

UCLA

UCLA Previously Published Works

Title

Theoretical constraints on the effects of pH, salinity, and temperature on clumped isotope signatures of dissolved inorganic carbon species and precipitating carbonate minerals

Permalink

<https://escholarship.org/uc/item/8pr0091n>

Authors

Hill, Pamela S
Tripathi, Aradhna K
Schauble, Edwin A

Publication Date

2014

DOI

10.1016/j.gca.2013.06.018

Peer reviewed



Theoretical constraints on the effects of pH, salinity, and temperature on clumped isotope signatures of dissolved inorganic carbon species and precipitating carbonate minerals

Pamela S. Hill*, Aradhna K. Tripathi*, Edwin A. Schauble

Department of Earth and Space Sciences, University of California, Los Angeles, 595 Charles Young Drive East, Box 951567, Los Angeles, CA 90095-1567, USA

Received 28 February 2013; accepted in revised form 13 June 2013; available online 25 June 2013

Abstract

The use of carbonate ‘clumped isotope’ thermometry as a geochemical technique to determine temperature of formation of a carbonate mineral is predicated on the assumption that the mineral has attained an internal thermodynamic equilibrium. If true, then the clumped isotope signature is dependent solely upon the temperature of formation of the mineral without the need to know the isotopic or elemental composition of coeval fluids. However, anomalous signatures can arise under disequilibrium conditions that can make the estimation of temperatures uncertain by several degrees Celsius. Here we use ab initio calculations to examine the potential disequilibrium mineral signatures that may arise from the incorporation of dissolved inorganic carbon (DIC) species (predominantly aqueous carbonate and bicarbonate ions) into growing crystals without full equilibration with the crystal lattice.

We explore theoretically the nature of clumping in the individual DIC species and the composite DIC pool under varying pH, salinity, temperature, and isotopic composition, and speculate about their effects upon the resultant disequilibrium clumping of the precipitates. We also calculate equilibrium clumped signatures for the carbonate minerals calcite, aragonite, and witherite. Our models indicate that each DIC species has a distinct equilibrium clumped isotope signature such that, $\Delta_{47}(\text{H}_2\text{CO}_3) > \Delta_{47}(\text{HCO}_3^-) > \Delta_{47}(\text{equilibrium calcite}) > \Delta_{47}(\text{CO}_3^{2-})$, and predict a difference between $\Delta_{47}(\text{HCO}_3^-)$ and $\Delta_{47}(\text{CO}_3^{2-}) > 0.033\text{‰}$ at 25 °C, and that $\Delta_{47}(\text{aragonite}) > \Delta_{47}(\text{calcite}) > \Delta_{47}(\text{witherite})$. We define the calcite clumped crossover pH as the pH at which the composite $\Delta_{47}(\text{DIC pool}) = \Delta_{47}(\text{equilibrium calcite})$. If disequilibrium $\Delta_{47}(\text{calcite})$ is misinterpreted as equilibrium $\Delta_{47}(\text{calcite})$, it is possible to overestimate or underestimate the growth temperature by small but significant amounts. Increases in salinity lower the clumped crossover pH and may cause larger effects. Extreme effects of pH, salinity, and temperature, such as between cold freshwater lakes at high latitudes to hot hypersaline environments, are predicted to have sizeable effects on the clumped isotope composition of aqueous DIC pools.

In order to determine the most reliable and efficient modeling methods to represent aqueous dissolved inorganic carbon (DIC) species and carbonate minerals, we performed convergence and sensitivity testing on several different levels of theory. We used 4 different techniques for modeling the hydration of DIC: gas phase, implicit solvation (PCM and SMD), explicit solvation (ion with 3 water molecules) and supermolecular clusters (ion plus 21 to 32 water molecules with geometries generated by molecular dynamics). For each solvation technique, we performed sensitivity testing by combining different levels of theory (up to 8 ab initio/hybrid methods, each with up to 5 different sizes of basis sets) to understand the limits of each technique. We looked at the degree of convergence with the most complex (and accurate) models in order to select the most

* Corresponding authors.

E-mail addresses: phill2014@gmail.com (P.S. Hill) and ripple@ess.ucla.edu or aradhna.tripati@gmail.com (A.K. Tripathi).

reliable and efficient modeling methods. The B3LYP method combined with the 6-311++G(2d,2p) basis set with supermolecular clusters worked well.

© 2013 Elsevier Ltd. All rights reserved.

1. INTRODUCTION

Carbonate ‘clumped isotope’ thermometry is a powerful isotopic technique being applied to both inorganic and biogenic precipitates to probe the temperature history and physical chemical characteristics of ancient environments. Based upon the attainment of internal bulk thermodynamic equilibrium (i.e., internal isotopic exchange equilibrium) among multiply substituted isotopologues¹ of carbon and oxygen within the lattice of a carbonate mineral, this technique can be used to determine the temperature of carbonate precipitation (i.e., temperature of formation) without the need to know the isotopic composition of coeval fluids (e.g., Ghosh et al., 2006; Eiler, 2007; Dennis and Schrag, 2010; Eagle et al., 2010; Tripathi et al., 2010). This is a significant advantage over other widely utilized oxygen-isotope or element-ratio paleo-temperature proxies (e.g. Urey, 1947; McCrea, 1950; Shackleton and Opdyke, 1973; Shackleton, 1974; Kim and O’Neil, 1997).

Most synthetic and natural carbonate minerals that have been measured (e.g., Ghosh et al., 2006; Dennis and Schrag, 2010; Eagle et al., 2010; Tripathi et al., 2010; Thiagarajan et al., 2011) appear to exhibit equilibrium clumped isotope compositions similar to those predicted from theory (Wang et al., 2004; Schauble et al., 2006; Guo et al., 2009; this work). However, disequilibrium clumped isotopic signatures have been reported, first in warm-water aragonitic corals (Ghosh et al., 2006) and subsequently in other biogenic carbonates (Tripathi et al., 2010; Thiagarajan et al., 2011; Eagle et al., 2013; Saenger et al., 2012), as well as speleothems (Affek et al., 2008; Daeron et al., 2011). Unrecognized anomalous signatures from *disequilibrium* conditions can potentially cause errors of several degrees Celsius in the estimation of temperatures and need to be addressed to avoid jeopardizing the reliability of clumping as a temperature proxy (e.g., Ghosh et al., 2006; Daeron et al., 2011).

In this work, we explore theoretically the nature of clumping in solutions containing dissolved inorganic carbon (DIC) species under a variety of conditions, including varying pH, salinity, temperature, and isotopic composition. We also examine the potential effects of speciation in the parent DIC pool on clumping signatures preserved in precipitating carbonate minerals, since it is possible that some of the scatter in temperature calibrations produced to date results from incorporation of dissolved inorganic carbon (predominantly aqueous CO_3^{2-} and HCO_3^- ions) into growing carbonate crystals without full equilibration within the crystal lattice. There may well be other causes for some

of the scatter, such as degassing (e.g., Guo, 2008) and/or other kinetic effects (e.g., in corals as in Saenger et al., 2012, or in speleothems as in Affek et al., 2008; Daeron et al., 2011); however, these effects are not considered in this study.

Ab initio modeling of solvated species such as DIC is known to be a complex problem and can be extremely computer intensive. Thus we also address the most efficient way to model clumped isotope fractionation in aqueous carbonate species and carbonate minerals. It is necessary to search for methods which are computer efficient, yet yield usefully accurate results, and to understand how these methods deviate from more accurate models. To this end, we have developed a series of electronic structure models that simulate aqueous and crystalline chemical environments. We compare the effects of both different levels of theory and different solvation simulation techniques upon the individual DIC species and upon the composite DIC pool. We used 4 different techniques for modeling the hydration of DIC: gas phase, implicit solvation, explicit solvation (ion with 3 water molecules) and supermolecular clusters (ion plus 21 or 32 water molecules with geometries generated by molecular dynamic time steps) (Fig. 1A). We sampled 10 different conformers for each DIC supermolecular cluster model, in order to approximate a distribution of dynamic solvation structures. For each solvation technique, we applied different levels of theory (up to 8 ab initio/hybrid methods, each with up to 5 different sizes of basis set). We looked at the degree of convergence with increasing complexity and computational cost, in order to select an efficient and reliable modeling method. Studies of oxygen isotope fractionation by Zeebe (2009) and carbon isotope fractionation by Rustad et al. (2008, 2010a,b) suggest that modeling of DIC species with aqueous clusters of 21 (Zeebe) to 30 (Rustad et al.) waters is necessary to attain good agreement with experimental oxygen and carbon isotope fractionations. An earlier study by Rudolph et al. (2006), comparing gas phase models to solvated DIC species surrounded by 1, 2, or 3 waters, also emphasizes the importance of including solvation. Liu and Tossell (2005) found that cluster models (containing up to 34 water molecules) gave robust results when used to simulate isotope fractionations between aqueous boron species.

We also look at calcite, aragonite, and witherite mineral clusters, employing Rustad et al.’s (2008, 2010b) method of building supermolecular clusters based on the conservation of Pauling bond strength (Fig. 1B and C). This permits the use of the same theoretical and computational framework (i.e., basis sets, model chemistries) for species of all phases: gas, aqueous, and mineral (Rustad et al., 2008, 2010b). Our comparisons of these different conditions allow us to determine a suitable method for the prediction of clumped isotope fractionation in the aqueous carbonate species. We also present and compare results from models of different

¹ Isotopologues are molecules of the same species that differ only in their isotopic composition, e.g., $^{12}\text{C}^{18}\text{O}^{16}\text{O}_2$ and $^{12}\text{C}^{16}\text{O}_3$. A multiply substituted isotopologue contains more than one rare isotope (e.g., $^{13}\text{C}^{18}\text{O}^{16}\text{O}_2$ and $^{12}\text{C}^{18}\text{O}^{17}\text{O}^{16}\text{O}$).

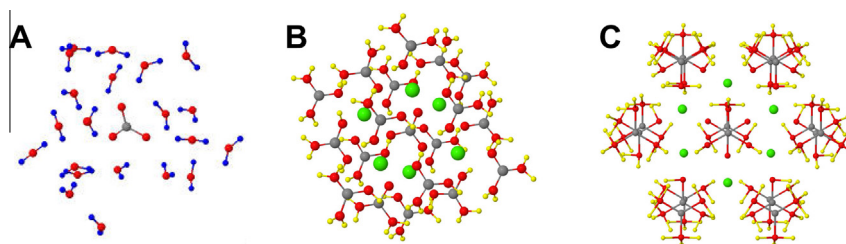


Fig. 1. Sample supermolecular cluster models. (A) $\text{CO}_3^{2-} * 21(\text{H}_2\text{O})$. (B) Calcite cluster model. (C) Aragonite cluster model (blue = H, red = O, gray = C, green = Ca, yellow = ghost atoms) (see Section 2.5). Images taken using *Jmol*. (For interpretation of the references to color in this figure legend, the reader is referred to the web version of this article.)

complexities to serve as a future guideline for judging computer efficiency versus accuracy of results.

2. METHODS

In this section we define $\Delta_{47}(\text{CO}_2)$, $\Delta_{63}(\text{CO}_3^{2-})$, and the isotope fractionation factors for $^{13}\text{C}/^{12}\text{C}$ ($\beta^{13}\text{C}$), $^{18}\text{O}/^{16}\text{O}$ ($\beta^{18}\text{O}$), and $^{17}\text{O}/^{16}\text{O}$ ($\beta^{17}\text{O}$) and then discuss the relation between $\Delta_{47}(\text{CO}_2)$ and $\Delta_{63}(\text{CO}_3^{2-})$ of a carbonate mineral, considerations in the theoretical modeling of DIC species and the calcite, aragonite, and witherite lattices, the Redlich Teller self-consistency test, and the calculation of composite reduced partition function ratios and equilibrium constants for the large cluster models with little or no symmetry. A detailed, multi-step procedure for the calculation of clumped isotope signatures for all multiply substituted isotopologues (Δ_{60} to Δ_{67}) is described in Appendix A.1.

2.1. Definition:² Clumped isotope signatures $\Delta_{63}(\text{CO}_3^{2-})$ and $\Delta_{47}(\text{CO}_2)$

The tendency of ^{13}C and ^{18}O to form bonds together in carbon dioxide is quantified by defining $\Delta_{47}(\text{CO}_2)$ as the permil (‰) deviation in the abundance of CO_2 molecules with a mass of 47 amu (=Mass47)³ from the abundance predicted by stochastic (random) mixing. In a similar fashion, $\Delta_{63}(\text{CO}_3^{2-})$ of a carbonate mineral² is defined as the permil deviation in the abundance of all CO_3^{2-} isotopologues of mass 63 amu (=Mass63)⁴ from the abundance predicted by random mixing. $\Delta_{63}(\text{CO}_3^{2-})$ cannot yet be measured directly; the carbonate must first be converted to CO_2 by phosphoric acid digestion, and then measured in a gas-source isotope ratio mass spectrometer (Ghosh et al., 2006; Guo et al., 2009).

The resulting clumped isotope signature Δ_{47} is dependent upon the sum of the concentrations of all isotopologues

of mass of 47 amu and is defined at a given temperature T as

$$\Delta_{47}(\text{CO}_2) = 10^3 * \left(\frac{[\text{Mass}47/\text{Mass}44]_{\text{sample}}}{[\text{Mass}47/\text{Mass}44]_{\text{random}}} - 1 \right) \quad (1)$$

Wang et al. (2004).⁵

In a similar fashion we define $\Delta_{63}(\text{CO}_3^{2-})$ of a carbonate mineral² at a given temperature T as the permil deviation in the abundance of all CO_3^{2-} isotopologues of mass 63 amu (=Mass63)⁴ from the abundance predicted by random mixing, such that

$$\Delta_{63}(\text{CO}_3^{2-}) = 10^3 * \left(\frac{[\text{Mass}63/\text{Mass}60]_{\text{sample}}}{[\text{Mass}63/\text{Mass}60]_{\text{random}}} - 1 \right) \quad (2)$$

In the present study we are interested in differences in Δ_{47} and Δ_{63} of less than 0.1‰, and so do not employ approximations like those suggested in Section 3.2 of Wang et al. (2004), since Δ_i of singly substituted isotopologues may not be <0.01‰ due to the asymmetry of the supermolecular clusters (see Table B.2 in Appendix B, the Electronic supplement, for examples of Δ_i). Cao and Liu (2012) have also proposed a slightly different method to approximate Δ_{47} , which is expected nonetheless to yield the same ultimate results.

The relative abundances of the isotopologues are dependent upon the thermodynamic equilibrium of the system at a given temperature T (i.e., the numerator in Eqs. (1) and (2)). The stochastic abundances (i.e., the denominator in Eq. (1) or Eq. (2)) are dependent upon the isotopic composition of the system. However, equilibrium Δ_{63} is independent of the system's isotopic makeup. The calculation of Δ_{63} is detailed in Appendix A.1. Computational routines for calculating isotopologue attributes were programmed in Scilab 5.3.3 (2011).

The quantities Δ_{44} , Δ_{45} , Δ_{46} , Δ_{48} , Δ_{49} , Δ_{60} , Δ_{61} , Δ_{62} , Δ_{64} , Δ_{65} , Δ_{66} , and Δ_{67} are defined in a similar manner. Note that $\Delta_{60} = 0$ and $\Delta_{44} = 0$ by definition.

² For simplicity we use $\Delta_{63}(\text{CO}_3^{2-})$ to represent any carbonate species of the form $\text{MCO}_3^{(x)}$ where M represents a cation or anion likely to combine with the carbonate ion, such as Ca^{2+} , Mg^{2+} , Fe^{2+} , H^+ , H_2 , etc., and x is the overall charge of the ion or molecule.

³ $\text{Mass}47 = \text{Mass}(^{13}\text{C}^{18}\text{O}^{16}\text{O}) + \text{Mass}(^{13}\text{C}^{17}\text{O}^{17}\text{O}) + \text{Mass}(^{12}\text{C}^{18}\text{O}^{17}\text{O})$ in amu; $\text{Mass}44 = \text{Mass}(^{12}\text{C}^{16}\text{O}^{16}\text{O})$ in amu.

⁴ $\text{Mass}63 = \text{Mass}(^{12}\text{C}^{16}\text{O}^{17}\text{O}^{18}\text{O}) + \text{Mass}(^{12}\text{C}^{17}\text{O}^{17}\text{O}^{17}\text{O}) + \text{Mass}(^{13}\text{C}^{16}\text{O}^{17}\text{O}^{17}\text{O}) + \text{Mass}(^{13}\text{C}^{16}\text{O}^{16}\text{O}^{18}\text{O})$ in amu; $\text{Mass}60 = \text{Mass}(^{12}\text{C}^{16}\text{O}^{16}\text{O}^{16}\text{O})$ in amu.

⁵ Huntington et al. (2009) discuss the practical applicability of this definition to measurement by gas-source isotope ratio mass spectrometry.

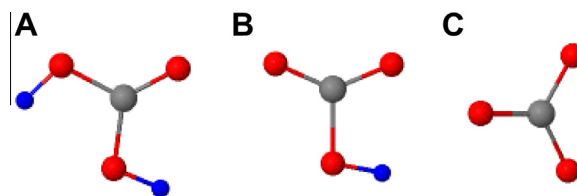


Fig. 2. DIC species as gas phase. (A) H_2CO_3 (*cis-trans*); (B) HCO_3^- ; (C) CO_3^{2-} . H_2CO_3 and HCO_3^- have C_1 symmetry in which each oxygen position is unique. CO_3^{2-} has D_{3h} symmetry in which the oxygen positions are indistinguishable (see Section 2.4). (blue = H, red = O, gray = C). Images taken using Jmol. (For interpretation of the references to color in this figure legend, the reader is referred to the web version of this article.)

2.2. Relation between Δ_{63} and Δ_{47} of a carbonate mineral

The Δ_{47} of a carbonate mineral is related to the Δ_{63} of the same carbonate sample by correcting for isotopic fractionation that occurs during phosphoric acid digestion, such that

$$\Delta_{47} = \Delta_{63} + y \quad (3)$$

where y is the fractionation factor for a given acid digestion temperature.

Guo et al. (2009) determined experimental and theoretical values for the acid digestion fractionation factor y as follows:⁶

$$\text{Experimental: } y = 0.232 \pm 0.015\text{‰ for acid digestion at } 25\text{ }^\circ\text{C} \quad (4)$$

$$\text{Theoretical: } y = 0.220\text{‰ for acid digestion at } 25\text{ }^\circ\text{C} \quad (5)$$

Acid fractionation effects at different temperatures are well known for oxygen isotopes (Swart et al., 1991).

The acid digestion fractionation is also expected to show a small compositional dependence. Guo et al.'s (2009) theoretical models predict an increase of $\sim 0.035\text{‰}$ in fractionation for every 1‰ increase in the Δ_{63} of the carbonate sample.

2.3. Definitions of isotope fractionation factors: $\beta^{18}\text{O}$, $\beta^{17}\text{O}$, $\beta^{13}\text{C}$, and $\alpha(A - B)$

The following common definitions are useful when discussing isotope fractionation (e.g., Faure and Mensing, 2004).

$\alpha(A - B)$ is the isotopic fractionation between 2 phases A and B such that

$$\begin{aligned} \alpha^{18\text{O}}(A - B) &= ({}^{18}\text{O}/{}^{16}\text{O})_A / ({}^{18}\text{O}/{}^{16}\text{O})_B \text{ and} \\ \alpha^{13\text{C}}(A - B) &= ({}^{13}\text{C}/{}^{12}\text{C})_A / ({}^{13}\text{C}/{}^{12}\text{C})_B \end{aligned} \quad (6)$$

$\beta^{13}\text{C}$ is defined as the ${}^{13}\text{C}/{}^{12}\text{C}$ partitioning between a given species and a gas phase carbon atom (i.e., carbon vapor). In a similar manner $\beta^{18}\text{O}$ and $\beta^{17}\text{O}$ are defined as the ${}^{18}\text{O}/{}^{16}\text{O}$

and ${}^{17}\text{O}/{}^{16}\text{O}$ isotope fractionation respectively between a given species and a gas phase oxygen atom.

$$\begin{aligned} \beta^{18}\text{O}(\text{CO}_3^{2-}) &= \alpha^{18\text{O}}(\text{CO}_3^{2-} - \text{O}(\text{g})) \text{ and} \\ \beta^{13}\text{C} &= \alpha^{13\text{C}}(\text{CO}_3^{2-} - \text{C}(\text{g})) \end{aligned} \quad (7)$$

It follows that

$$\alpha(A - B) = \beta(A) / \beta(B). \quad (8)$$

$\beta^{18}\text{O}$, $\beta^{17}\text{O}$, and $\beta^{13}\text{C}$ are calculated from reduced partition function ratios as detailed in Appendix A.1.1 and Eqs. (A5)–(A9).

2.4. Composite fractionation factors ${}^{18}\text{O}/{}^{16}\text{O}$ ($\beta^{18}\text{O}$), ${}^{17}\text{O}/{}^{16}\text{O}$ ($\beta^{17}\text{O}$), ${}^{13}\text{C}/{}^{12}\text{C}$ ($\beta^{13}\text{C}$), and equilibrium constants (K3866 and K2876)

In the gas phase the trigonal planar carbonate ion has D_{3h} symmetry, while the linear carbon dioxide molecule demonstrates $\text{D}_{\infty h}$ symmetry. In these cases, the isotopomers⁷ of an isotopologue¹ describing the different sites of the oxygen isotopes are indistinguishable. For example, the isotopologue ${}^{13}\text{C}^{18}\text{O}^{16}\text{O}^{16}\text{O}^{2-}$ of the carbonate ion has 3 isotopomers: ${}^{13}\text{C}^{18}\text{O}^{16}\text{O}^{16}\text{O}^{2-}$, ${}^{13}\text{C}^{16}\text{O}^{18}\text{O}^{16}\text{O}^{2-}$, and ${}^{13}\text{C}^{16}\text{O}^{16}\text{O}^{18}\text{O}^{2-}$, which are all equivalent by symmetry, and their vibrational frequencies and derived attributes (such as $\beta^{18}\text{O}$, $\beta^{17}\text{O}$, and $\beta^{13}\text{C}$) are equal (Fig. 2C).

However, in a carbonate species with little or no symmetry in which each O site is distinct, such as HCO_3^- or H_2CO_3 or $\text{CO}_3^{2-} * 21(\text{H}_2\text{O})$ (Figs. 1A and 2A and 2B), the isotopologue (e.g., $\text{H}_2^{12}\text{C}^{18}\text{O}^{16}\text{O}^{16}\text{O}$) has 3 distinct isotopomers (e.g., $\text{H}_2^{12}\text{C}^{18}\text{O}^{16}\text{O}^{16}\text{O}$, $\text{H}_2^{12}\text{C}^{16}\text{O}^{18}\text{O}^{16}\text{O}$, and $\text{H}_2^{12}\text{C}^{16}\text{O}^{16}\text{O}^{18}\text{O}$), each of which has distinct vibrational frequencies and derived attributes. In this case, we must calculate the composite attributes for an isotopologue as a function of the individual isotopomer attributes.

⁷ Isotopomers (short for isotope isomer) are isotopes with the same chemical formula but different arrangements of the isotopes (e.g., $\text{H}^{12}\text{C}^{18}\text{O}^{17}\text{O}^{17}\text{O}^-$, $\text{H}^{12}\text{C}^{17}\text{O}^{18}\text{O}^{17}\text{O}^-$, and $\text{H}^{12}\text{C}^{17}\text{O}^{17}\text{O}^{18}\text{O}^-$). Here we denote individual isotopomers with an underscore, following the notation of Guo et al. (2009). Thus, ${}^{13}\text{C}^{18}\text{O}^{16}\text{O}^{16}\text{O}$ represents only one isotopomer while ${}^{13}\text{C}^{18}\text{O}^{16}\text{O}^{16}\text{O}$ represents all three isotopomers: ${}^{13}\text{C}^{18}\text{O}^{16}\text{O}^{16}\text{O}$, ${}^{13}\text{C}^{16}\text{O}^{18}\text{O}^{16}\text{O}$, and ${}^{13}\text{C}^{16}\text{O}^{16}\text{O}^{18}\text{O}$. For consistency, we use the same notation for isotopomers of a given isotopologue even if the isotopomers are not distinct. (Charges are omitted for simplicity.)

⁶ Use of the polynomial regression equation as expressed in Eq. (23) in Guo et al. (2009) gives a theoretical fractionation factor of 0.237‰ for acid digestion at $25\text{ }^\circ\text{C}$.

We define the composite β factors as the geometric mean⁸ of the individual isotopomer β s; for example, for isotopologue $^{12}\text{C}^{18}\text{O}^{16}\text{O}^{16}\text{O}$

$$\beta^{18\text{O}2866} = (\beta^{18\text{O}2866} * \beta^{18\text{O}2686} * \beta^{18\text{O}2668})^{(1/3)} \quad (9)$$

Following the notation in [Schauble et al. \(2006\)](#), we use the shortcut notation ‘2866’ to represent attributes of the isotopologue $^{12}\text{C}^{18}\text{O}^{16}\text{O}^{16}\text{O}$; ‘3866’ for $^{13}\text{C}^{18}\text{O}^{16}\text{O}^{16}\text{O}$, etc.

The composite equilibrium constants K (see [Appendix A.1](#) for a definition of K , Eqs. (A11) and (A12)), however, must be calculated directly from the isotopomer abundances. The composite equilibrium constant for isotopologue 2876 is

$$K_{2876} = \frac{\{[^{12}\text{C}^{18}\text{O}^{17}\text{O}^{16}\text{O}] * [^{12}\text{C}^{16}\text{O}^{16}\text{O}^{16}\text{O}]\}}{\{[^{12}\text{C}^{18}\text{O}^{16}\text{O}^{16}\text{O}] * [^{12}\text{C}^{17}\text{O}^{16}\text{O}^{16}\text{O}]\}} \\ = (x_{2876} * x_{2666}) / (x_{2866} * x_{2766}) \quad (10)$$

where x_i is the fractional mass of isotopologue i and \underline{x}_i is the fractional mass of isotopomer i . From here on we use the unsigned ‘CO₃’ to represent any carbonate of interest in these equations.

Substituting the individual isotopomer masses for the composite isotopologue masses gives⁹

$$K_{2876} = \frac{\{(x_{2876} + \underline{x}_{2867} + \underline{x}_{2786} + \underline{x}_{2768} + \underline{x}_{2678} \\ + \underline{x}_{2687}) * (x_{2666})\}}{\{(x_{2866} + \underline{x}_{2686} \\ + \underline{x}_{2668}) * (x_{2766} + \underline{x}_{2676} + \underline{x}_{2667})\}} \quad (11)$$

The composite ratio of K_i/K_{i-r} (used by [Wang et al., 2004](#), in discussions of the relationship between K and Δ) can be calculated as a weighted average such that

$$(K_{2876}/K_{2876-r}) = \left\{ \frac{(x_{2876} * K_{2876}/K_{2876-r}) \\ + (x_{2867} * K_{2867}/K_{2867-r}) \\ + (x_{2786} * K_{2786}/K_{2786-r}) \\ + (x_{2768} * K_{2768}/K_{2768-r}) \\ + (x_{2678} * K_{2678}/K_{2678-r}) \\ + (x_{2687} * K_{2687}/K_{2687-r}) \right\} / x_{2876} \quad (12)$$

⁸ It is also possible to define the composite $\beta^{18\text{O}}$ as the simple arithmetic average or as the weighted arithmetic average of the 3 isotopomer β values. Differences in these definitions in our models are exceedingly small, on the order of 0.001‰ or less.

⁹ For the carbonate ion systems, the individual isotopomer equilibrium constants for the isotopologue 2876 (i.e., K_{2876} , K_{2867} , K_{2786} , K_{2768} , K_{2678} , and K_{2687}) will each be greater than 1 when calculated for a molecular system with C1 symmetry (e.g., all the supermolecular CO₃²⁻ * n(H₂O) clusters). However, when the composite equilibrium constant K_{2876} or K_{287} is calculated (Eq. (11)) for a system with inherent symmetry (e.g., CO₃²⁻ and CO₂ respectively), the composite K_{2876} or K_{287} will be less than 1 ($K_{2876} \sim 0.67$ for CO₃²⁻ and $K_{287} \sim 0.5$ for CO₂). The stochastic value for each individual isotopomer of K_{2876} is 1, but the stochastic value for the composite K_{2876} is 2/3. Similarly, for CO₂ the stochastic value for individual isotopomers of K_{287} is 1, and the composite K_{287} stochastic (classical) value is 1/2. These stochastic values arise from the inherent symmetry of CO₃²⁻ and CO₂.

where K_{2876-r} is the stochastic composite equilibrium constant K_{2876} and the isotopomer stochastic equilibrium constants are denoted as K_{2876-r} , K_{2867-r} , K_{2786-r} , K_{2768-r} , K_{2678-r} , and K_{2687-r} .

In a similar fashion the composite equilibrium constant K_{3866} can be calculated as

$$K_{3866} = (x_{3866} * x_{2666}) / (x_{2866} * x_{3666}) \\ = \frac{(x_{3866} * \underline{x}_{3686} * \underline{x}_{3668} * x_{2666})}{(x_{2866} \\ * \underline{x}_{2686} * \underline{x}_{2668} * x_{3666})} \quad (13)$$

2.5. Ab initio and solvation models of aqueous DIC species and carbonate mineral lattices

In this section we describe the models and tests used to determine an optimal combination of ab initio method, basis set, and solvation technique for calculating Δ_{63} , $\beta^{18\text{O}}$, $\beta^{17\text{O}}$, and $\beta^{13\text{C}}$ that is reasonably computationally efficient, yet yields usefully accurate results, and to determine how this method deviates from more accurate models constructed using higher levels of theory.

2.5.1. Prior work using large molecular clusters to model solvation in DIC species

Accurate vibrational frequencies are the most critical output from electronic structure models for the determination of isotope partitioning and isotopologue abundances. Earlier studies indicate that modeling an aqueous species is significantly improved by the inclusion of explicit waters of hydration. [Rudolph et al. \(2006\)](#) showed that modeling small clusters of DIC species (with 1 to 3 waters of hydration) gives a better match with measured vibrational frequencies than models of the DIC species in the gas phase. [Zeebe \(2009\)](#) found that the inclusion of increasing numbers of waters of hydration (up to 22) surrounding a carbonate ion (CO₃²⁻) improved the accuracy of the model’s prediction of the oxygen isotope fractionation between CO₃²⁻ and water. He found good agreement between theory and experiment with about fifteen or more waters of hydration. [Rustad et al. \(2008, 2010b\)](#) performed an in-depth study of the use of supermolecular clusters to predict carbon isotope fractionation in DIC aqueous species. When comparing gas phase models to implicit solvation models and to supermolecular clusters of different sizes (7 to 64 waters of hydration) using different ab initio methods and basis set combinations, they concluded that supermolecular clusters are better predictors of carbon isotope fractionation than gas models or implicit solvation models. However, the potential energy surfaces of the supermolecular cluster systems are very flat due to the weak H bonds and overall system complexity as would be expected given the dynamism of solutions (i.e., because solutions are dynamic and not at the global minimum energy configuration most of the time). With such a system, any optimized geometry is likely to be a local energy minimum rather than the global minimum. Thus it is necessary to take the average value of several conformers to obtain a reasonable estimate of cluster system properties. [Rustad et al.](#) concluded that an average of ten conformers is sufficient to predict ¹³C/¹²C fractionation within a standard error

of the mean (se) of 0.3 to 0.5‰ at 25 °C. They evaluated ab initio/hybrid methods such as PBE and B3LYP, combined with basis sets 6-31G*, 6-311G*, and aug-cc-pVDZ (see next section for references). They concluded that the B3LYP/aug-cc-pVDZ combination was “probably the most accurate. . . showing that hybrid functionals and diffuse basis functions improve the description of hydrogen bonding in aqueous systems (Xantheas, 1995; Sim et al., 1992; Hamman, 1997)” (page 552, Rustad et al., 2008). Since the aug-cc-pVDZ basis set is computationally very expensive, they also concluded that the PBE/6-31G* combination with conformers of about 30 waters of hydration was a reasonable alternative and can predict $\beta^{13}\text{C}$ for gas, aqueous, and solid state carbonate system within 3‰ se. They further concluded that use of the B3LYP/aug-cc-pVDZ can reduce the standard error of $\beta^{13}\text{C}$ to about 1‰.

2.5.2. Convergence and sensitivity testing for Δ_{63} , $\beta^{18}\text{O}$, and $\beta^{13}\text{C}$ at different levels of theory

We performed sensitivity and convergence testing for the modeling of aqueous DIC species by combining different levels of theory with different sized basis sets for a select set of carbonate species: $\text{CO}_2(\text{g})$, $\text{CO}_3^{2-}(\text{g})$, $\text{H}_2\text{CO}_3(\text{g})$, $\text{H}_2\text{CO}_3 * 3(\text{H}_2\text{O})$, and $\text{HCO}_3^- * 3(\text{H}_2\text{O})$. The species were chosen to allow us to compare a variety of ionic charges and the effect of 2 different (simple) solvation techniques. The use of simple species also allowed us to test more complex ab initio methods. We looked at the degree of convergence of each combination of method and basis set with the most complex (and presumably accurate) models in order to select the most reliable and efficient modeling methods. We used ab initio/hybrid methods: RHF (restricted Hartree Fock), DFT (Density Functional Theory) including B3LYP (a versatile and popular hybrid method which combines the exact electron exchange treatment of Hartree-Fock theory with the Lee, Yang and Parr correlation functional: Becke, 1993; Lee et al., 1988), PBE (the exchange functional combined with the gradient-corrected functional of (Perdew et al., 1996, 1997), and functionals from the newer M06 series: Zhao and Truhlar, 2008a,b; Yang et al., 2010), MP2 (Møller-Plesset perturbation theory level 2: Head-Gordon et al., 1988), CCSD (Coupled-Cluster Singles and Doubles: Cizek, 1969; Scuseria et al., 1988), and QCISD (Quadratic Configuration Interaction with Single and Double Excitation: Pople et al., 1987).

The CCSD and QCISD ab initio methods are the most accurate approaches considered here, but the computational cost becomes prohibitive for studies of large molecules (e.g., Johnson et al., 1993; Thomas et al., 1993a,b; Oliphant and Bartlett, 1994; Bartlett, 1995; Bartlett and Musial (2007); Scott and Radom, 1996 and references therein). Results from hybrid DFT methods on aqueous clusters may perform as well as the MP2 method (Xantheas, 1995). The RHF method can be a good first order approximation, but is typically outperformed by other methods at higher levels of theory (e.g., Lee and Scuseria, 1995; Johnson et al., 1993; Thomas et al., 1993a,b; Oliphant and Bartlett, 1994; Bartlett, 1995; Scott and Radom, 1996 and references therein; Wong, 1996; Halls and Schlegel, 1998; Crawford and Schaefer, (2000).

We combined progressively larger Pople basis sets with each method, increasing the number of polarizing and diffuse Gaussian orbitals. We used 6-31G* (split valence double zeta with polarization) (Hariharan and Pople, 1973; Rassolov et al., 1998), 6-311G* (split valence triple zeta plus polarization) (Blau-deau et al., 1997), and 6-311++G(2d,2p) (split valence triple zeta with polarization and added diffuse functions) (Krishnan et al., 1980; Blau-deau et al., 1997). We compared the Pople basis sets against the Dunning group correlation-consistent polarized basis sets cc-pVTZ (valence triple zeta with polarization) and aug-cc-pVTZ (augmented with added diffuse functions) (e.g., Kendall et al., 1992; Woon and Dunning, 1993). We used aug-cc-pVTZ for direct comparison with 6-311++G(2d,2p) instead of the smaller aug-cc-pVDZ (valence double zeta, used by Rustad et al. (2008)). The largest two basis sets, 6-311++G(2d,2p) and aug-cc-pVTZ, appear to be near reasonable basis set convergence thresholds for the chosen density functionals (e.g., Molnar et al., 2009; Bryantsev et al., 2009; Suárez et al., 2011).

2.5.3. Comparison of Δ_{63} , $\beta^{18}\text{O}$, and $\beta^{13}\text{C}$ calculated using different solvation techniques

We generated electronic structure models for each of the DIC species: H_2CO_3 (*cis-trans* conformer – Fig. 2A), HCO_3^- , and CO_3^{2-} (Fig. 2B and C). For each DIC species we applied 4 different solvation techniques: (1) simple gas phase models of isolated DIC species, (2) implicit solvation (self consistent reaction field – SCRf), (3) explicit solvation using three water molecules surrounding each DIC species, and (4) supermolecular cluster models containing 21 to 32 water molecules (Fig. 1A).

The different solvation approaches mentioned above employ increasingly complex simulations of the aqueous environment. Implicit solvation models attempt to capture some of the chemical properties of a solute species, at reduced computational expense, by surrounding a cluster of atoms (including explicitly designated water molecules if desired) with a continuous dielectric medium approximating the properties of liquid water. We used the polarizable continuum model (PCM) of Miertus et al. (1981) with a dielectric constant equal to that of pure water (80.1 at 20 °C). We also used the SMD model (Marenich et al., 2009), a sophisticated self-consistent reaction field implicit solvation model that has worked well with the M06 series DFT functionals developed by the Truhlar/Cramer group in previous studies (Cramer and Truhlar, 2008; Chamberlin et al., 2008).

For the explicit solvation method (also known as the water droplet method), we simulated the solvent by surrounded each DIC species with 3 water molecules distributed symmetrically around and in the same plane as the central ion (patterned after Rudolph et al., 2006).

The fourth solvation method consisted of supermolecular clusters, in which the DIC species is surrounded by 21 or 32 water molecules, numbers suggested by Zeebe (2007) and Rustad et al. (2008) respectively. Molecular dynamics has been shown to be useful in setting up representative solvation structures around reactant and product molecules – which can then be “quenched”, i.e., relaxed and subjected to static

vibrational frequency calculations (e.g., bulk isotope partitioning studies by Rustad and Bylaska, 2007; Rustad et al., 2008, 2010a,b; Zeebe, 2009). The molecular dynamics simulation program Moldy (Refson, 2000) was used to generate the supermolecular clusters as described above. Lennard-Jones potentials and partial charges for DIC species and water were taken from Zeebe (2011) and references therein. Isotopic partitioning results for each DIC species are the average of up to 10 conformers. We had to omit 3 conformers in which the DIC species morphed into another species during optimization. Obtaining optimized geometries for such large systems requires frequent user intervention (Appendix A.4).

2.5.4. Modeling calcite, aragonite, and witherite lattices as supermolecular clusters

The calcite and aragonite mineral lattices were modeled as supermolecular clusters patterned after the cluster representation of mineral lattices by Rustad et al. (2008, 2010b) (Fig. 1B and C). Each mineral cluster has an inner layer consisting of a central carbonate (CO_3^{2-}) surrounded by six Ca–O polyhedra. (Each O in the central carbonate group of calcite (aragonite) is bonded to two (three) Ca ions as part of a Ca–O polyhedron; each Ca in calcite (aragonite) is bonded to six (nine) oxygens.) The outer layer is a secondary “ring” of carbonate groups (CO_3^{2-}). Each Ca atom in all the oxygen-calcium bonds from this outer layer (i.e., that is not part of the inner six Ca–O polyhedra) is replaced by a ghost atom at a distance of 1 Å from the oxygen atom (along the vector of the Ca–O bond) with a charge equal to the Pauling bond valence (+1/3 for calcite and +2/9 for aragonite). The cluster has an overall neutral charge. The positions of all atoms in the outer layer are frozen during the geometry optimization calculations. All ab initio calculations on the outer, frozen atoms were performed with the 3-21G basis set; calculations on the inner, moveable atoms were performed by a variety of basis sets, as did Rustad et al. on their molecular clusters. All ab initio calculations were performed with Gaussian09, Revision B.01 (Gaussian 09, Revision B.01, 2010) on the UCLA Hoffman2 computer cluster.

We also modeled witherite (BaCO_3) as a supermolecular cluster for comparison with experimental runs. Witherite belongs to the same space group as aragonite. However, the 6-311++G(2d,2p) basis set cannot be used with Ba, so we used the small SDD basis set (without polarization or diffuse functions), which combines the D95 basis set (Dunning and Hay, 1976) with the Stuttgart RSC 1997 ECP basis set (e.g., Fuentealba et al., 1985). Comparison with species run with both the Pople and SDD basis sets allowed us to estimate results for the witherite cluster compared to calcite and aragonite clusters run with B3LYP/6-311++G(2d,2p).

The use of supermolecular cluster models allows comparison of crystal lattices with aqueous species within a consistent computational and theoretical framework (Zeebe, 2009; Rustad et al., 2008, 2010b). Such an approach should help cancel out systematic errors. This is the first time this technique has been applied to model

clumped isotope signatures of crystals and supermolecular aqueous clusters together.

2.6. Self-consistency test: Redlich Teller Product Rule

The Redlich Teller Product Rule (Redlich, 1935; Herzberg, 1966) provides a check on the numerical self-consistency of the calculated vibrational frequencies.

$$1.5 * \ln \left\langle \frac{1m}{2m} \right\rangle + 1.5 * \ln \left\langle \frac{2M}{1M} \right\rangle + \ln \left\langle \left(\frac{2I_x}{1I_x} \right) * \left(\frac{2I_y}{1I_y} \right) * \left(\frac{2I_z}{1I_z} \right) \right\rangle = \sum_i \ln \left(\frac{2v_i}{1v_i} \right) \quad (14)$$

where superscripts 1 and 2 refer to isotopically light or heavy atoms respectively, “m” = mass of the carbonate atom, “M” = mass of molecular system, v = vibrational frequency, and I_x , I_y , and I_z are the moments of inertia around the x , y , and z axes respectively with the origin at the center of mass of the molecular system (Nakamoto, 1997). In the case of single molecules in the gas phase, then “m” = the mass of the substituted isotope(s). For ^{13}C substitutions in molecules with a center of symmetry, such as symmetric isotopomers of CO_2 and CO_3^{2-} in the gas phase, the moments of inertia will cancel to 1. For other molecular systems without a center of symmetry, the product of the ratios of the moments of inertia is not 1, but should still be relatively close to unity ($\sim 1 \pm 10^{-3}$ to 10^{-6} depending on the molecular system). Sometimes the moments of inertia are omitted from the equation and the computed value of the left-hand side of Eq. (15) is used to evaluate the numerical self-consistency of large systems (see Rustad et al., 2008).

$$1.5 * \ln \left\langle \frac{1m}{2m} \right\rangle + 1.5 * \ln \left\langle \frac{2M}{1M} \right\rangle = \sum_i \ln \left(\frac{2v_i}{1v_i} \right) \quad (15)$$

All models used in the present study are found to obey the Redlich Teller relations: models with isotopesubstitution at a center of symmetry obey exactly (within likely rounding errors in calculated vibrational frequencies), while models with asymmetric substitution deviate by slightly more, but are still within the expected range (Rustad et al., 2008).

3. RESULTS

In this section we summarize the reasons for our choice of the B3LYP/6-311++G(2d,2p) supermolecular cluster model for the calculation of Δ_{63} , $\beta^{13}\text{C}$, and $\beta^{18}\text{O}$. We also present general trends for Δ_{63} , $\beta^{13}\text{C}$, and composite $\beta^{18}\text{O}$ for each of the DIC species and the calcite and aragonite clusters as well as comparison of model predictions with other theoretical and experimental work.

3.1. Choice of best model for Δ_{63} , $\beta^{18}\text{O}$, and $\beta^{13}\text{C}$ of DIC, calcite, and aragonite clusters

Here we present the summary results of the convergence and sensitivity testing, in which we evaluate the effectiveness

of different levels of theory and solvation techniques in predicting values of Δ_{63} , $\beta^{13}\text{C}$, and $\beta^{18}\text{O}$ for selected DIC species. Section 2.5 has a detailed discussion of the models used in the tests, including solvation techniques, ab initio methods and basis sets as well as summaries of prior relevant work. A more complete examination of the results with tables and graphs, including ab initio/hybrid methods – basis set combinations, solvation techniques, comparison of chosen species with experimental bond lengths and vibrational frequencies, and the effect of scaling factors can be found in Appendix A.2.

3.1.1. Convergence test for different ab initio/hybrid methods – basis set combinations

We compared values of Δ_{63} , $\beta^{13}\text{C}$, and $\beta^{18}\text{O}$ calculated by different levels of theory for $\text{CO}_2(\text{g})$, $\text{CO}_3^{2-}(\text{g})$, $\text{H}_2\text{CO}_3(\text{g})$, $\text{HCO}_3^- * 3(\text{H}_2\text{O})$, and $\text{H}_2\text{CO}_3 * 3(\text{H}_2\text{O})$ (Table A2, Fig. A1A–E and Section 2.5.2). Each ab initio/hybrid method was paired with 3 to 5 basis sets of different complexities. Overall, we found similar chemical trends and convergence behavior for all species investigated.

Models constructed using the 2 largest basis sets 6-311++G(2d,2p) and aug-cc-pVTZ were similar, with Δ_{63} values deviating from each other by less than 0.001‰ on average (range 0.000 to 0.006‰), most likely indicating approach to the complete basis set limit for hybrid density functionals (e.g., Molnar et al., 2009; Bryantsev et al., 2009; Suárez et al., 2011). The 6-311++G(2d,2p) basis set has fewer basis functions and allows faster computations than aug-cc-pVTZ.

Rustad et al. (2008) tested a range of basis sets and model chemistries for estimating $^{13}\text{C}/^{12}\text{C}$ fractionation, and concluded that the hybrid B3LYP method combined with the double-zeta aug-cc-pVDZ basis set gave the best match to experiment for $\beta^{13}\text{C}$. We find that trends in Δ_{63} in our convergence study are similar to those of $\beta^{13}\text{C}$, and the B3LYP method produces results that are close to those of higher levels of theory (viz., CCSD and QCISD). The B3LYP models in the convergence study also do well matching experimental vibrational frequencies and bond lengths from higher-order methods. We found no statistically significant differences between results from clusters with 21 waters or 32 waters (see Appendix A.2 for detailed results of the convergence studies, comparison of theoretical predictions of vibrational frequencies and bond lengths with measured values, and effect of scaling factors.)

Therefore, we conclude that the B3LYP/6-311++G(2d,2p) model is a reasonable compromise between accuracy and computer efficiency for the calculation of Δ_{63} , $\beta^{13}\text{C}$, and $\beta^{18}\text{O}$. The B3LYP/6-311++G(2d,2p) cluster models of the calcite and aragonite lattices, built following Rustad et al. (2008, 2010a), also perform very well when compared to both the experimental calibration curve of Dennis and Schrag (2010) and the theoretical curve of Guo et al. (2009) and Schauble et al. (2006) (Section 3.4.4).

3.1.2. Comparison of solvation techniques

We compared values of Δ_{63} , $\beta^{13}\text{C}$, and $\beta^{18}\text{O}$ at 25°C for each DIC species calculated with each of the four sol-

vation techniques: (1) gas phase, (2) implicit solvation, (3) explicit solvation (with 3 waters), and (4) supermolecular clusters (see Section 2.5.3) using the B3LYP method paired with the 3 Pople basis sets for each DIC species (Fig. A2A–C and the first 5 columns of Table A3). Within a given method, basis set, and solvation method, $\Delta_{63}(\text{H}_2\text{CO}_3) > \Delta_{63}(\text{HCO}_3^-) > \Delta_{63}(\text{CO}_3^{2-})$. However, the relative size of Δ_{63} does not vary consistently with changing basis set, solvation technique, or species. Based on the superior performance of large molecular clusters in prior evaluations of the accuracy of solvation techniques (Liu and Tossell, 2005; Rudolph et al., 2006; Rustad et al., 2008, 2010a,b; Zeebe, 2009), we have concentrated our efforts on supermolecular clusters using the B3LYP method with the 6-311++G(2d,2p) basis set. The supermolecular clusters are also better predictors of oxygen and carbon isotope fractionation than the other solvation techniques (Section 3.4.1).

The B3LYP models in the convergence studies also do well matching experimental vibrational frequencies and bond lengths from higher-order methods (see Appendix A.2). Predictions of $^{13}\text{C}/^{12}\text{C}$ and $^{18}\text{O}/^{16}\text{O}$ fractionation match well with experimental values. Effects of scaling the vibrational frequencies are discussed in A2.4.

3.2. Δ_{63} , $\beta^{13}\text{C}$, and composite $\beta^{18}\text{O}$ for DIC species (B3LYP/6-311++G(2d,2p) supermolecular cluster models)

The models predict distinct values of Δ_{63} for each of the 3 DIC species, such that $\Delta_{63}(\text{H}_2\text{CO}_3) > \Delta_{63}(\text{HCO}_3^-) > \Delta_{63}(\text{CO}_3^{2-})$. This is also true of $\beta^{13}\text{C}$, and composite $\beta^{18}\text{O}$ (Table A1 and Fig. 3). As detailed in Section 2.5, for each supermolecular cluster we sampled up to 10 different conformers, in order to approximate a distribution of dynamic solvation structures. The geometry of each individual conformer was generated from the quenching of different time steps from a molecular dynamics simulation. This is very similar to the approach taken successfully by Rustad et al. (2008), in which they used ab initio molecular dynamics. Values of Δ_{63} , $\beta^{13}\text{C}$, and composite $\beta^{18}\text{O}$ of individual conformers for each

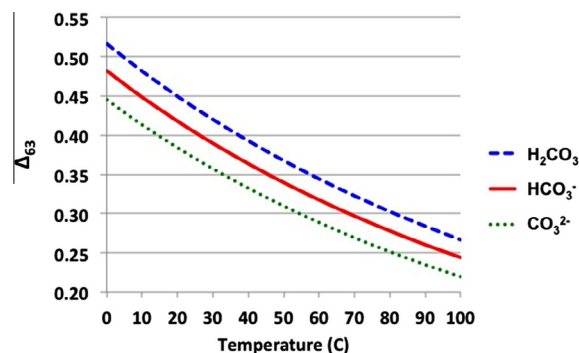


Fig. 3. Δ_{63} of DIC species calculated the B3LYP/6-311++G(2d,2p) models averaged over ten individual conformers (see Fig. 4) for temperatures from 0 to 100 °C (Table A1).

Table 1

Δ_{63} , $\beta^{13}\text{C}$, composite $\beta^{18}\text{O}$, and composite $\beta^{17}\text{O}$ of the individual conformers for each set of supermolecular clusters for the 3 DIC species at 25 °C as calculated by the B3LYP/6-311++G(2d,2p) models. Averages and standard errors are included for each set (Fig. 4). Values are unscaled. Also included are the O isotope fractionation factor between the DIC species and liquid water $\alpha^{18\text{O}}(\text{CO}_3^{2-} - \text{H}_2\text{O}(\text{l}))$ and C isotope fractionation factor between the DIC species and carbon dioxide $\alpha^{13\text{C}}(\text{CO}_3^{2-} - \text{CO}_2(\text{g}))$. RT diff is the numerical difference between the two sides of the Redlich Teller product equation (Eq. (15)).

Conformer	# Waters	$\beta^{13}\text{C}$	Comp $\beta^{18}\text{O}$	Comp $\beta^{17}\text{O}$	Δ_{63}	RT diff	$\alpha^{18\text{O}}(\text{CO}_3^{2-} - \text{H}_2\text{O}(\text{l}))$	$\alpha^{13\text{C}}(\text{CO}_3^{2-} - \text{CO}_2(\text{g}))$
<i>CO₃²⁻</i>								
1a	21	1.1993	1.0986	1.0510	0.3696	6.4E–06	1.0207	1.0030
2a	21	1.1992	1.0990	1.0512	0.3707	–2.8E–04	1.0211	1.0029
3a	21	1.1987	1.0980	1.0507	0.3678	–2.2E–04	1.0201	1.0025
4a	21	1.1995	1.0996	1.0515	0.3698	–2.3E–04	1.0216	1.0032
5a	21	1.1987	1.0978	1.0505	0.3728	–9.7E–05	1.0199	1.0025
7a	21	1.1977	1.0969	1.0501	0.3644	–3.6E–05	1.0191	1.0016
9a	21	1.2002	1.0995	1.0514	0.3719	–3.0E–04	1.0215	1.0037
11a	32	1.2015	1.1009	1.0521	0.3747	–3.1E–05	1.0228	1.0048
Average		1.1993	1.0988	1.0511	0.3702	–1.5E–04	1.0209	1.0030
Standard error		±0.0004	±0.0004	±0.0002	±0.0011	±4.3E–05	±0.0004	±0.0003
Conformer	# Waters	$\beta^{13}\text{C}$	Comp $\beta^{18}\text{O}$	Comp $\beta^{17}\text{O}$	Δ_{63}	RT diff	$\alpha(\text{HCO}_3^- - \text{H}_2\text{O}(\text{l}))$	$\alpha(\text{HCO}_3^- - \text{CO}_2(\text{g}))$
<i>HCO₃⁻</i>								
1b	21	1.2027	1.1079	1.0557	0.3986	–4.7E–04	1.0293	1.0058
2b	21	1.2058	1.1100	1.0567	0.4065	–8.3E–06	1.0313	1.0085
3b	21	1.2019	1.1080	1.0557	0.4060	–2.6E–04	1.0295	1.0052
4b	21	1.2031	1.1084	1.0559	0.4038	–1.9E–04	1.0298	1.0062
5b	21	1.2005	1.1065	1.0550	0.4028	–8.3E–04	1.0280	1.0039
6b	21	1.2006	1.1059	1.0547	0.4097	–1.6E–03	1.0275	1.0041
7b	21	1.2012	1.1080	1.0557	0.4031	–1.9E–03	1.0294	1.0046
8b	21	1.2042	1.1089	1.0562	0.4066	–9.4E–05	1.0299	1.0060
9b	21	1.2030	1.1085	1.0560	0.3982	–3.6E–04	1.0292	1.0052
10b	21	1.2019	1.1078	1.0556	0.3980	–8.8E–05	1.0292	1.0052
Average		1.2025	1.1080	1.0557	0.4033	–5.8E–04	1.0293	1.0057
Standard error		±0.0005	±0.0004	±0.0002	±0.0013	±2.1E–04	±0.0003	±0.0004
Conformer	# Waters	$\beta^{13}\text{C}$	Comp $\beta^{18}\text{O}$	Comp $\beta^{17}\text{O}$	Δ_{63}	RT diff		
<i>H₂CO₃</i>								
1c	21	1.2077	1.1175	1.0605	0.4352	–9.1E–04		
2c	21	1.2118	1.1205	1.0620	0.4291	–8.0E–05		
3c	21	1.2130	1.1214	1.0624	0.4512	–1.3E–04		
4c	21	1.2086	1.1180	1.0607	0.4312	–4.8E–04		
6c	21	1.2106	1.1188	1.0611	0.4401	–5.7E–04		
7c	21	1.2137	1.1214	1.0624	0.4393	–1.3E–05		
8c	32	1.2113	1.1195	1.0615	0.4275	–5.8E–05		
9c	32	1.2100	1.1186	1.0611	0.4313	–2.8E–04		
10c	32	1.2104	1.1189	1.0612	0.4372	–1.3E–04		
Average		1.2105	1.1191	1.0613	0.4344	–3.3E–04		
Standard error		±0.0006	±0.0004	±0.0002	±0.0016	±9.9E–05		

DIC species are shown in Table 1 and Fig. 4; average values of DIC species, calcite, and aragonite from 0° to 1000 °C are shown in Table A1.

At 25 °C the average values for supermolecular cluster B3LYP/6-311++G(2d,2p) models give $\Delta_{63}(\text{CO}_3^{2-}) = 0.3702 \pm 0.0011\text{‰}$, $\Delta_{63}(\text{HCO}_3^-) = 0.4033 \pm 0.0013\text{‰}$, and $\Delta_{63}(\text{H}_2\text{CO}_3) = 0.4344 \pm 0.0016\text{‰}$. (Errors are given as standard error of the mean). As expected, Δ_{63} decreases with increasing temperature. The differences between Δ_{63} of the DIC species also decrease with temperature; for example, the difference between $\Delta_{63}(\text{CO}_3^{2-})$ and $\Delta_{63}(\text{HCO}_3^-)$ is 0.0368 at 0 °C, 0.0331‰ at 25 °C,

0.0300‰ at 50 °C, and 0.0255‰ at 90 °C (see Table A1 and Fig. 3).

We performed the Student *t* test comparing the groups of conformers of $\Delta_{63}(\text{CO}_3^{2-})$ vs. $\Delta_{63}(\text{HCO}_3^-)$ and then $\Delta_{63}(\text{HCO}_3^-)$ vs. $\Delta_{63}(\text{H}_2\text{CO}_3)$ for the B3LYP/6-311++G(2d,2p) models at 25 °C. Both tests were highly significant with $p < 0.001$ ($t = -6.04$, $df = 18$ and $t = -7.44$, $df = 18$ respectively), implying that Δ_{63} of the set of conformers for HCO_3^- is statistically different from the two other DIC species.

Our calculations using different isotopic compositions of the carbonate species confirmed that Δ_{63} is dependent upon only temperature.

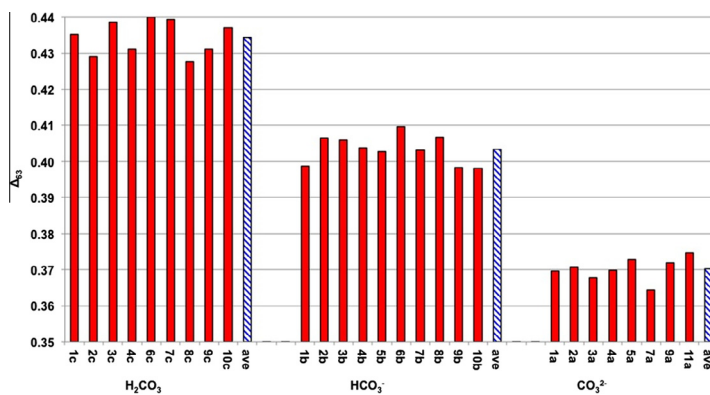


Fig. 4. Comparison of Δ_{63} of individual supermolecular cluster conformers of each DIC species from B3LYP/6-311++G(2d,2p) models at 25 °C. Each blue striped bar is the average of the set of ten red conformers to its left (Table 1). (For interpretation of the references to color in this figure legend, the reader is referred to the web version of this article.)

3.3. Δ_{63} , $\beta^{13}\text{C}$, and composite $\beta^{18}\text{O}$ for the carbonate mineral clusters

As expected, Δ_{63} , composite $\beta^{18}\text{O}$, composite $\beta^{17}\text{O}$, and $\beta^{13}\text{C}$ of the calcite and aragonite cluster models all decrease with increasing temperature. Table A1 shows these values for the B3LYP/6-311++G(2d,2p) model from 0 °C to 1000 °C. At 25 °C values for calcite (and aragonite) B3LYP/6-311++G(2d,2p) cluster model Δ_{63} are 0.394‰ (and 0.4060‰), $\beta^{13}\text{C}$ are 1.2077 (and 1.2110), and composite $\beta^{18}\text{O}$ are 1.1060 (and 1.1075).

Table A3 (final rows) shows a comparison of $\beta^{13}\text{C}$, composite $\beta^{18}\text{O}$, and Δ_{63} at 25 °C for the B3LYP/6-311++G(2d,2p), B3LYP/6-311G*, and B3LYP/6-31G* calcite and aragonite cluster models. Ranges in model differences for calcite (aragonite) $\beta^{13}\text{C}$, $\beta^{18}\text{O}$, and Δ_{63} are 10‰ (8.4‰), 7‰ (4.5‰), and 0.041‰ (0.033‰), respectively. These are similar to the average differences in the B3LYP aqueous models, indicating that choice of basis set when calculating Δ_{63} can be significant for both aqueous and mineral species.

Δ_{63} of the witherite cluster model could not be compared directly with the B3LYP/6-311++G(2d,2p) calcite or aragonite models because the 6-311++G(2d,2p) basis set does not handle the barium atom (see Section 2.5.4). We used B3LYP/SDD model to compare all 3 mineral clusters. At 25 °C, the B3LYP/SDD models for Δ_{63} are 0.3556‰ for witherite and 0.3671‰ for calcite. Based on these results, we project that in general, Δ_{63} for witherite will be about 0.01‰ smaller than Δ_{63} for calcite and about 0.015 to 0.02‰ smaller than Δ_{63} for aragonite for most models.

3.4. Comparison with previous experiments and theory

3.4.1. Oxygen and carbon isotope fractionation

To estimate oxygen isotope fractionations we compared B3LYP models constructed with three basis sets (6-31G*, 6-311G*, and 6-311++G(2d,2p)) to measured oxygen isotope fractionations between DIC species and liquid water (Beck et al., 2005) (Table 3). Following a procedure similar to that in Zeebe (2009) we define (from Eq. (8))

$$\alpha^{180}(\text{H}_2\text{O}(l) - \text{H}_2\text{O}(g)) = (\beta^{180}(\text{H}_2\text{O}(l)) / \beta^{180}(\text{H}_2\text{O}(g))) \quad (16)$$

Since the oxygen fractionation between liquid water and water vapor is 1.0094 at 25 °C (Majoube, 1971; Horita and Wesolowski, 1994), it follows that

$$\begin{aligned} \alpha^{180}(\text{CO}_3^{2-} - \text{H}_2\text{O}(l)) &= (\beta^{180}(\text{CO}_3^{2-}) / \beta^{180}(\text{H}_2\text{O}(g))) \\ &\quad * (1 / \alpha^{180}(\text{H}_2\text{O}(l) - \text{H}_2\text{O}(g))) \\ &= \beta^{180}(\text{CO}_3^{2-}) / (1.0094 * \beta^{180}(\text{H}_2\text{O}(g))) \end{aligned} \quad (17)$$

In the above equations, for each $\beta^{180}(\text{CO}_3^{2-})$, we calculated the corresponding $\beta^{180}(\text{H}_2\text{O}(g))$ using the same method/basis set combination (Table 2). Similar equations hold for $\alpha^{180}(\text{HCO}_3^- - \text{H}_2\text{O}(l))$.

We tested model predictions of carbon isotope fractionation between DIC species and $\text{CO}_2(g)$ using experimental results from (Zhang et al., 1995) (Table 4).

$$\alpha^{13\text{C}}(\text{CO}_3^{2-} - \text{CO}_2(g)) = (\beta^{13\text{C}}(\text{CO}_3^{2-}) / \beta^{13\text{C}}(\text{CO}_2(g))) \quad (18)$$

We used the corresponding model of $\beta^{13\text{C}}(\text{CO}_2(g))$ for each $\beta^{13\text{C}}(\text{CO}_3^{2-})$ (Table A2). Similar equations hold for $\alpha^{13\text{C}}(\text{HCO}_3^- - \text{CO}_2(g))$.

The supermolecular clusters are better predictors of oxygen isotope fractionation $\alpha^{180}(\text{DIC} - \text{H}_2\text{O}(l))$ than the non-cluster models (Table A3, column 7, and Fig. A3). For both CO_3^{2-} and HCO_3^- , $\alpha^{180}(\text{gas model}) < \alpha^{180}(\text{implicit solvation}) < \alpha^{180}(\text{explicit solvation}) < \alpha^{180}(\text{supermolecular clusters})$. Within each solvation technique, α^{180} decreases as the size of the basis set increases. The average supermolecular cluster $\alpha^{180}(\text{CO}_3^{2-} - \text{H}_2\text{O}(l)) [\alpha^{180}(\text{HCO}_3^- - \text{H}_2\text{O}(l))]$ for B3LYP/6-31G*, B3LYP/6-311G*, and B3LYP/6-311++G(2d,2p) models are $1.0256 \pm 0.0003\%$ [1.0334 ± 0.0013], $1.0237 \pm 0.0003\%$ [1.0321 ± 0.0013], and $1.0209 \pm 0.0004\%$ [1.0293 ± 0.0010] respectively compared to the measured α^{180} $1.0245 \pm 0.0003\%$ [1.0315 ± 0.0002] from Beck et al. (2005) (Table 3). Error intervals in this section are given in terms of standard deviation instead of standard

Table 2

$\beta^{17}\text{O}$ and $\beta^{18}\text{O}$ for H_2O as calculated with different combinations of ab initio/hybrid methods and basis sets at temperatures 20, 22, and 25 °C. Values are unscaled.

Method	Basis set	T (°C)	$\beta^{17}\text{O}(\text{H}_2\text{O})$	$\beta^{18}\text{O}(\text{H}_2\text{O})$
B3LYP	6-31G*	20	1.0348	1.0667
		22	1.0346	1.0662
		25	1.0342	1.0654
B3LYP	6-311G*	20	1.0352	1.0674
		22	1.0349	1.0668
		25	1.0345	1.066
B3LYP	6-311++G(2d,2p)	20	1.0353	1.0677
		22	1.035	1.0671
		25	1.0346	1.0663
B3LYP	cc-pVTZ	20	1.035	1.0671
		22	1.0348	1.0666
		25	1.0343	1.0658
M06	6-31G*	20	1.0358	1.0686
		22	1.0355	1.068
		25	1.0351	1.0672
M06	6-311G*	20	1.0359	1.0688
		22	1.0356	1.0682
		25	1.0352	1.0674
M06	cc-pVTZ	20	1.0358	1.0686
		22	1.0355	1.068
		25	1.0351	1.0672
HF	6-31G*	20	1.0388	1.0745
		22	1.0385	1.0739
		25	1.0381	1.073
HF	6-311G*	20	1.0395	1.0758
		22	1.0392	1.0752
		25	1.0387	1.0743

error to compare with Beck et al.'s and Zhang et al.'s measurements.

Overall, the supermolecular clusters yield the best match to observed carbon isotope fractionation (Table A3, column 8, and Fig. A4). Within each solvation technique, $\alpha^{13\text{C}}$ decreases as the size of the basis set increases. The average supermolecular cluster $\alpha^{13\text{C}}(\text{CO}_3^{2-} - \text{CO}_2(\text{g}))$ [$\alpha^{13\text{C}}(\text{HCO}_3^- - \text{CO}_2(\text{g}))$] B3LYP/6-31G*, B3LYP/6-311G*, and B3LYP/6-311++G(2d,2p) values are $1.0109 \pm 0.0003\text{‰}$ [1.0132 ± 0.0016], $1.0049 \pm 0.0003\text{‰}$ [1.0075 ± 0.0018], $1.0030 \pm 0.0003\text{‰}$ [1.0057 ± 0.0013] respectively compared to the measured $\alpha^{13\text{C}}$ $1.0059 \pm 0.0007\text{‰}$ [1.0080 ± 0.0001] from Zhang et al. (1995) (Table 4).

Table 3

Experimental oxygen isotope fractionation between liquid water and DIC species (from Beck et al., 2005). The measured values are converted to O isotopic fractionation factors α such that $1000 \ln \alpha = d$ and then used for comparison with predicted oxygen isotope fractionation values ($\alpha^{18\text{O}}$) (Section 3.4.1). Error bars are standard deviation.

	$d = \text{measured value}$	$\alpha^{18\text{O}} = \exp(d/1000)$	Max	Min
Beck et al. (2005) at 25 °C				
$\alpha^{18\text{O}}(\text{CO}_2 - \text{H}_2\text{O}(\text{l}))$	40.49 ± 0.14	1.0413	1.0415	1.0412
$\alpha^{18\text{O}}(\text{CO}_3^{2-} - \text{H}_2\text{O}(\text{l}))$	24.19 ± 0.26	1.0245	1.0248	1.0242
$\alpha^{18\text{O}}(\text{HCO}_3^- - \text{H}_2\text{O}(\text{l}))$	31.00 ± 0.15	1.0315	1.0316	1.0313

3.4.2. $^{13}\text{C}/^{12}\text{C}$ reduced partition function ratios ($\beta^{13\text{C}}$)

Table 5 shows a comparison of reduced partition function ratios for $^{13}\text{C}/^{12}\text{C}$ ($\beta^{13\text{C}}$) for selected gas and supermolecular cluster models from Rustad et al. (2008) and this work. $\beta^{13\text{C}}$ from the same models are within 0.001 (1‰) of each other, except for B3LYP/6-31G*, which differs by 0.003 (3‰). $\beta^{13\text{C}}$ from aug-cc-pVDZ and aug-cc-pVTZ for the same species and solvation model are within 0.002 (2‰) of each other.

3.4.3. $\Delta_i(\text{CO}_2(\text{g}))$

We compared the predicted values of Δ_{47} , Δ_{48} , and Δ_{49} (CO_2) from our models with the predictions of Wang et al. (2004). They used two different sets of vibrational frequencies for their calculations for the clumped isotope signatures of CO_2 at 200 K, 300 K and 1000 K. We made the same calculations for several different method/basis sets combinations (Table A8, Fig. A5). The predicted values of Δ_{47} from the B3LYP, MP2, CCSD, and QCISD models are very close to the two predictions of Wang et al. (0.9138 and 0.9243 at 300 K). The M06 and M06-2X models yield slightly higher Δ_{47} than Wang et al. (2004) while the PBE models are lower. Δ_{47} from the B3LYP/6-311++G(2d,2p) model is 0.9019‰ at 300K.

3.4.4. Calcite and aragonite Δ_{47}

We compared our equilibrium cluster model of calcite to the experimental calibration of Ghosh et al. (2006) (1–50 °C), Dennis and Schrag (2010) (7.5–77 °C), and the theoretical curve from Guo et al. (2009), which combines a model acid digestion fractionation factor with predicted clumping equilibria from Schauble et al. (2006) (Table 6, Fig. 5). We first convert Δ_{63} from the B3LYP/6-311++G(2d,2p) model to Δ_{47} by adding Guo's experimental and theoretical acid digestion fractionation factors (Eqs. (3)–(5)). For all conversions of Δ_{63} to Δ_{47} we assume that the temperature of the phosphoric acid digestion processes on the calcite samples is 25 °C. The temperature at which the acid digestion takes place should not to be confused with the temperature of formation of the calcite crystal.

The slope of the B3LYP/6-311++G(2d,2p) calcite vs. temperature model is very similar to both the Dennis and Schrag (2010) curve and the Guo et al. (2009) curve below about 40 °C; above 40 °C our result is slightly less sensitive to temperature. All three are less sensitive to temperature than the Ghosh et al. (2006) calibration. The vertical position of the B3LYP/6-311++G(2d,2p) depends upon the acid digestion fractionation factor (Eqs. (3)–(5)). To illustrate this, the B3LYP/6-311++G(2d,2p) model result is shown both (1) as corrected with Guo et al.'s (2009)

Table 4

Experimental carbon isotope fractionation between CO₂(g) and DIC species (from Zhang et al., 1995). The measured values are converted to fractionation factors ($\alpha^{13\text{C}}$) such that $1000 \ln \alpha = d$ and then used for comparison with predicted carbon isotope fractionation values ($\alpha^{13\text{C}}$) (Section 3.4.1). Error bars are standard deviation.

	d = measured value	$\alpha^{13\text{C}} = \exp(d/1000)$	Max	Min
Zhang et al. (1995), at 25 °C				
$\alpha^{13\text{C}}(\text{CO}_3^{2-} - \text{CO}_2(\text{g}))$	5.92 ± 0.65	1.0059	1.0066	1.0053
$\alpha^{13\text{C}}(\text{HCO}_3^- - \text{CO}_2(\text{g}))$	7.93 ± 0.08	1.0080	1.0080	1.0079

Table 5

Comparison of reduced partition function ratios for ¹³C/¹²C ($\beta^{13\text{C}}$) for gas phase and supermolecular cluster models with other works. Values from this work and from Rustad et al. (2008) are unscaled.

	Method/basis set	$\beta^{13\text{C}}$ (Rustad et al., 2008)	$\beta^{13\text{C}}$ (This work)
Gas Phase Models			
CO ₂ (g)	B3LYP/6-31G*	1.1909	1.1941
	B3LYP/aug-cc-pVDZ	1.1935	
	B3LYP/aug-cc-pVTZ	1.1948	1.1956
	MP2/aug-cc-pVDZ	1.1914	
	MP2/aug-cc-pVTZ	1.1930	1.1937
	PBE/aug-cc-pVDZ	1.1864	1.1873
	Experiment ^{a,b}	1.1943 (1.1910 ^c)	
H ₂ CO ₃ (g)	B3LYP/aug-cc-pVDZ	1.2099	
	B3LYP/aug-cc-pVTZ		1.2075
	MP2/aug-cc-pVDZ	1.2098	
	MP2/aug-cc-pVTZ		1.2108
HCO ₃ ⁻ (g)	–		
	B3LYP/aug-cc-pVDZ	1.1874	
	B3LYP/aug-cc-pVTZ		1.1989
	MP2/aug-cc-pVDZ	1.1855	
	MP2/6-311++G(2d,2p)		1.1985
CO ₃ ²⁻ (g)	B3LYP/aug-cc-pVDZ	1.1756	
	B3LYP/aug-cc-pVTZ		1.1742
	MP2/aug-cc-pVDZ	1.1721	
	MP2/aug-cc-pVTZ		1.1749
	PBE/ aug-cc-pVDZ	1.1613	
	PBE/ aug-cc-pVTZ		1.1576
Supermolecular clusters – averages			
CO ₃ ²⁻ (aq)	B3LYP/6-31G*	1.2064	1.2072 ± 0.0004
	B3LYP/aug-cc-pVDZ	1.1991	
	B3LYP/6-311++G(2d,2p)		1.1993 ± 0.0004
	Empirical estimate for CO ₃ ²⁻ (aq)	1.1967	
HCO ₃ ⁻ (aq)	B3LYP/6-31G*	1.2103	1.2098 ± 0.00056
	B3LYP/aug-cc-pVDZ	1.2036	
	B3LYP/6-311++G(2d,2p)		1.2025 ± 0.0005

^a Zeebe and Wolf-Gladrow (2001).

^b Richet et al. (1977).

^c Includes anharmonicity constants for the potential energy.

experimentally determined acid fractionation factor of $0.232 \pm .015$; and (2) as corrected with their theoretical factor of 0.220‰. The B3LYP/6-311++G(2d,2p) result corrected with either acid fractionation factor falls well within one standard deviation of the Dennis & Schrag calibration.¹⁰

¹⁰ $\Delta_{47} = \left(\frac{(0.0337 \pm 0.0018) \times 10^6}{T^2} \right) + (0.2470 \pm 0.0194)$ (Dennis and Schrag, 2010, Eq. (4)).

We also compared the theoretical predictions from our calcite and aragonite cluster models of oxygen and carbon isotope fractionation ($\beta^{18\text{O}}$ and $\beta^{13\text{C}}$ respectively) with previous theoretical and experimental results (Table 7). The calcite crystal lattice model of Schauble et al. (2006) uses first-principles lattice dynamics (i.e., density functional perturbation theory with norm-conserving pseudopotentials) to predict $\beta^{18\text{O}}$, $\beta^{13\text{C}}$, K3866, and K2876. Chacko et al. (1991) computed reduced partition function ratios (β factors) using statistical mechanics and the measured vibrational mode frequencies of the

Table 6

Comparison of Δ_{63} and Δ_{47} of calcite mineral at equilibrium for several experimental and theoretical models. The comparison plots from Ghosh et al. (2006), Dennis and Schrag (2010), and Guo et al. (2009) (using K values from Schauble et al. (2006)) are calculated from their polynomial fit equations. Our B3LYP/6-311++G(2d,2p) model is shown with both the experimental acid digestion fractionation factor ($0.232 \pm 0.015\text{‰}$) and the theoretical factor (0.220‰) (fractionation factors from Guo et al., 2009). $\Delta_{47} = \Delta_{63} + \text{factor}$ (Eqs. (3)–(5)). The B3LYP/6-311++G(2d,2p) plot with either fractionation factor falls within 1σ of the Dennis & Schrag curve (Section 3.4.4, Fig. 5). Values from this work are unscaled.

T (°C)	Ghosh et al. (2006)	Combined Guo et al. (2009), with Schauble et al. (2006)	Dennis and Schrag (2010)	B3LYP/6-311++G(2d,2p) Δ_{63} ($\Delta_{47} = \Delta_{63} + 0.232$)	B3LYP/6-311++G(2d,2p) Δ_{63} ($\Delta_{47} = \Delta_{63} + 0.220$)
0	0.773	0.724	–	0.470 (0.702)	0.470 (0.690)
10	0.718	0.690	0.667	0.438 (0.670)	0.438 (0.658)
20	0.669	0.658	0.639	0.408 (0.640)	0.408 (0.628)
22	0.660	0.652	0.634	0.402 (0.634)	0.402 (0.622)
25	0.646	0.643	0.626	0.394 (0.626)	0.394 (0.614)
30	0.624	0.629	0.614	0.381 (0.613)	0.381 (0.601)
40	0.584	0.601	0.591	0.355 (0.587)	0.355 (0.575)
50	0.547	0.576	0.570	0.332 (0.564)	0.332 (0.552)
60	–	0.553	0.551	0.310 (0.542)	0.310 (0.530)
70	–	0.531	0.533	0.290 (0.522)	0.290 (0.510)
80	–	0.511	0.517	0.271 (0.503)	0.271 (0.491)
90	–	0.493	–	0.254 (0.486)	0.254 (0.474)
100	–	0.476	–	0.238 (0.470)	0.238 (0.458)

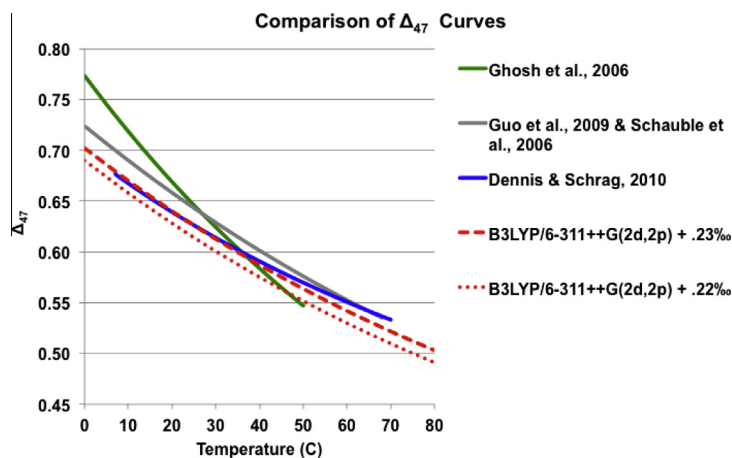


Fig. 5. Comparison of the calcite model from this work with other theoretical and experimental models of calcite Δ_{47} at equilibrium. Order of entries in the legend is the order of the plots at 22°C. The plots for the Ghosh et al. (2006), Dennis and Schrag (2010), and combined Guo et al. and Schauble et al. (from Guo et al., 2009) are calculated from their polynomial fit equations. The B3LYP/6-311++G(2d,dp) calcite model (this study) is shown with both the experimental acid digestion fractionation factor ($0.232 \pm 0.015\text{‰}$) and the theoretical factor (0.220‰) for acid digestion at 25 °C (Eqs. (3)–(5)) (Guo et al., 2009). (See Table 6.) These graphs are drawn in the original reference frame (i.e., relative to a stochastic distribution) and not in the “absolute reference frame” of Dennis et al. (2011).

calcite lattice. Rustad et al.’s (2008, 2010a,b) supermolecular calcite clusters are the basis for our calcite and aragonite models. The present isotope fractionation factors are very close to these. Our equilibrium constants K3866 and K2876 for both calcite and aragonite are slightly higher than those of Schauble et al. (2006). O and C isotopic fractionation between aragonite and calcite are also slightly larger.

3.5. Relation between Δ_{63} and other Δ_i

Fig. A6 shows the average values of each Δ_i plotted against Δ_{63} for the supermolecular cluster models of the 3

DIC species for all temperatures calculated (Table B.3 in Appendix B, the Electronic supplement). As expected all Δ_i are roughly proportional to temperature squared at Earth surface temperatures.

4. DISCUSSION

In this section we discuss theoretical predictions for attributes of the composite DIC pool, and their possible effect on the clumped isotope signature of carbonate minerals precipitating from that pool without reaching full internal equilibrium.

Table 7

Comparison of theoretical carbon ($\beta^{13}\text{C}$) and oxygen ($\beta^{18}\text{O}$) fractionation factors and equilibrium constants K_{3866} and K_{2876} for calcite and aragonite from other studies to this work. Also included are C and O fractionation factors between calcite and aragonite. Three different models from this work are presented for calcite. Values from this study are unscaled.

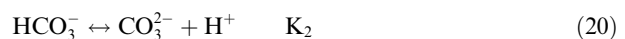
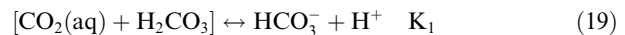
Calcite								
T (°C)	$\beta^{18}\text{O}$ 0	$\beta^{18}\text{O}$ 25	$\beta^{13}\text{C}$ 0	$\beta^{13}\text{C}$ 25	K_{3866} 0	K_{3866} 25	K_{2876} 0	K_{2876} 25
Schauble et al. (2006)	1.11942	1.10328	1.23450	1.20430	1.000490	1.000410	0.666729	0.666715
Chacko and Deines (2008)	1.1192	1.1031						
Chacko et al. (1991)			1.2339	1.2037				
Deines (2004)				1.1973				
Rustad et al. (2008) (B3LYP/6-31G*/3-21G)			1.2107					
Rustad et al. (2008) (PBE//6-31G*/3-21G)			1.1994					
This work:								
B3LYP/6-31G*	1.130	1.113	1.249	1.217	1.00055468	1.00046896	0.66672364	0.66671073
B3LYP/6-311G*	1.125	1.109	1.241	1.211	1.00052046	1.00043778	0.66672484	0.66671167
B3LYP/6-311++G(2d,2p)	1.1226	1.1060	1.2384	1.2078	1.00050642	1.00042475	0.66672448	0.66671132
Aragonite								
T (°C)	$\beta^{18}\text{O}$ 0	$\beta^{18}\text{O}$ 25	$\beta^{13}\text{C}$ 0	$\beta^{13}\text{C}$ 25	K_{3866} 0	K_{3866} 25	K_{2876} 0	K_{2876} 25
Schauble et al. (2006)	1.11923	1.10319	1.23718	1.20669	1.000513	1.000430		
Rustad et al. (2008) (PBE/6-31G*/3-21G)				1.2014				
This work:								
B3LYP/6-311++G(2d,2p)	1.1242	1.1075	1.2420	1.2110	1.00052059	1.00043780	0.66672414	0.66671092
Calcite–Aragonite								
T (°C)	$\alpha^{18}\text{O}(\text{arag-cal})$ 25	$\alpha^{13}\text{C}(\text{arag-cal})$ 25	$\Delta_{63}(\text{arag})-\Delta_{63}(\text{cal})$ 0 25					
Schauble et al. (2006)	0.99992	1.00198						
Rustad et al. (2008) (PBE/6-31G*/3-21G)		1.0017						
This work: B3LYP/6-311++G(2d,2p)	1.0013	1.0026	.0130	.0120				
Romanek et al. (1992) (inorganic carbonates)	$\epsilon^{18}\text{O}(\text{arag-cal})^a$	$\epsilon^{13}\text{C}(\text{arag-cal})$						
		$1.7 \pm 0.4\text{‰}$						
Lécuyer et al. (2012) (mollusk shells-temperature to tropical)	$\sim 0.4\text{‰}$, probably due to bias from acid digestion	$0.95 \pm 0.81\text{‰}$						

^a Aragonite–calcite fractionation in permil.

4.1. Composite Δ_{63} of DIC pool

4.1.1. Dependence of relative abundances of DIC species on pH, temperature, and salinity

A solution of dissolved inorganic carbon (DIC) contains carbonic acid and dissolved carbon dioxide [$\text{H}_2\text{CO}_3 + \text{CO}_2(\text{aq})$], bicarbonate (HCO_3^-), and carbonate (CO_3^{2-}). The relative abundances of the DIC species are determined by the pH of the solution, based on the following equations and the associated equilibrium constants K_1 and K_2 .



The pH at which crossover points occur (i.e., when the concentrations of two of the species are equal) is dependent upon the equilibrium constants of the dissociation reactions. K_1 and K_2 are usually presented as $\text{p}K_1$ and $\text{p}K_2$ where $\text{p}K_1 = -\log(K_1)$ and $\text{p}K_2 = -\log(K_2)$. We calculated the speciation of DIC at different temperatures and salinities using the experimental curves for K_1 and K_2 from Millero et al. (2006) in conjunction with Eqs. (19) and (20)

Table 8

Equilibrium dissociation constants (pK_1 and pK_2) for carbonic acid (Eqs. (19) and (20), respectively) for varying temperature and salinity, calculated from the Millero et al. (2006) empirical formulas (valid for temperatures 0 to 50 °C and salinities from 0 to 50). Values below were calculated from their polynomial equations as fitted to experimental values.

Temperature (°C)	Salinity					
	0 pK_1	0 pK_2	35 pK_1	35 pK_2	50 pK_1	50 pK_2
0	6.578	10.629	6.111	9.372	6.052	9.164
22	6.369	10.357	5.867	9.011	5.816	8.831
25	6.351	10.330	5.840	8.964	5.788	8.785
50	6.287	10.172	5.659	8.586	5.597	8.406

Table 9

Fractional abundances (f) of the DIC species vs. pH for different temperatures (T) and salinities (S). The equilibrium constants pK_1 and pK_2 change with T and S (Table 8, Fig. 6) (Millero et al., 2006). Note that the sum of the fractional abundances of the 3 species is unity, i.e., $f([\text{H}_2\text{CO}_3 + \text{CO}_2(\text{aq})]) + f(\text{HCO}_3^-) + f(\text{CO}_3^{2-}) = 1$.

pH	T = 0 °C, S = 0			T = 25 °C, S = 0			T = 50 °C, S = 0		
	$f([\text{CO}_2(\text{aq}) + \text{H}_2\text{CO}_3])$	$f(\text{HCO}_3^-)$	$f(\text{CO}_3^{2-})$	$f([\text{CO}_2(\text{aq}) + \text{H}_2\text{CO}_3])$	$f(\text{HCO}_3^-)$	$f(\text{CO}_3^{2-})$	$f([\text{CO}_2(\text{aq}) + \text{H}_2\text{CO}_3])$	$f(\text{HCO}_3^-)$	$f(\text{CO}_3^{2-})$
0	1.000	0.000	0.000	1.000	0.000	0.000	1.000	0.000	0.000
1	1.000	0.000	0.000	1.000	0.000	0.000	1.000	0.000	0.000
2	1.000	0.000	0.000	1.000	0.000	0.000	1.000	0.000	0.000
3	1.000	0.000	0.000	1.000	0.000	0.000	0.999	0.001	0.000
4	0.997	0.003	0.000	0.996	0.004	0.000	0.995	0.005	0.000
5	0.974	0.026	0.000	0.957	0.043	0.000	0.951	0.049	0.000
6	0.791	0.209	0.000	0.692	0.308	0.000	0.659	0.341	0.000
7	0.275	0.725	0.000	0.183	0.816	0.000	0.162	0.837	0.001
8	0.036	0.961	0.002	0.022	0.974	0.005	0.019	0.975	0.007
9	0.004	0.973	0.023	0.002	0.953	0.045	0.002	0.935	0.063
10	0.000	0.809	0.190	0.000	0.681	0.319	0.000	0.598	0.402
11	0.000	0.299	0.701	0.000	0.176	0.824	0.000	0.129	0.871
12	0.000	0.041	0.959	0.000	0.021	0.979	0.000	0.015	0.985
13	0.000	0.004	0.996	0.000	0.002	0.998	0.000	0.001	0.999
14	0.000	0.000	1.000	0.000	0.000	1.000	0.000	0.0001	0.9999
pH	T = 0 °C, S = 35			T = 25 °C, S = 35			T = 25 °C, S = 50		
	$f([\text{CO}_2(\text{aq}) + \text{H}_2\text{CO}_3])$	$f(\text{HCO}_3^-)$	$f(\text{CO}_3^{2-})$	$f([\text{CO}_2(\text{aq}) + \text{H}_2\text{CO}_3])$	$f(\text{HCO}_3^-)$	$f(\text{CO}_3^{2-})$	$f([\text{CO}_2(\text{aq}) + \text{H}_2\text{CO}_3])$	$f(\text{HCO}_3^-)$	$f(\text{CO}_3^{2-})$
0	1.000	0.000	0.000	1.000	0.000	0.000	1.000	0.000	0.000
1	1.000	0.000	0.000	1.000	0.000	0.000	1.000	0.000	0.000
2	1.000	0.000	0.000	1.000	0.000	0.000	1.000	0.000	0.000
3	0.999	0.001	0.000	0.999	0.001	0.000	0.997	0.003	0.000
4	0.992	0.008	0.000	0.986	0.014	0.000	0.975	0.025	0.000
5	0.928	0.072	0.000	0.874	0.126	0.000	0.798	0.202	0.000
6	0.563	0.437	0.000	0.409	0.591	0.001	0.283	0.714	0.003
7	0.114	0.882	0.004	0.064	0.926	0.010	0.037	0.927	0.036
8	0.012	0.948	0.040	0.006	0.896	0.097	0.003	0.716	0.281
9	0.001	0.701	0.298	0.000	0.479	0.521	0.000	0.203	0.797
10	0.000	0.190	0.809	0.000	0.084	0.916	0.000	0.025	0.975
11	0.000	0.023	0.977	0.000	0.009	0.991	0.000	0.003	0.997
12	0.000	0.002	0.998	0.000	0.001	0.999	0.000	0.000	1.000
13	0.000	0.000	1.000	0.000	0.000	1.000	0.000	0.000	1.000
14	0.000	0.000	1.000	0.000	0.000	1.000	0.000	0.000	1.000

(Table 8). These values are valid for temperatures from 0 to 50 °C and salinities from 0 to 50.

The relative abundances of the DIC species are affected primarily by pH and secondarily by salinity and temperature (Table 9, Fig. 6). An increase in either salinity or tem-

perature effects a decrease in K_1 and K_2 (Table 8), resulting in a shift of the species abundance crossovers toward lower pH (Fig. 6). The effect of decreasing salinity is greater than that of decreasing temperature. An increase in salinity also slightly lowers the maximum value of HCO_3^- and the pH at

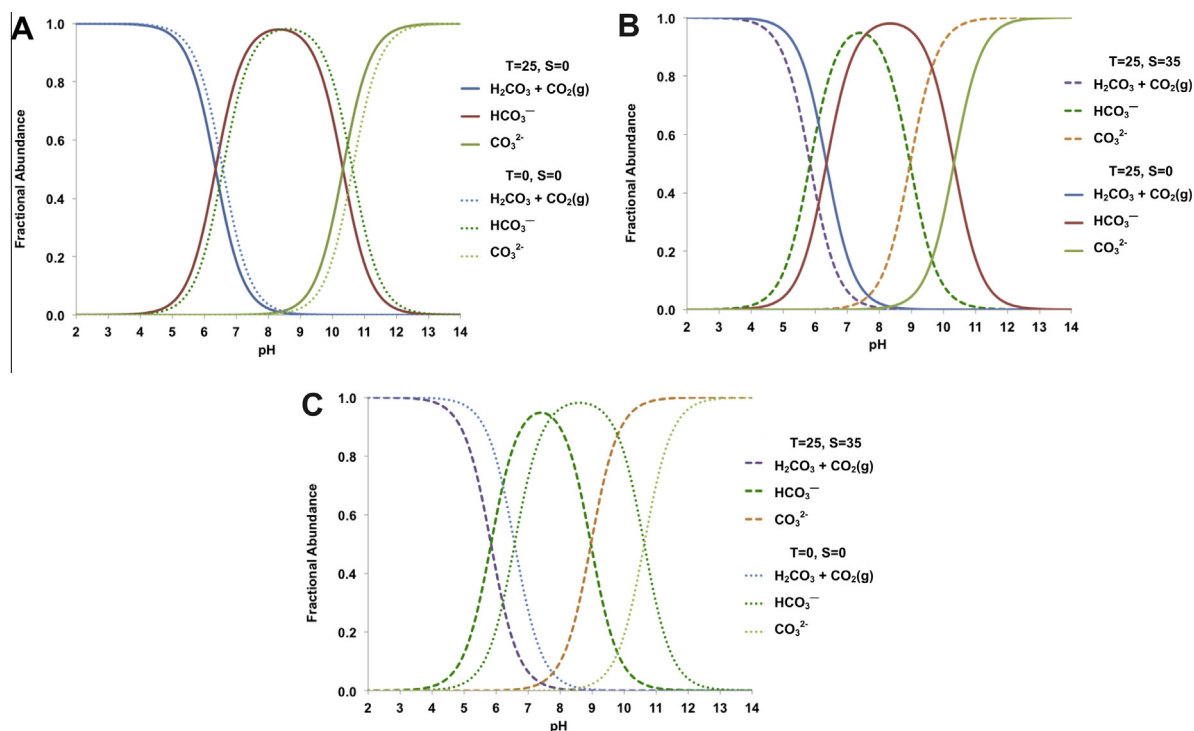


Fig. 6. Effects of salinity (S) and temperature (T) on relative abundances of DIC species vs. pH. The fractional abundances of the dissolved inorganic carbon (DIC) species depend primarily on the pH of the solution and secondarily on the salinity and temperature of the solution. Species abundances are calculated from the empirical formulas of Millero et al. (2006), in conjunction with Eqs. (19) and (20) (Table 9). Note that the maximum abundance of HCO_3^- decreases as salinity increases. Millero et al.'s equations are valid for temperatures (T) ranging from 0 to 50 °C and salinities from 0 to 50. (A) pH vs. DIC Species: constant salinity (S=0), changing temperature (T=0, 25°C). (B) pH vs. DIC Species: constant temperature (T=25°C), changing salinity (S=0, 35). (C) pH vs. DIC Species: changing salinity (S=0, 35), changing temperature (T=0, 25°C).

which the maximum occurs. Note that in Table 9, the sum of the relative abundances of the 3 DIC species, $f([\text{H}_2\text{CO}_3 + \text{CO}_2(\text{aq})]) + f(\text{HCO}_3^-) + f(\text{CO}_3^{2-})$ is unity.

At low pH, the amount of H_2CO_3 relative to $\text{CO}_2(\text{aq})$ is extremely small, less than 0.2% (Falcke and Eberle, 1990; Tossell, 2006; Adamczyk et al., 2009; England et al., 2011; Soli and Byrne, 2002).

4.1.2. Assumptions and equations needed to calculate composite Δ_{63} for the DIC pool

The composite Δ_{63} for the DIC pool is easily calculated at $\text{pH} \geq 8$, when the amount of $\text{CO}_2(\text{aq})$ is negligible; then Δ_{63} is the weighted average of Δ_{63} of CO_3^{2-} and HCO_3^- . However, determination of a composite Δ_{63} for the entire DIC pool from which a carbonate mineral can precipitate becomes problematic at low pH, when $[\text{CO}_2(\text{aq}) + \text{H}_2\text{CO}_3]$ is high, because $\text{CO}_2(\text{aq})$ does not have the three oxygen atoms necessary to form a carbonate (MCO_3) directly and $\text{CO}_2 \leftrightarrow \text{H}_2\text{CO}_3$ interconversion is slow, similar to the time-scale of overall DIC equilibration rates.

In order to calculate a composite Δ_{63} for the DIC pool at low pH, we make the following assumptions. Since the hydration of $\text{CO}_2(\text{aq})$ occurs at a much slower rate than the deprotonation of H_2CO_3 to HCO_3^- (i.e., stripping off a proton occurs much more rapidly than acquiring an extra O to form a carbonate ion) (Adamczyk et al., 2009), we

assume that any carbonate mineral precipitating rapidly from a DIC pool at low pH will form from the instantaneous H_2CO_3 and HCO_3^- components of the DIC pool and not directly from $\text{CO}_2(\text{aq})$. For the purpose of the current first order calculations, we ignore any subsequent conversion of $\text{CO}_2(\text{aq})$ to H_2CO_3 or HCO_3^- . We also assume that the DIC species are at equilibrium with one another and with the solution water.

The amount of H_2CO_3 relative to $\text{CO}_2(\text{aq})$ is about 0.1% in the temperature range of 15 °C to 32.5 °C and salinity close to that of sea water (Soli and Byrne, 2002). For the purposes of the following calculations, we also assume that the ratio of H_2CO_3 to $\text{CO}_2(\text{aq})$ is a constant 0.001.

We then calculate Δ_{63} of the composite DIC pool from Δ_{63} of the three DIC species containing CO_3 weighted by their relative abundances at a given pH such that

$$\Delta_{63}(\text{DIC pool}) = f(\text{H}_2\text{CO}_3) * \Delta_{63}(\text{H}_2\text{CO}_3) + f'(\text{HCO}_3^-) * \Delta_{63}(\text{HCO}_3^-) + f''(\text{HCO}_3^-) * \Delta_{63}(\text{CO}_3^{2-}) \quad (21)$$

$$\text{and } f(\text{H}_2\text{CO}_3) + f'(\text{HCO}_3^-) + f''(\text{CO}_3^{2-}) = 1$$

where $f(\text{H}_2\text{CO}_3)$, $f'(\text{HCO}_3^-)$, and $f''(\text{CO}_3^{2-})$ are the fractional abundances of H_2CO_3 , HCO_3^- , and CO_3^{2-} respectively in the DIC pool (without the $\text{CO}_2(\text{aq})$) and

Table 10

Δ_{63} of composite DIC solution at different temperatures ($^{\circ}\text{C}$) and salinities calculated with the supermolecular cluster model B3LYP/6-311++G(2d,2p) based on relative amounts of H_2CO_3 , HCO_3^- , and CO_3^{2-} . Possible contributions from $\text{CO}_2(\text{aq})$ are not included in these calculations – see Sections 4.1.2 and A.3 and Fig. 7. Values are unscaled.

pH	T = 0 $^{\circ}\text{C}$, S = 0	T = 25 $^{\circ}\text{C}$, S = 0	T = 25 $^{\circ}\text{C}$, S = 35	T = 25 $^{\circ}\text{C}$, S = 50	T = 50 $^{\circ}\text{C}$, S = 0	T = 50 $^{\circ}\text{C}$, S = 50
0.0	0.516	0.434	0.434	0.434	0.367	0.367
1.0	0.516	0.434	0.434	0.434	0.367	0.367
2.0	0.515	0.433	0.430	0.430	0.366	0.362
3.0	0.509	0.425	0.416	0.415	0.358	0.348
4.0	0.491	0.409	0.405	0.405	0.344	0.341
5.0	0.483	0.404	0.404	0.404	0.340	0.340
5.2	0.482	0.404	0.403	0.403	0.340	0.340
6.0	0.482	0.403	0.403	0.403	0.340	0.339
6.5	0.482	0.403	0.403	0.403	0.340	0.339
7.0	0.482	0.403	0.403	0.403	0.340	0.338
7.1	0.482	0.403	0.403	0.403	0.340	0.338
7.2	0.482	0.403	0.403	0.403	0.340	0.338
7.3	0.482	0.403	0.403	0.402	0.340	0.337
7.4	0.482	0.403	0.402	0.402	0.340	0.337
7.5	0.482	0.403	0.402	0.402	0.340	0.336
7.6	0.482	0.403	0.402	0.401	0.340	0.336
7.7	0.482	0.403	0.402	0.401	0.339	0.335
7.8	0.482	0.403	0.401	0.400	0.339	0.334
7.9	0.482	0.403	0.401	0.400	0.339	0.332
8.0	0.482	0.403	0.400	0.399	0.339	0.331
8.1	0.481	0.403	0.399	0.398	0.339	0.330
8.2	0.481	0.403	0.398	0.397	0.339	0.328
8.3	0.481	0.403	0.397	0.395	0.339	0.326
8.4	0.481	0.403	0.396	0.394	0.339	0.325
8.5	0.481	0.403	0.395	0.392	0.339	0.323
8.6	0.481	0.403	0.393	0.390	0.339	0.321
8.7	0.481	0.403	0.392	0.388	0.339	0.320
8.8	0.481	0.402	0.390	0.386	0.338	0.318
8.9	0.481	0.402	0.388	0.385	0.338	0.317
9.0	0.481	0.402	0.386	0.383	0.338	0.316
9.5	0.479	0.399	0.378	0.376	0.334	0.312
10.0	0.475	0.393	0.373	0.372	0.328	0.310
11.0	0.456	0.376	0.371	0.370	0.314	0.310
12.0	0.446	0.371	0.370	0.370	0.310	0.310
13.0	0.445	0.370	0.370	0.370	0.310	0.310
14.0	0.445	0.370	0.370	0.370	0.310	0.310

$f(\text{H}_2\text{CO}_3 + \text{CO}_2(\text{aq}))$, $f(\text{HCO}_3^-)$, and $f(\text{CO}_3^{2-})$ are the fractional abundances of H_2CO_3 , HCO_3^- , and CO_3^{2-} respectively in the DIC pool (with the $\text{CO}_2(\text{aq})$), and $f(\text{H}_2\text{CO}_3) = .001^* f(\text{H}_2\text{CO}_3 + \text{CO}_2(\text{aq}))$. Note that the values of $f(\text{HCO}_3^-)$ and $f(\text{CO}_3^{2-})$ from Table 10 must be renormalized with $f(\text{H}_2\text{CO}_3)$ such that $f(\text{H}_2\text{CO}_3) + f'(\text{HCO}_3^-) + f'(\text{CO}_3^{2-}) = 1$ before applying Eq. (21) (see Appendix A.3 for details and an example.)

The composite DIC Δ_{63} mainly reflects the Δ_{63} of the most abundant species at a given pH. DIC Δ_{63} is lowest at high pH when CO_3^{2-} is dominant and increases as pH decreases to more neutral values where HCO_3^- is the dominant species. At low, acidic pH the dominant species are $[\text{H}_2\text{CO}_3 + \text{CO}_2(\text{aq})]$. However, since the amount of H_2CO_3 is so small, Δ_{63} of HCO_3^- continues to dominate the portion of the DIC pool from which we assume the calcite crystal will precipitate. As pH drops and the amount of HCO_3^- decreases, Δ_{63} of the MCO_3 pool increases toward the Δ_{63} of H_2CO_3 . Note that the $\text{CO}_2(\text{aq})$ has significant

Δ_{47} , but cannot exhibit Δ_{63} clumping. Three plateaus in the composite Δ_{63} with changing pH, corresponding to dominance by H_2CO_3 , HCO_3^- , and CO_3^{2-} , are thus expected (Table 10 and Fig. 7).

4.1.3. Other isotopic attributes of composite DIC pool

Composite $\beta^{13}\text{C}$ and $\beta^{18}\text{O}$ for the DIC pool (neglecting water) can be calculated as above using the fractional abundances of the DIC species times the individual $\beta^{13}\text{C}$ or $\beta^{18}\text{O}$ respectively of each DIC species. This should be a reasonable approximation for $\text{pH} \geq 8$ (i.e., when the amount of $\text{CO}_2(\text{aq})$ is negligible). At lower pH, it is not clear how $\beta^{13}\text{C}$ or $\beta^{18}\text{O}$ of $\text{CO}_2(\text{aq})$ interacts with $\beta^{13}\text{C}$ or $\beta^{18}\text{O}$ of HCO_3^- .

However, to calculate the composite $\beta^{18}\text{O}$ of the DIC pool including the water, the concentrations of each DIC species in the solution as well as $\beta^{18}\text{O}$ of the water in the solution must be considered (see Zeebe, 2007, for a detailed discussion of $\beta^{18}\text{O}$ in the DIC pool).

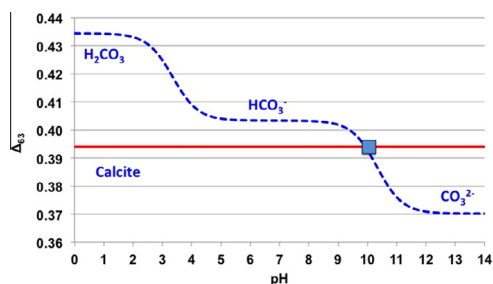


Fig. 7. Composite DIC Δ_{63} (dotted blue line) compared to equilibrium calcite Δ_{63} (solid red line) vs. pH at 25 °C from the B3LYP/6-311++G(2d,2p) models. Changes in Δ_{63} DIC with pH reflect the changing relative abundances of the DIC species (Table 11). Possible contributions from $\text{CO}_2(\text{aq})$ are not included in these calculations – see Section 4.1.2. At equilibrium Δ_{63} of calcite is independent of pH and of the DIC solution. (For interpretation of the references to color in this figure legend, the reader is referred to the web version of this article.)

4.2. Precipitating carbonate minerals and the DIC pool; possible effects of temperature, pH, and salinity

4.2.1. Precipitation rate

The rate of precipitation may be an important factor modulating whether DIC speciation effects on clumping are recorded in carbonate minerals (Tripathi et al., 2010). Because CO_3^{2-} and HCO_3^- ions have distinct clumping equilibria, the state of bond ordering recorded by carbonates precipitated in disequilibrium may vary depending on the pH of the solution at the site of precipitation. This supposes that when a calcite crystal precipitates from a DIC pool slowly enough that it has time to come to internal bulk equilibrium, its clumped isotope signature is independent of the pH of the parent solution. Thus while the Δ_{63} of the DIC pool will change with pH, the Δ_{63} of a slowly precipitating carbonate crystal will be dependent only upon the temperature of the pool. However, this effect should be modulated by precipitation rate, with rapid precipitation tending to favor disequilibrium incorporation of part or all of the clumped isotope signature of the DIC pool into the crystal lattice and slow precipitation favoring attainment of independent clumped isotope equilibration throughout the lattice. We note that there are other factors, such as kinetic effects, that may also affect the disequilibrium Δ_{63} of a carbonate mineral precipitating in disequilibrium, but we do not address those factors in the current study.

4.2.2. Calcite clumped crossover pH

The above hypothesis (Section 4.2.1) implies that when a calcite crystal precipitates from a DIC pool sufficiently rapidly that it does not have time to reach an internal bulk equilibrium, then it may inherit all or part of the Δ_{63} of the DIC pool. To help quantify this effect, we define the *clumped crossover pH* as the pH at which the calcite Δ_{63} at equilibrium is equal to Δ_{63} of the DIC pool at equilibrium. The clumped crossover pH determines the pH at which the disequilibrium Δ_{63} of a precipitating calcite min-

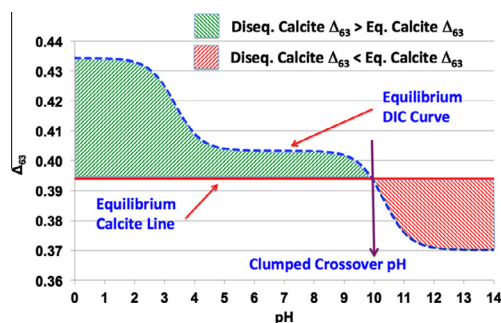


Fig. 8. Range of possible pH dependencies of calcite Δ_{63} if the crystal precipitates at disequilibrium at 25 °C and salinity = 0. The clumped crossover pH is the pH at which calcite Δ_{63} equilibrium = DIC Δ_{63} at equilibrium. If pH < clumped crossover pH, then the disequilibrium calcite Δ_{63} > equilibrium calcite Δ_{63} (green striped area) and the “apparent temperature” underestimates temperature; if pH > clumped crossover pH, then the disequilibrium calcite Δ_{63} < equilibrium calcite Δ_{63} (pink striped area) and the “apparent temperature” overestimates temperature. Δ_{63} values are from the B3LYP/6-311++G(2d,2p) models (see Section 4.2.2). (For interpretation of the references to color in this figure legend, the reader is referred to the web version of this article.)

eral may be misinterpreted as either an overestimation (high pH) or an underestimation (low pH) of temperature of formation if the ‘apparent Δ_{63} ’ (i.e., measured Δ_{63}) is assumed to be the calcite equilibrium Δ_{63} value (Table 11).

For pH values less than the clumped crossover pH, the DIC Δ_{63} is greater than the equilibrium calcite Δ_{63} , and the disequilibrium calcite Δ_{63} will be greater than the equilibrium calcite Δ_{63} . This can result in an underestimation of temperature from ‘apparent Δ_{63} ’ for example, at pH = 7, T = 25 °C, S = 0, temperature is underestimated by 3.2 °C (Fig. 8) if calcite inherits the composite DIC Δ_{63} .

For pH greater than the clumped crossover pH, the DIC Δ_{63} is less than the equilibrium calcite Δ_{63} . Thus the disequilibrium calcite Δ_{63} will be less than the equilibrium calcite Δ_{63} , resulting in an overestimation of the ‘apparent Δ_{63} ’ temperature; for example, at pH = 12, T = 25 °C, S = 0, temperature will be overestimated by 8.7 °C (Fig. 8). The situation for aragonite is somewhat different since the clumped crossover pH for aragonite occurs at lower pH than calcite due to its higher Δ_{63} . Thus, apparent temperatures derived from disequilibrium aragonite Δ_{63} for pH greater than about 4 (depending upon salinity) will potentially overestimate the actual temperature of formation (Figs. 7 and 8). Conversely, if our estimate for witherite is correct, then the clumped crossover pH for witherite would be higher (by about ~0.8 pH units) than that for calcite at 25 °C.

4.2.3. Effects of salinity and temperature on DIC pool Δ_{63} and clumped crossover pH

Natural carbonates and carbonate-bearing solutions occur over a wide range of temperatures, pH, and salinities. We investigated the effects of salinity on the composite DIC Δ_{63} and clumped crossover pH for 3 different environments, each with a range of temperatures: salinity = 0

(fresh water), salinity = 35 (common seawater) and salinity = 50 (brine). Although seawater and briny solutions will be affected by the presence of other ions and possibly ion pairing, we considered only salinity in the following calculations. These effects, however, are not likely to be important for all carbonates, but only for carbonates that are precipitated at rapid growth rates.

The effect of increased salinity is to lower the pH at which the inflection points in the DIC Δ_{63} curve occur (Fig. 9 and Tables 8 and 9). As a result, the clumped crossover pH also decreases (Fig. 9A). Salinity does not affect the calcite equilibrium Δ_{63} . At 25 °C the crossover pH is 9.90 for $S=0$, 8.55 for $S=35$, and 8.4 for $S=50$ (Table 10). Since the calcite clumped crossover pH intersects the DIC Δ_{63} curve at a location of rapid change (i.e., steep slope), a typical experimental Δ_{63} standard error of, say, $\pm 0.005\text{‰}$ would correspond to an uncertainty in the crossover pH of about 0.3 to 0.4 and an uncertainty in temperature of roughly 1 to 2 °C.

The effect of a temperature increase is twofold; the primary effect is a reduction in Δ_{63} of the composite DIC pool as well as the calcite equilibrium Δ_{63} , since Δ_{63} is thermodynamically dependent upon temperature. A secondary effect is the lowering of the DIC equilibrium constants (pKs), which also shifts changes in the relative DIC abundances to lower pH, also causing a slight decrease in the crossover pH (Fig. 9B, Tables 9 and 10). At a salinity of 0, the crossover pH is 10.30 for $T=0\text{ °C}$ and 9.70 for $T=50\text{ °C}$ (Table 11). Calcite Δ_{63} at equilibrium is 0.470 ‰ at $T=0\text{ °C}$ and 0.332‰ at $T=50\text{ °C}$.

The combined effects of temperature and salinity increases can be seen in Fig. 9C. and Table 10. At $T=0\text{ °C}$ and $S=0$, the clumped crossover pH is 10.30 and calcite Δ_{63} at equilibrium is 0.470‰, while at $T=50\text{ °C}$ and $S=50$, the clumped crossover pH is 7.94 and calcite Δ_{63} at equilibrium is 0.332‰. Changes in the clumped crossover pH will affect both the direction and magnitude of the disequilibrium calcite Δ_{63} (Fig. 8). This affects the

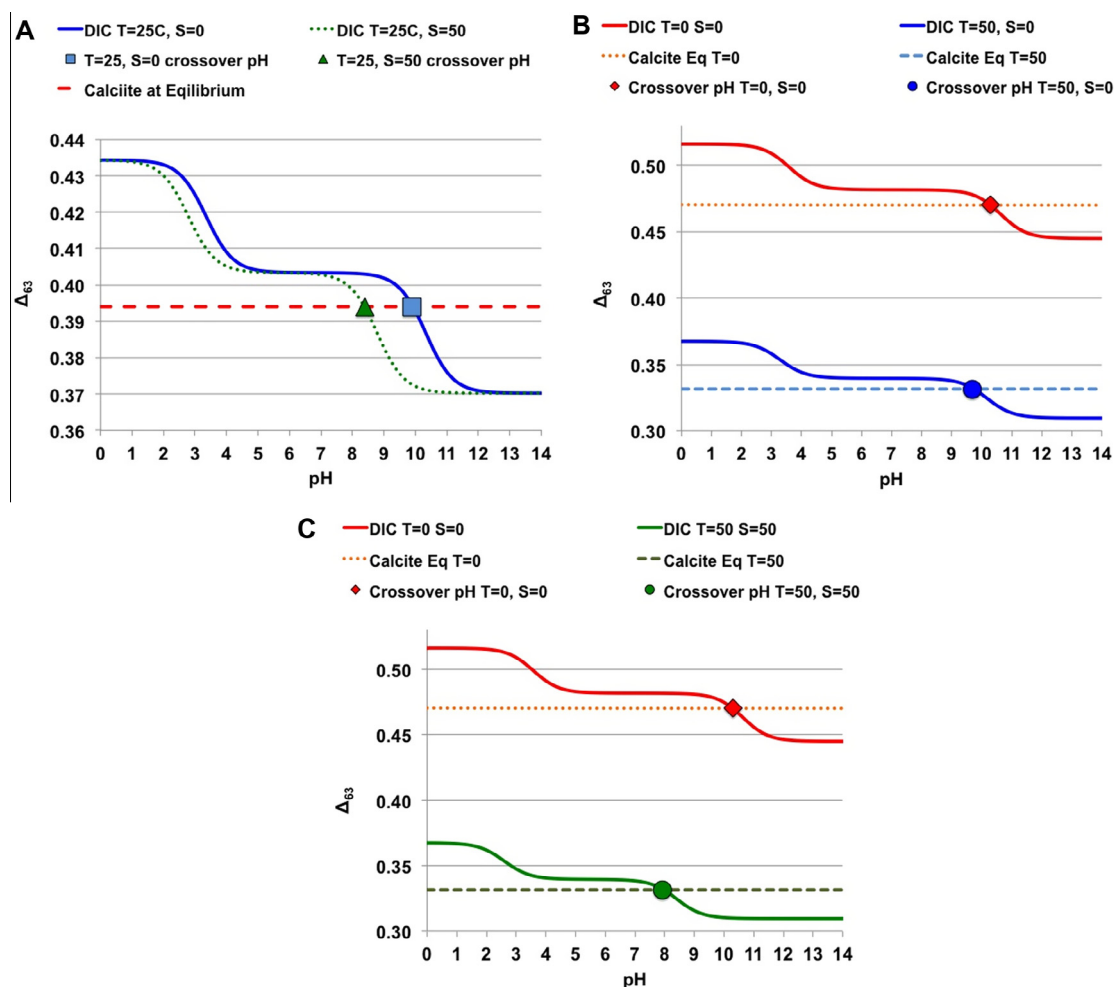


Fig. 9. Effects of (A) salinity, (B) temperature, and (C) both salinity and temperature on Δ_{63} of the DIC pool and the calcite clumped crossover pH (Table 10). (A). As salinity increases from 0 to 50 at a constant temperature = 25 °C, the crossover pH changes from pH = 9.9 to 8.40. (B). As temperature changes from 0 °C to 50 °C at salinity = 0, the crossover pH changes from pH = 10.3 to 9.74. The calcite equilibrium Δ_{63} also changes from 0.470 to 0.332‰. (C). As salinity increases from 0 to 50 and temperature increases from 0 °C to 50 °C, the crossover pH changes from pH = 10.30 to 7.94. The calcite equilibrium Δ_{63} also changes from 0.470 to 0.332‰.

Table 11

Calcite clumped crossover pH and calcite equilibrium Δ_{63} for a range of temperatures and salinities calculated with the B3LYP/6-311++G(2d,2p) supermolecular models and apparent temperatures based upon misinterpretation of calcite disequilibrium Δ_{63} (inherited from equilibrium DIC Δ_{63}) as the equilibrium calcite Δ_{63} for a range of temperatures (T) and salinities (S) at pH = 5 and pH = 12 (Sections 4.2.2, 4.2.3, and 4.3). As either salinity or temperature increases, the clumped crossover pH decreases. The effect of salinity is greater than that of temperature. The calcite equilibrium Δ_{63} also decreases with temperature, but is independent of salinity and pH (Fig. 7, Tables 10 and A1). Values are unscaled.

T (°C), S	Clumped crossover pH	Calcite Δ_{63eq}	pH = 7			pH = 12			Range of apparent T (°C)
			DIC Δ_{63}	Apparent T (°C)	Under estimation of actual T	DIC Δ_{63}	Apparent T (°C)	Over Estimation of actual T	
S = 0, T = 0 °C	10.30	0.4701	0.482	−3.6	−3.6	0.446	7.5	7.5	11.1
S = 0, T = 25 °C	9.90	0.3940	0.403	21.8	−3.2	0.371	33.7	8.7	11.9
S = 0, T = 50 °C	9.70	0.3316	0.340	46.4	−3.6	0.310	59.9	9.9	13.5
S = 35, T = 25 °C	8.55	0.3940	0.404	21.8	−3.2	0.370	34.1	9.1	12.3
S = 50, T = 25 °C	8.40	0.3940	0.404	21.8	−3.2	0.370	34.1	9.1	12.3
S = 50, T = 50 °C	7.94	0.3316	0.340	46.4	−3.6	0.310	59.9	9.9	13.5

interpretation of the disequilibrium Δ_{63} as being an over or underestimation of the actual temperature of formation. Table 11 shows the potential over or underestimation of temperature by misinterpretation of the calcite disequilibrium Δ_{63} (inherited from the DIC Δ_{63}) for a range of pH, temperatures, and salinities. The clumped crossover pH for aragonite and witherite will also be affected by salinity and temperature, occurring at lower or higher pH respectively than calcite.

4.3. Implications

From our modeling results, we conclude that the composite clumped isotope signature of a DIC pool at equilibrium with the water in the solution at a given temperature depends primarily on pH (since pH determines the relative combinations of DIC species), and secondly upon salinity of the solution (due to its added effect on DIC speciation). Temperature also has a small effect on the speciation. Our best models show a difference of about 0.033‰ between a DIC pool consisting mostly of bicarbonate (HCO_3^-) at pH ~ 7 and a solution of mostly carbonate (CO_3^{2-}) at pH $> \sim 12$ at 25 °C. A calcite mineral precipitating from a DIC solution slowly enough to reach internal bulk equilibrium should have a Δ_{63} independent of the DIC pool (Fig. 7). In contrast, if the precipitation rate of calcite is so rapid that the calcite lattice does not have time to come to an internal isotopic equilibrium, and if the above mechanism for recording DIC speciation in carbonate minerals is correct (Section 4.2.1), then the calcite may inherit all or part of the clumped isotope signature of the DIC in the parent solution (Figs. 7 and 8).

At pH values lower than the calcite clumped crossover pH (Section 4.2.3), with the above mechanism we would expect the disequilibrium Δ_{63} of the rapidly precipitated calcite lattice to be greater than the expected calcite equilibrium value, resulting in a possible underestimation of formation temperature. As the pH decreases, the difference between disequilibrium and equilibrium values will in-

crease. For pH values that are higher than the clumped crossover pH we would expect the disequilibrium Δ_{63} of the calcite lattice to be less than its equilibrium value, resulting in a possible overestimation of formation temperature. The clumped crossover pH (where DIC and calcite equilibria are equivalent) varies primarily with salinity and secondarily with temperature (Fig. 9). The effect of salinity can be significant; for example, the crossover pH for fresh water (S = 0) is predicted to be 9.90 compared to 8.55 in seawater (S = 35) at 25 °C.

Our findings may in part explain some of the variability observed in calibration datasets. Differences in the temperature- Δ_{47} calibrations for inorganic calcite reported by Ghosh et al. (2006) and Dennis and Schrag (2010) could partially reflect pH effects. It is possible that some of the systematic scatter observed in biogenic calibration data may also arise from pH (Ghosh et al., 2006; Tripathi et al., 2010; Thiagarajan et al., 2011; Eagle et al., 2013). Future studies may show there are systematic environmental and biological differences in calibrations between taxa originating from DIC speciation effects. At least some marine calcifiers (such as corals, e.g. Al-Horani et al., 2003) can maintain calcifying fluid pH values that are significantly different from that of seawater and probably retain the ability to buffer their internal pH from changes in external pH. Organisms that elevate their pH substantially to calcify may have Δ_{47} systematically offset to lower values compared to organisms that calcify at near ambient pH. Hence we do not expect all marine calcifiers to be passive tracers of pH and salinity effects on the isotopic distributions in seawater DIC. Further, assuming a calcifying fluid pH similar to ambient waters, then it is possible that calcifiers characterized by rapid growth rates that are living at greater depth in the ocean and thus at lower temperatures, and typically lower pH, might exhibit higher Δ_{47} values due to increased HCO_3^- concentrations. We might also expect to find lower Δ_{47} disequilibrium values in highly alkaline environments, such as California's Mono Lake, pH of ~ 10 , in conditions of rapid growth.

Thus, the potential effects of pH, salinity, and temperature upon the misinterpretation of “apparent temperature” of a calcite crystal that precipitates under disequilibrium conditions can be quite large if the disequilibrium Δ_{63} is misinterpreted as the equilibrium Δ_{63} . For example, at 25 °C and $S = 0$, a spurious difference of 11.9 °C could be implied between the “apparent temperatures” of pH = 7 and pH = 12 (Table 11). If we add a change in salinity from $S = 0$ (fresh water) to $S = 35$ (sea water), then the difference in apparent temperatures becomes 12.3 °C. If we consider the difference between cold freshwater environments at high latitudes ($S = 0$, $T = 0$ °C, pH ~ 7) and warm hypersaline environments ($S \geq 50$, $T = 50$ °C, and pH ~ 12), the difference in apparent temperature in disequilibrium conditions could be as high as 63.5 °C compared to the actual temperature difference of 50 °C. In subsurface environments the range in conditions and other parameters could be considerably bigger. For potential application of clumped isotope thermometry to processes in the shallow crust, the range in temperature and solution chemistry could be even larger. These theoretical calculations emphasize the need for further study to understand the potential effects of DIC speciation and solution chemistry on Δ_{63} and Δ_{47} from carbonates precipitating from diverse environments at both equilibrium and disequilibrium.

5. CONCLUSIONS

In this work, we have investigated pH as a possible driver of the clumped isotope fractionation of precipitating carbonate minerals that fail to reach an internal bulk isotopic equilibrium. Many carbonate minerals precipitate from some kind of solution containing dissolved inorganic carbon (DIC). Here we explore theoretically the nature of clumping in the individual DIC species and the composite solution under a variety of conditions, including varying pH, salinity, temperature, and isotopic composition, and speculate about their effects upon the resultant disequilibrium clumping of the precipitates.

In order to find the best models for determining clumped isotope, oxygen, and carbon fractionation of aqueous dissolved inorganic carbon (DIC) species and carbonate minerals, we performed convergence and sensitivity testing on several different levels of theory combined with four different solvation techniques. We determined the B3LYP/6-311++G(2d,2p) to be a reasonable compromise between model accuracy and computer efficiency for solvated DIC species. We have also demonstrated that supermolecular clusters of 21 or more water molecules surrounding a single species are better predictors of Δ_{63} , $^{13}\text{C}/^{12}\text{C}$, and $^{18}\text{O}/^{16}\text{O}$ for the DIC species than gas phase, implicit solvation or explicit solvation (with 3 waters) models.

We calculated Δ_{63} , $^{13}\text{C}/^{12}\text{C}$, and $^{18}\text{O}/^{16}\text{O}$ for each of the DIC species and the calcite and aragonite minerals using cluster models with B3LYP/6-311++G(2d,2p). This is the first time this cluster modeling technique has been applied to both crystals and aqueous species, allowing comparison of clumped isotope signatures of all species within a consis-

tent computational and theoretical framework. We then calculated the composite Δ_{63} for the total DIC pool at equilibrium with water and determined its dependence on pH, salinity, and temperature. We compared the equilibrium calcite lattice Δ_{63} values with the DIC values for a given temperature and predicted the size and direction (i.e., over or underestimation of interpreted temperature) of possible disequilibrium Δ_{63} that the calcite lattice might inherit from the DIC species if the calcite crystal does not have enough time to equilibrate fully during precipitation. We defined the clumped crossover pH of a crystal precipitating at disequilibrium, showed its dependence on salinity and temperature, and discussed the implications for over or underestimation of apparent temperature. We also suggested under what conditions disequilibrium conditions might be found.

ACKNOWLEDGMENTS

We would like to thank Dr. Fernando R. Clemente of Gaussian, Inc., for his very helpful suggestions with some of the advanced features in Gaussian09. We would also like to thank Anastassia Alexandrova, Bill Casey, Rob Eagle, Ben Elliott, Chuck Hill, Jim Rustad, and Ben Schwartz for their insightful input. A.K.T. acknowledges support from National Science Foundation grants EAR-0949191 and ARC-1215551, ACS grant 51182-DNI2, DOE grant DE-FG02-13ER16402, a Hellman Fellowship, and a UCLA Career Development Award, and E.A.S. acknowledges support from National Science Foundation grant EAR-1047668.

APPENDIX A

A.1. Calculation of equilibrium Δ_{63}

Here we describe the steps in the calculation of Δ_{63} as defined in Eq. (2) in Section 2.1. Section A.1.1 describes the calculation of the equilibrium constants and relative abundances of the isotopologues of a carbonate phase that has attained an internal thermodynamic equilibrium. Section A.1.2 details the internal isotopic exchange reactions needed to calculate the equilibrium constants, and Section A.1.3 demonstrates the calculation of the stochastic isotopologue abundances.

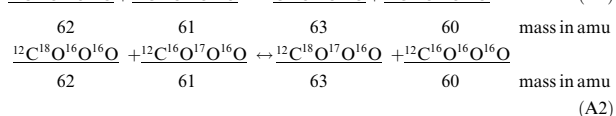
The supermolecular clusters used in this study contain multiple water molecules with geometries generated by molecular dynamics (Section 2.5) and thus have C1 (i.e., no) symmetry. In such models carbonate, bicarbonate, and carbonic acid species each have 54 distinct isotopomers⁷ ($2^* 3^* 3^* 3^* 3 = 54$). (Supermolecular clusters with carbon dioxide have 18 distinct isotopomers ($2^* 3^* 3 = 18$.) The calculation of $\Delta_{47}(\text{CO}_2)$ is similar to that for $\Delta_{63}(\text{CO}_3^{2-})$ and is detailed in Wang et al. (2004).

In order to calculate the relative abundances of each isotopomer, we set up 50 isotopomer exchange reaction equations in which 50 isotopomers are expressed in terms of the remaining 4 independent isotopomers. Each equation i has its own temperature-dependent equilibrium constant K_i . The K_s are calculated from the reduced partition function ratios for each isotopomer. The relative isotopomer masses

are then calculated by solving the isotopomer exchange reaction equations and the mass balance equations as a series of dependent equations (using the *fsolve* function in either MATLAB or SciLab 5.3.3, which employs the Powell dogleg method of solving systems of nonlinear algebraic equations (Powell, 1970)). For systems with a higher symmetry, isotopologue abundances can be calculated by summing the abundances of all isotopomers associated with a given isotopologue.

A.1.1. Calculation of the relative isotopomer equilibrium abundances for a given temperature *T*

To find the relative isotopomer abundances we set up the isotopomer exchange equations for each isotopomer, relating the equilibrium constants K_i to the relative isotopomer concentrations (see Section A.1.2). Using the unsigned ‘CO₃’ to represent any carbonate of interest, we start with the exchange reactions for $^{13}\text{C}^{18}\text{O}^{16}\text{O}^{16}\text{O}$ and $^{12}\text{C}^{18}\text{O}^{17}\text{O}^{16}\text{O}$ as an example⁷



Each reaction *i* has an equilibrium constant K_i , related to the isotopomer abundances as

$$\begin{aligned} \underline{K3866} &= \frac{\{^{13}\text{C}^{18}\text{O}^{16}\text{O}^{16}\text{O}\} * \{^{12}\text{C}^{16}\text{O}^{16}\text{O}^{16}\text{O}\}}{\{^{12}\text{C}^{18}\text{O}^{16}\text{O}^{16}\text{O}\} * \{^{13}\text{C}^{16}\text{O}^{16}\text{O}^{16}\text{O}\}} \\ \underline{K2876} &= \frac{\{^{12}\text{C}^{18}\text{O}^{17}\text{O}^{16}\text{O}\} * \{^{12}\text{C}^{16}\text{O}^{16}\text{O}^{16}\text{O}\}}{\{^{12}\text{C}^{18}\text{O}^{16}\text{O}^{16}\text{O}\} * \{^{12}\text{C}^{16}\text{O}^{17}\text{O}^{16}\text{O}\}} \end{aligned} \quad (\text{A3})$$

where $\underline{K3866}$ is the equilibrium constant for the exchange reaction for $^{13}\text{C}^{18}\text{O}^{16}\text{O}^{16}\text{O}$ (Eq. (A1)), $\underline{K2876}$, the equilibrium constant for the exchange reaction for $^{12}\text{C}^{18}\text{O}^{17}\text{O}^{16}\text{O}$ (Eq. (A2)), and [x] is the concentration of isotopomer x. Recall that the underlining indicates an individual isotopomer⁷.

Next the values of the equilibrium constants must be determined. From thermodynamics

$$K_i = \exp(-\Delta E/RT) \quad (\text{A4})$$

where *R* is the universal gas constant, *T* is temperature in Kelvin, and ΔE is the change of Gibbs free energy of the reaction between the products and reactants. The equilibrium constants are calculated from the reduced partition function ratios of the isotopomers, a measure of the relative energies or probabilities of the products vs. the reactants (see Schauble, 2004, for a detailed discussion, and Urey, 1947; Bigeleisen and Mayer, 1947, for the seminal derivations).

The reduced partition functions are calculated from the vibrational frequencies derived from ab initio models of each isotopomer, such that

$$Q_i = \{1/(\sigma_i)\} \prod_{i=1}^{3N-6} \{hc(v_i)/kT\} \left\{ \frac{\exp(-hc(v_i)/2kT)}{1 - \exp(-hc(v_i)/kT)} \right\} \quad (\text{A5})$$

where Q_i is the reduced partition function of isotopologue *i*, v_i is the *i*th vibrational frequency (in cm^{-1}) and σ is the rotational symmetry number of isotopologue *i*, *h* is Planck’s constant, *k* is Boltzmann’s constant, *c* is the speed of light (in cm/sec), and *T* is the temperature in Kelvin. The accuracy of the results depends upon the accuracy of the ab initio models and the underlying assumptions of the level of theory used in the program (Section 2.5).

The equilibrium constants for each exchange reaction are determined from the relevant reduced partition function ratios for each isotopomer such that (for example)

$$\begin{aligned} \underline{K3866} &= \frac{(Q_{3866} * Q_{2666})}{(Q_{3666} * Q_{2866})} \\ &= \frac{(Q_{3866}/Q_{2666})}{\{(Q_{3666}/Q_{2666}) \\ &\quad * Q_{2866}/(Q_{2666})\}} \\ &= \underline{R}_{3866}/(\underline{R}_{3666} * \underline{R}_{2866}) \end{aligned} \quad (\text{A6})$$

$$\begin{aligned} \underline{K2876} &= \frac{(Q_{2876} * Q_{2666})}{(Q_{2866} * Q_{2766})} \\ &= \frac{(Q_{2876}/Q_{2666})}{\{(Q_{2866}/Q_{2666}) \\ &\quad * Q_{2766}/(Q_{2666})\}} \\ &= \underline{R}_{2876}/(\underline{R}_{2866} * \underline{R}_{2766}) \end{aligned} \quad (\text{A7})$$

etc.

where R_j is the reduced partition function ratio (RPFR) and defined as

$$R_j = Q_j/Q_{2666} \quad (\text{A8})$$

Q_{2666} is the reduced partition function of the most abundant (and non-substituted) carbonate isotopologue $^{12}\text{C}^{16}\text{O}_3$. Calculation of the isotopologue composite values of $\underline{K3866}$ and $\underline{K2876}$ are determined from the isotopomer K_s as described in Section 2.4.

$$\begin{aligned} \text{Note that } \beta^{18}\text{O}(\underline{^{12}\text{C}^{18}\text{O}^{16}\text{O}^{16}\text{O}}) \\ = \underline{R}_{2866} \text{ and } \beta^{13}\text{C}(\underline{^{13}\text{C}^{16}\text{O}^{16}\text{O}^{16}\text{O}}) = \underline{R}_{3666}, \text{ etc.} \end{aligned} \quad (\text{A9})$$

Calculation of the composite values of $\beta^{18}\text{O}$ is also described in Section 2.4.

A.1.2. Isotopomer exchange reactions, relative abundance equations, and mass balance equations

Four isotopomers are chosen as the independent variables in the following equations. Their values are calculated from the isotopic composition of the carbonate system of interest.

$$\begin{aligned} &^{12}\text{C}^{16}\text{O}^{16}\text{O}^{16}\text{O} \\ &^{13}\text{C}^{16}\text{O}^{16}\text{O}^{16}\text{O} \\ &\underline{^{12}\text{C}^{18}\text{O}^{16}\text{O}^{16}\text{O}} \\ &\underline{^{12}\text{C}^{17}\text{O}^{16}\text{O}^{16}\text{O}} \end{aligned} \quad (\text{A10})$$

The remaining 50 isotopomer equations are expressed in terms of the independent variables.

$$\begin{aligned}
& {}^{13}\text{C}^{16}\text{O}^{16}\text{O}^{16}\text{O} + {}^{12}\text{C}^{16}\text{O}^{18}\text{O}^{16}\text{O} + {}^{12}\text{C}^{16}\text{O}^{16}\text{O}^{17}\text{O} \\
& \leftrightarrow 2 * {}^{12}\text{C}^{16}\text{O}^{16}\text{O}^{16}\text{O} + {}^{13}\text{C}^{16}\text{O}^{18}\text{O}^{17}\text{O} \\
& {}^{13}\text{C}^{16}\text{O}^{16}\text{O}^{16}\text{O} + {}^{12}\text{C}^{17}\text{O}^{16}\text{O}^{16}\text{O} + {}^{12}\text{C}^{16}\text{O}^{16}\text{O}^{18}\text{O} \\
& \leftrightarrow 2 * {}^{12}\text{C}^{16}\text{O}^{16}\text{O}^{16}\text{O} + {}^{13}\text{C}^{17}\text{O}^{16}\text{O}^{18}\text{O} \\
& {}^{13}\text{C}^{16}\text{O}^{16}\text{O}^{16}\text{O} + {}^{12}\text{C}^{17}\text{O}^{16}\text{O}^{16}\text{O} + {}^{12}\text{C}^{16}\text{O}^{18}\text{O}^{16}\text{O} \\
& \leftrightarrow 2 * {}^{12}\text{C}^{16}\text{O}^{16}\text{O}^{16}\text{O} + {}^{13}\text{C}^{17}\text{O}^{18}\text{O}^{16}\text{O} \\
& {}^{13}\text{C}^{16}\text{O}^{16}\text{O}^{16}\text{O} + {}^{12}\text{C}^{18}\text{O}^{16}\text{O}^{16}\text{O} + {}^{12}\text{C}^{16}\text{O}^{16}\text{O}^{17}\text{O} \\
& \leftrightarrow 2 * {}^{12}\text{C}^{16}\text{O}^{16}\text{O}^{16}\text{O} + {}^{13}\text{C}^{18}\text{O}^{16}\text{O}^{17}\text{O} \\
& {}^{13}\text{C}^{16}\text{O}^{16}\text{O}^{16}\text{O} + {}^{12}\text{C}^{18}\text{O}^{16}\text{O}^{16}\text{O} + {}^{12}\text{C}^{16}\text{O}^{17}\text{O}^{16}\text{O} \\
& \leftrightarrow 2 * {}^{12}\text{C}^{16}\text{O}^{16}\text{O}^{16}\text{O} + {}^{13}\text{C}^{18}\text{O}^{17}\text{O}^{16}\text{O} \\
& {}^{13}\text{C}^{16}\text{O}^{16}\text{O}^{16}\text{O} + {}^{12}\text{C}^{17}\text{O}^{16}\text{O}^{16}\text{O} + {}^{12}\text{C}^{16}\text{O}^{17}\text{O}^{16}\text{O} \\
& \quad + {}^{12}\text{C}^{16}\text{O}^{16}\text{O}^{17}\text{O} \leftrightarrow 3 * {}^{12}\text{C}^{16}\text{O}^{16}\text{O}^{16}\text{O} + {}^{13}\text{C}^{17}\text{O}^{17}\text{O}^{17}\text{O} \\
& {}^{13}\text{C}^{16}\text{O}^{16}\text{O}^{16}\text{O} + {}^{12}\text{C}^{18}\text{O}^{16}\text{O}^{16}\text{O} + {}^{12}\text{C}^{16}\text{O}^{18}\text{O}^{16}\text{O} \\
& \quad + {}^{12}\text{C}^{16}\text{O}^{16}\text{O}^{18}\text{O} \leftrightarrow 3 * {}^{12}\text{C}^{16}\text{O}^{16}\text{O}^{16}\text{O} + {}^{13}\text{C}^{18}\text{O}^{18}\text{O}^{18}\text{O}
\end{aligned}
\tag{A11}$$

The relative isotopomer masses (x_i) are calculated from Eq. (A12) (obtained from substituting the K 's into Eq. (A11) as exemplified with Eq. (A3)), combined with 4 mass balance equations Eqs. (A14)–(A17).

$$\begin{aligned}
x_{2667} &= (K_{2667} * x_{2766}) \\
x_{2668} &= (K_{2668} * x_{2866}) \\
x_{2676} &= (K_{2676} * x_{2766}) \\
x_{2677} &= (K_{2677} * x_{2667}) / (x_{2666} / x_{2676}) \\
x_{2678} &= (K_{2678} * x_{2668}) / (x_{2666} / x_{2676}) \\
x_{2686} &= (K_{2686} * x_{2866}) \\
x_{2687} &= (K_{2687} * x_{2667}) / ((x_{2666} / x_{2686})) \\
x_{2688} &= (K_{2688} * x_{2668}) / ((x_{2666} / x_{2686})) \\
x_{2767} &= (K_{2767} * x_{2667}) / ((x_{2666} / x_{2766})) \\
x_{2768} &= (K_{2768} * x_{2668}) / ((x_{2666} / x_{2766})) \\
x_{2776} &= (K_{2776} * x_{2676}) / ((x_{2666} / x_{2766})) \\
x_{2777} &= (K_{2777} * x_{2667}) / ((x_{2666} / x_{2766}) * (x_{2666} / x_{2676})) \\
x_{2778} &= (K_{2778} * x_{2668}) / ((x_{2666} / x_{2766}) * (x_{2666} / x_{2676})) \\
x_{2786} &= (K_{2786} * x_{2686}) / ((x_{2666} / x_{2766})) \\
x_{2787} &= (K_{2787} * x_{2667}) / ((x_{2666} / x_{2766}) * (x_{2666} / x_{2686})) \\
x_{2788} &= (K_{2788} * x_{2668}) / ((x_{2666} / x_{2766}) * (x_{2666} / x_{2686})) \\
x_{2867} &= (K_{2867} * x_{2667}) / ((x_{2666} / x_{2866})) \\
x_{2868} &= (K_{2868} * x_{2668}) / ((x_{2666} / x_{2866})) \\
x_{2876} &= (K_{2876} * x_{2676}) / ((x_{2666} / x_{2866})) \\
x_{2877} &= (K_{2877} * x_{2667}) / ((x_{2666} / x_{2866}) * (x_{2666} / x_{2676})) \\
x_{2878} &= (K_{2878} * x_{2668}) / ((x_{2666} / x_{2866}) * (x_{2666} / x_{2676})) \\
x_{2886} &= (K_{2886} * x_{2686}) / ((x_{2666} / x_{2866}))
\end{aligned}$$

$$\begin{aligned}
x_{2887} &= (K_{2887} * x_{2667}) / ((x_{2666} / x_{2866}) * (x_{2666} / x_{2686})) \\
x_{2888} &= (K_{2888} * x_{2668}) / ((x_{2666} / x_{2866}) * (x_{2666} / x_{2686})) \\
x_{3667} &= (K_{3667} * x_{3666}) / ((x_{2666} / x_{2667})) \\
x_{3668} &= (K_{3668} * x_{3666}) / ((x_{2666} / x_{2668})) \\
x_{3676} &= (K_{3676} * x_{3666}) / ((x_{2666} / x_{2676})) \\
x_{3677} &= (K_{3677} * x_{3666}) / ((x_{2666} / x_{2676}) * (x_{2666} / x_{2667})) \\
x_{3678} &= (K_{3678} * x_{3666}) / ((x_{2666} / x_{2676}) * (x_{2666} / x_{2668})) \\
x_{3686} &= (K_{3686} * x_{3666}) / ((x_{2666} / x_{2686})) \\
x_{3687} &= (K_{3687} * x_{3666}) / ((x_{2666} / x_{2686}) * (x_{2666} / x_{2667})) \\
x_{3688} &= (K_{3688} * x_{3666}) / ((x_{2666} / x_{2686}) * (x_{2666} / x_{2668})) \\
x_{3766} &= (K_{3766} * x_{3666}) / ((x_{2666} / x_{2766})) \\
x_{3767} &= (K_{3767} * x_{3666}) / ((x_{2666} / x_{2766}) * (x_{2666} / x_{2667})) \\
x_{3768} &= (K_{3768} * x_{3666}) / ((x_{2666} / x_{2766}) * (x_{2666} / x_{2668})) \\
x_{3776} &= (K_{3776} * x_{3666}) / ((x_{2666} / x_{2766}) * (x_{2666} / x_{2676})) \\
x_{3777} &= (K_{3777} * x_{3666}) / ((x_{2666} / x_{2766}) \\
& \quad * (x_{2666} / x_{2676}) * (x_{2666} / x_{2667})) \\
x_{3778} &= (K_{3778} * x_{3666}) / ((x_{2666} / x_{2766}) \\
& \quad * (x_{2666} / x_{2676}) * (x_{2666} / x_{2668})) \\
x_{3786} &= (K_{3786} * x_{3666}) / ((x_{2666} / x_{2766}) * (x_{2666} / x_{2686})) \\
x_{3787} &= (K_{3787} * x_{3666}) / ((x_{2666} / x_{2766}) \\
& \quad * (x_{2666} / x_{2686}) * (x_{2666} / x_{2667})) \\
x_{3788} &= (K_{3788} * x_{3666}) / ((x_{2666} / x_{2766}) \\
& \quad * (x_{2666} / x_{2686}) * (x_{2666} / x_{2668})) \\
x_{3866} &= (K_{3866} * x_{3666}) / ((x_{2666} / x_{2866})) \\
x_{3867} &= (K_{3867} * x_{3666}) / ((x_{2666} / x_{2866}) * (x_{2666} / x_{2667})) \\
x_{3868} &= (K_{3868} * x_{3666}) / ((x_{2666} / x_{2866}) * (x_{2666} / x_{2668})) \\
x_{3876} &= (K_{3876} * x_{3666}) / ((x_{2666} / x_{2866}) * (x_{2666} / x_{2676})) \\
x_{3877} &= (K_{3877} * x_{3666}) / ((x_{2666} / x_{2866}) \\
& \quad * (x_{2666} / x_{2676}) * (x_{2666} / x_{2667})) \\
x_{3878} &= (K_{3878} * x_{3666}) / ((x_{2666} / x_{2866}) \\
& \quad * (x_{2666} / x_{2676}) * (x_{2666} / x_{2668})) \\
x_{3886} &= (K_{3886} * x_{3666}) / ((x_{2666} / x_{2866}) * (x_{2666} / x_{2686})) \\
x_{3887} &= (K_{3887} * x_{3666}) / ((x_{2666} / x_{2866}) \\
& \quad * (x_{2666} / x_{2686}) * (x_{2666} / x_{2667})) \\
x_{3888} &= (K_{3888} * x_{3666}) / ((x_{2666} / x_{2866}) \\
& \quad * (x_{2666} / x_{2686}) * (x_{2666} / x_{2668}))
\end{aligned}
\tag{A12}$$

The mass balance equations for the above system are as follows, where x_{16O} , x_{17O} , x_{18O} , x_{13C} , and x_{12C} are the relative abundances of ^{13}C , ^{12}C , ^{18}O , ^{17}O , and ^{16}O in the carbonate, such that

$$x_{12C} * x_{13C} = 1 \text{ and } x_{16O} * x_{17O} * x_{18O} = 1. \tag{A13}$$

Table A1

Δ_{63} , $\beta^{13}\text{C}$, composite $\beta^{18}\text{O}$, and composite $\beta^{17}\text{O}$ for the 3 DIC species, calcite lattice, and aragonite lattice from 0 °C to 1000 °C as calculated by the B3LYP/6-311++G(2d,2p) supermolecular models. DIC values are the averages of the set of 10 conformers for each species. Values are unscaled. Standard errors (se) are included for each set of supermolecular clusters (Fig. 3).

Temp (°C)	Δ_{63}	$\Delta_{63}\text{se}$	$\beta^{13}\text{C}$	$\beta^{13}\text{C se}$	Comp $\beta^{18}\text{O}$	Comp $\beta^{18}\text{O se}$	Comp $\beta^{17}\text{O}$	Comp $\beta^{17}\text{O se}$
<i>CO₃²⁻</i>								
0	0.4448	±0.0012	1.2289	±0.0004	1.1141	±0.0005	1.0588	±0.0003
10	0.4131	±0.0012	1.2163	±0.0004	1.1076	±0.0005	1.0555	±0.0002
20	0.3839	±0.0011	1.2048	±0.0004	1.1016	±0.0005	1.0525	±0.0002
22	0.3784	±0.0011	1.2026	±0.0004	1.1004	±0.0005	1.0519	±0.0002
25	0.3702	±0.0011	1.1993	±0.0004	1.0988	±0.0004	1.0511	±0.0002
30	0.3571	±0.0011	1.1941	±0.0004	1.0961	±0.0004	1.0497	±0.0002
40	0.3324	±0.0011	1.1843	±0.0004	1.0910	±0.0004	1.0471	±0.0002
50	0.3096	±0.0011	1.1753	±0.0004	1.0863	±0.0004	1.0448	±0.0002
60	0.2887	±0.0010	1.1668	±0.0003	1.0820	±0.0004	1.0426	±0.0002
70	0.2693	±0.0010	1.1590	±0.0003	1.0779	±0.0004	1.0405	±0.0002
80	0.2514	±0.0010	1.1517	±0.0003	1.0742	±0.0003	1.0386	±0.0002
90	0.2349	±0.0009	1.1449	±0.0003	1.0707	±0.0003	1.0368	±0.0002
100	0.2196	±0.0009	1.1386	±0.0003	1.0675	±0.0003	1.0352	±0.0002
200	0.1162	±0.0006	1.0927	±0.0002	1.0444	±0.0002	1.0233	±0.0001
300	0.0655	±0.0004	1.0661	±0.0002	1.0313	±0.0002	1.0165	±0.0001
400	0.0391	±0.0003	1.0494	±0.0001	1.0232	±0.0001	1.0122	±0.0001
500	0.0245	±0.0002	1.0382	±0.0001	1.0179	±0.0001	1.0094	±0.0000
600	0.0160	±0.0001	1.0304	±0.0001	1.0142	±0.0001	1.0075	±0.0000
700	0.0109	±0.0001	1.0248	±0.0001	1.0115	±0.0001	1.0061	±0.0000
800	0.0076	±0.0001	1.0205	±0.0001	1.0095	±0.0000	1.0050	±0.0000
900	0.0055	±0.0001	1.0173	±0.0001	1.0080	±0.0000	1.0042	±0.0000
1000	0.0040	±0.0000	1.0148	±0.0000	1.0068	±0.0000	1.0036	±0.0000
<i>HCO₃⁻</i>								
0	0.4816	±0.0014	1.2322	±0.0006	1.1242	±0.0004	1.0638	±0.0002
10	0.4483	±0.0014	1.2196	±0.0006	1.1173	±0.0004	1.0604	±0.0002
20	0.4177	±0.0013	1.2080	±0.0005	1.1110	±0.0004	1.0572	±0.0002
22	0.4119	±0.0013	1.2057	±0.0005	1.1097	±0.0004	1.0566	±0.0002
25	0.4033	±0.0013	1.2025	±0.0005	1.1080	±0.0004	1.0557	±0.0002
30	0.3895	±0.0012	1.1973	±0.0005	1.1051	±0.0003	1.0543	±0.0002
40	0.3636	±0.0012	1.1874	±0.0005	1.0997	±0.0003	1.0516	±0.0002
50	0.3396	±0.0012	1.1783	±0.0005	1.0948	±0.0003	1.0490	±0.0002
60	0.3174	±0.0011	1.1698	±0.0004	1.0901	±0.0003	1.0467	±0.0001
70	0.2969	±0.0011	1.1619	±0.0004	1.0859	±0.0003	1.0445	±0.0001
80	0.2779	±0.0010	1.1546	±0.0004	1.0819	±0.0003	1.0425	±0.0001
90	0.2604	±0.0010	1.1477	±0.0004	1.0782	±0.0002	1.0406	±0.0001
100	0.2440	±0.0010	1.1413	±0.0004	1.0747	±0.0002	1.0389	±0.0001
200	0.1323	±0.0007	1.0950	±0.0003	1.0499	±0.0001	1.0261	±0.0001
300	0.0759	±0.0005	1.0680	±0.0002	1.0356	±0.0001	1.0187	±0.0001
400	0.0459	±0.0003	1.0510	±0.0001	1.0267	±0.0001	1.0141	±0.0000
500	0.0290	±0.0002	1.0396	±0.0001	1.0207	±0.0001	1.0109	±0.0000
600	0.0191	±0.0002	1.0316	±0.0001	1.0166	±0.0000	1.0087	±0.0000
700	0.0130	±0.0001	1.0257	±0.0001	1.0135	±0.0000	1.0071	±0.0000
800	0.0092	±0.0001	1.0214	±0.0001	1.0112	±0.0000	1.0059	±0.0000
900	0.0066	±0.0001	1.0180	±0.0000	1.0095	±0.0000	1.0050	±0.0000
1000	0.0049	±0.0001	1.0154	±0.0000	1.0081	±0.0000	1.0043	±0.0000
<i>H₂CO₃</i>								
0	0.5161	±0.0017	1.2411	±0.0007	1.1366	±0.0005	1.0700	±0.0002
10	0.4814	±0.0017	1.2281	±0.0006	1.1292	±0.0004	1.0663	±0.0002
20	0.4494	±0.0016	1.2161	±0.0006	1.1223	±0.0004	1.0629	±0.0002
22	0.4433	±0.0016	1.2138	±0.0006	1.1210	±0.0004	1.0622	±0.0002
25	0.4344	±0.0016	1.2105	±0.0006	1.1191	±0.0004	1.0613	±0.0002
30	0.4199	±0.0015	1.2051	±0.0006	1.1160	±0.0004	1.0597	±0.0002
40	0.3927	±0.0015	1.1949	±0.0005	1.1102	±0.0004	1.0568	±0.0002
50	0.3675	±0.0014	1.1855	±0.0005	1.1048	±0.0003	1.0541	±0.0002
60	0.3442	±0.0014	1.1768	±0.0005	1.0998	±0.0003	1.0516	±0.0002
70	0.3226	±0.0013	1.1687	±0.0005	1.0951	±0.0003	1.0492	±0.0002
80	0.3026	±0.0013	1.1611	±0.0005	1.0908	±0.0003	1.0470	±0.0001
90	0.2840	±0.0012	1.1540	±0.0004	1.0868	±0.0003	1.0450	±0.0001

Table A1 (*continued*)

Temp (°C)	Δ_{63}	$\Delta_{63\text{Se}}$	$\beta^{13}\text{C}$	$\beta^{13}\text{C se}$	Comp $\beta^{18}\text{O}$	Comp $\beta^{18}\text{O se}$	Comp $\beta^{17}\text{O}$	Comp $\beta^{17}\text{O se}$
100	0.2667	±0.0012	1.1474	±0.0004	1.0830	±0.0003	1.0431	±0.0001
200	0.1470	±0.0009	1.0995	±0.0003	1.0559	±0.0002	1.0292	±0.0001
300	0.0855	±0.0006	1.0715	±0.0002	1.0402	±0.0001	1.0211	±0.0001
400	0.0522	±0.0004	1.0538	±0.0002	1.0303	±0.0001	1.0159	±0.0000
500	0.0333	±0.0003	1.0418	±0.0001	1.0236	±0.0001	1.0124	±0.0000
600	0.0220	±0.0002	1.0334	±0.0001	1.0189	±0.0000	1.0100	±0.0000
700	0.0151	±0.0002	1.0272	±0.0001	1.0155	±0.0000	1.0082	±0.0000
800	0.0106	±0.0001	1.0226	±0.0001	1.0129	±0.0000	1.0068	±0.0000
900	0.0077	±0.0001	1.0191	±0.0001	1.0109	±0.0000	1.0058	±0.0000
1000	0.0057	±0.0001	1.0163	±0.0000	1.0093	±0.0000	1.0049	±0.0000
Temp (°C)	Δ_{63}		$\beta^{13}\text{C}$		$\beta^{18}\text{O}$		$\beta^{17}\text{O}$	
<i>Calcite</i>								
0	0.4701		1.2384		1.1226		1.0630	
10	0.4378		1.2254		1.1155		1.0595	
20	0.4080		1.2134		1.1091		1.0562	
22	0.4024		1.2111		1.1078		1.0556	
25	0.3940		1.2078		1.1060		1.0547	
30	0.3805		1.2024		1.1031		1.0533	
40	0.3551		1.1922		1.0977		1.0505	
50	0.3316		1.1827		1.0926		1.0480	
60	0.3098		1.1740		1.0880		1.0456	
70	0.2897		1.1659		1.0836		1.0434	
80	0.2710		1.1583		1.0796		1.0414	
90	0.2537		1.1513		1.0759		1.0395	
100	0.2376		1.1447		1.0724		1.0377	
200	0.1276		1.0970		1.0476		1.0249	
300	0.0726		1.0693		1.0336		1.0177	
400	0.0435		1.0518		1.0249		1.0131	
500	0.0273		1.0401		1.0192		1.0101	
600	0.0179		1.0319		1.0152		1.0080	
700	0.0122		1.0260		1.0123		1.0065	
800	0.0085		1.0216		1.0102		1.0054	
900	0.0061		1.0182		1.0086		1.0045	
1000	0.0045		1.0155		1.0073		1.0039	
<i>Aragonite</i>								
0	0.4831		1.2420		1.1242		1.0638	
10	0.4504		1.2288		1.1171		1.0603	
20	0.4202		1.2167		1.1105		1.0570	
22	0.4144		1.2144		1.1093		1.0564	
25	0.4060		1.2110		1.1075		1.0554	
30	0.3923		1.2055		1.1045		1.0540	
40	0.3664		1.1952		1.0990		1.0512	
50	0.3425		1.1856		1.0939		1.0486	
60	0.3203		1.1768		1.0892		1.0462	
70	0.2998		1.1685		1.0848		1.0440	
80	0.2807		1.1608		1.0807		1.0419	
90	0.2630		1.1537		1.0770		1.0400	
100	0.2465		1.1470		1.0734		1.0382	
200	0.1333		1.0986		1.0483		1.0253	
300	0.0762		1.0705		1.0341		1.0179	
400	0.0458		1.0528		1.0253		1.0133	
500	0.0289		1.0409		1.0195		1.0103	
600	0.0190		1.0326		1.0154		1.0082	
700	0.0129		1.0265		1.0125		1.0066	
800	0.0090		1.0220		1.0104		1.0055	
900	0.0065		1.0185		1.0087		1.0046	
1000	0.0048		1.0158		1.0074		1.0039	

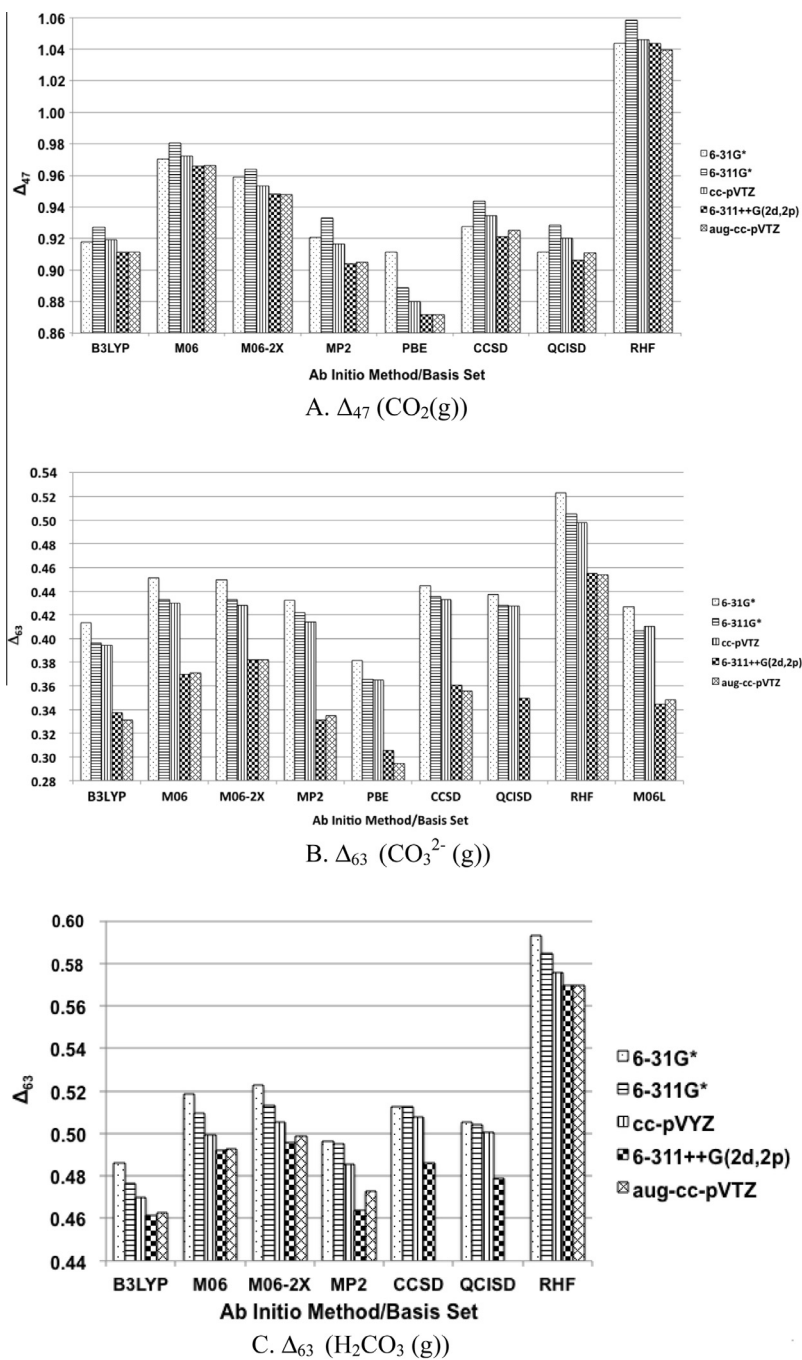


Fig. A1. Results of convergence study: comparison of Δ_{47}/Δ_{63} calculated by different combinations of ab initio/hybrid methods and basis sets (Table A2). (A) Δ_{47} ($\text{CO}_2(\text{g})$) (B) Δ_{63} ($\text{CO}_3^{2-}(\text{g})$) (C) Δ_{63} ($\text{H}_2\text{CO}_3(\text{g})$) (D) Δ_{63} ($\text{HCO}_3^- * 3(\text{H}_2\text{O})$) (E) Δ_{63} ($\text{H}_2\text{CO}_3 * 3(\text{H}_2\text{O})$).

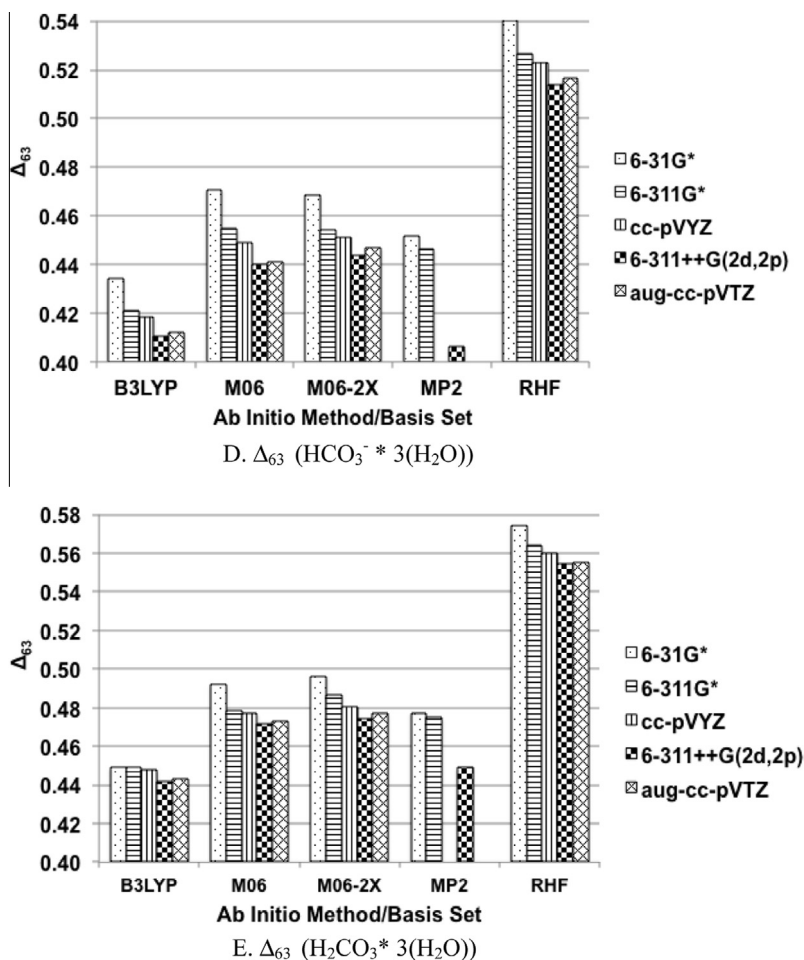


Fig A1. (continued)

$$\begin{aligned}
 & \underline{x2666} + \underline{x2766} + \underline{x2866} + \underline{x3666} + \underline{x2667} + \underline{x2668} \\
 & + \underline{x2676} + \underline{x2677} + \underline{x2678} + \underline{x2686} + \underline{x2687} + \underline{x2688} \\
 & + \underline{x2767} + \underline{x2768} + \underline{x2776} + \underline{x2777} + \underline{x2778} + \underline{x2786} \\
 & + \underline{x2787} + \underline{x2788} + \underline{x2867} + \underline{x2868} + \underline{x2876} + \underline{x2877} \\
 & + \underline{x2878} + \underline{x2886} + \underline{x2887} + \underline{x2888} + \underline{x3667} + \underline{x3668} \\
 & + \underline{x3676} + \underline{x3677} + \underline{x3678} + \underline{x3686} + \underline{x3687} + \underline{x3688} \\
 & + \underline{x3766} + \underline{x3767} + \underline{x3768} + \underline{x3776} + \underline{x3777} + \underline{x3778} \\
 & + \underline{x3786} + \underline{x3787} + \underline{x3788} + \underline{x3866} + \underline{x3867} + \underline{x3868} \\
 & + \underline{x3876} + \underline{x3877} + \underline{x3878} + \underline{x3886} + \underline{x3887} + \underline{x3888} = 1
 \end{aligned}
 \tag{A14}$$

$$\begin{aligned}
 & \underline{x3666} + \underline{x3667} + \underline{x3668} + \underline{x3676} + \underline{x3677} + \underline{x3678} \\
 & + \underline{x3686} + \underline{x3687} + \underline{x3688} + \underline{x3766} + \underline{x3767} + \underline{x3768} \\
 & + \underline{x3776} + \underline{x3777} + \underline{x3778} + \underline{x3786} + \underline{x3787} + \underline{x3788} \\
 & + \underline{x3866} + \underline{x3867} + \underline{x3868} + \underline{x3876} + \underline{x3877} + \underline{x3878} \\
 & + \underline{x3886} + \underline{x3887} + \underline{x3888} = \underline{x13C}
 \end{aligned}
 \tag{A15}$$

$$\begin{aligned}
 & 3 * \underline{x2666} + 2 * \underline{x2766} + 2 * \underline{x2866} + 3 * \underline{x3666} + 2 * \underline{x2667} \\
 & + 2 * \underline{x2668} + 2 * \underline{x2676} + \underline{x2677} + \underline{x2678} + 2 * \underline{x2686} \\
 & + \underline{x2687} + \underline{x2688} + \underline{x2767} + \underline{x2768} + \underline{x2776} + \underline{x2786} \\
 & + \underline{x2867} + \underline{x2868} + \underline{x2876} + \underline{x2886} + 2 * \underline{x3667} \\
 & + 2 * \underline{x3668} + 2 * \underline{x3676} + \underline{x3677} + \underline{x3678} + 2 * \underline{x3686} \\
 & + \underline{x3687} + \underline{x3688} + 2 * \underline{x3766} + \underline{x3767} + \underline{x3768} + \underline{x3776} \\
 & + \underline{x3786} + 2 * \underline{x3866} + \underline{x3867} + \underline{x3868} + \underline{x3876} \\
 & + \underline{x3886} = 3 * \underline{x16O}
 \end{aligned}
 \tag{A16}$$

$$\begin{aligned}
 & \underline{x2866} + \underline{x2668} + \underline{x2678} + \underline{x2686} + \underline{x2687} + 2 * \underline{x2688} \\
 & + \underline{x2768} + \underline{x2778} + \underline{x2786} + \underline{x2787} + 2 * \underline{x2788} + \underline{x2867} \\
 & + 2 * \underline{x2868} + \underline{x2876} + \underline{x2877} + 2 * \underline{x2878} + 2 * \underline{x2886} \\
 & + 2 * \underline{x2887} + 3 * \underline{x2888} + \underline{x3668} + \underline{x3678} + \underline{x3686} \\
 & + \underline{x3687} + 2 * \underline{x3688} + \underline{x3768} + \underline{x3778} + \underline{x3786} \\
 & + \underline{x3787} + 2 * \underline{x3788} + \underline{x3866} + \underline{x3867} + 2 * \underline{x3868} \\
 & + \underline{x3876} + \underline{x3877} + 2 * \underline{x3878} + 2 * \underline{x3886} \\
 & + 2 * \underline{x3887} + 3 * \underline{x3888} = 3 * \underline{x18O}
 \end{aligned}
 \tag{A17}$$

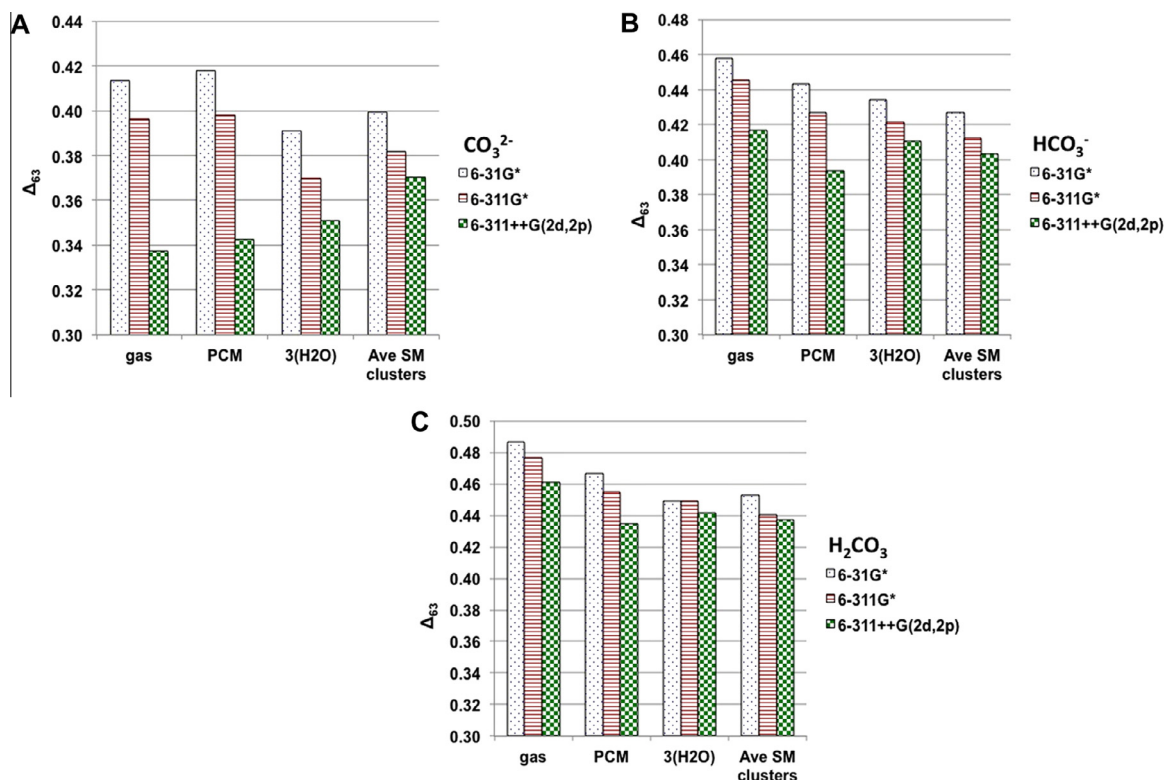


Fig. A2. Comparison of Δ_{63} calculated using 4 different solvation techniques using B3LYP models with 3 different Pople basis sets (Table A3). (A) $\Delta_{63}(\text{CO}_3^{2-})$, (B) $\Delta_{63}(\text{HCO}_3^-)$, (C) $\Delta_{63}(\text{H}_2\text{CO}_3)$.

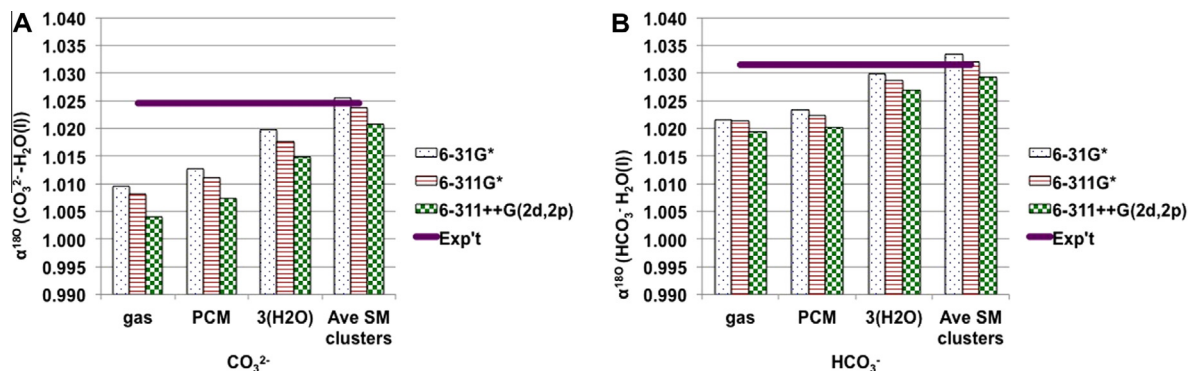


Fig. A3. Results of the oxygen isotope fractionation test in which the predicted fractionation between (A) CO_3^{2-} and liquid water $\{\alpha^{18\text{O}}(\text{CO}_3^{2-} - \text{H}_2\text{O}(l))\}$ and between (B) HCO_3^- and liquid water $\{\alpha^{18\text{O}}(\text{HCO}_3^- - \text{H}_2\text{O}(l))\}$ are compared to experimental data from Beck et al. (2005) (Table 3). The purple horizontal lines represent the experimental data for each fractionation. Values for the supermolecular clusters (far right) are the averages of sets of 10 individual conformers (Tables 1 and A3, col. 7). (For interpretation of the references to color in this figure legend, the reader is referred to the web version of this article.)

Eq. (A14) sets the sum of all the isotopomer relative abundances to unity. Eq (A15) - (A17) set the sum of all isotopomers containing ^{13}C or ^{16}O or ^{18}O to the total fractional amount of the relative isotope in the carbonate phase. Note that isotopomers containing multiple isotopes are counted more than once; for example, $^{12}\text{C}^{16}\text{O}^{18}\text{O}^{18}\text{O}$ is counted twice in Eq. (A17).

The abundance of an isotopologue with more than one isotopomer is the sum of the abundances of each

isotopomer (whether its isotopomers are distinct or not); for example,

$$x_{3866} = x_{\underline{3866}} + x_{\underline{3686}} + x_{\underline{3668}} \quad (\text{A18})$$

Note that the direction of the isotope exchange reaction equations in Wang et al. (2004) is set up in the reverse order of later papers listing the exchange reactions, such as Schauble et al. (2006); Guo et al. (2009), and this work.

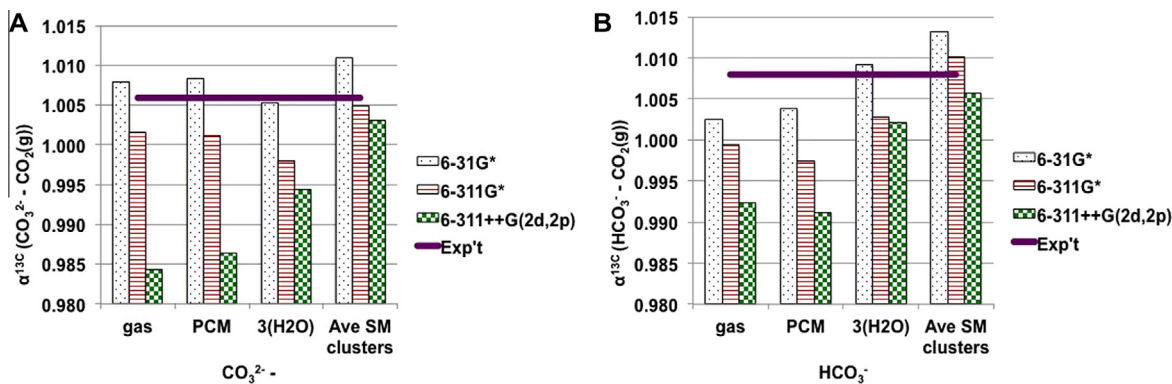


Fig. A4. Results of the carbon isotope fractionation test in which the predicted fractionation between (A) CO_3^{2-} and $\text{CO}_2(\text{g})$ $\{\alpha^{13\text{C}}(\text{CO}_3^{2-} - \text{CO}_2(\text{g}))\}$ and between (B) HCO_3^- and $\text{CO}_2(\text{g})$ $\{\alpha^{13\text{C}}(\text{HCO}_3^- - \text{CO}_2(\text{g}))\}$ are compared to experimental data from Zhang et al. (1995) (Table 4). The horizontal purple lines represent the experimental data for each fractionation. Values for the supermolecular clusters (far right) are the averages of sets of 10 individual conformers. (Tables 1 and A3, col. 8). (For interpretation of the references to color in this figure legend, the reader is referred to the web version of this article.)

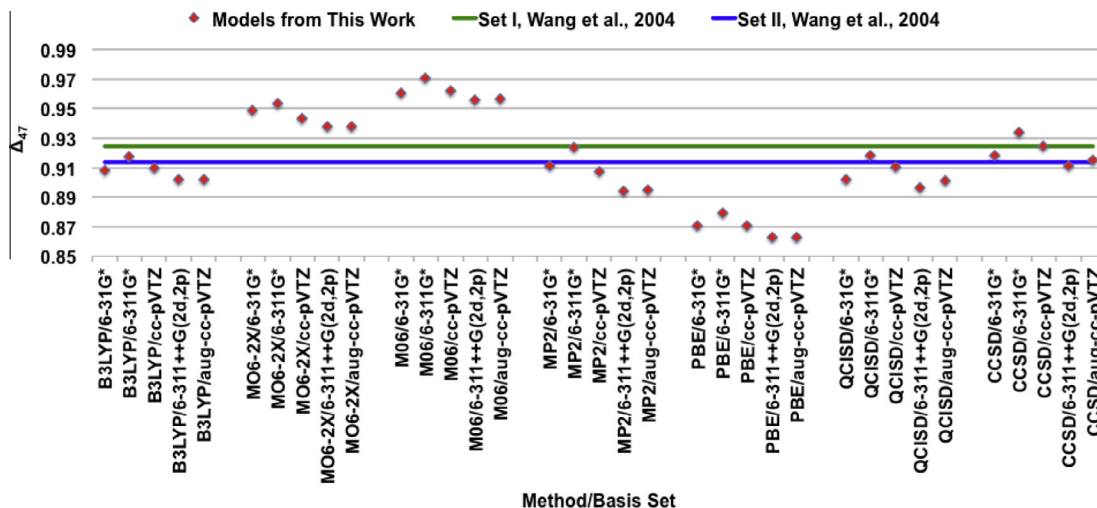


Fig. A5. Comparison of $\Delta_{47}(\text{CO}_2(\text{g}))$ at $T = 300 \text{ K}$ (26.85°C) predicted by several models from this study with the two models presented in Wang et al. (2004). The B3LYP, MP2, QCISD, and CCSD models are the best fit with the Wang et al. models (Table A8).

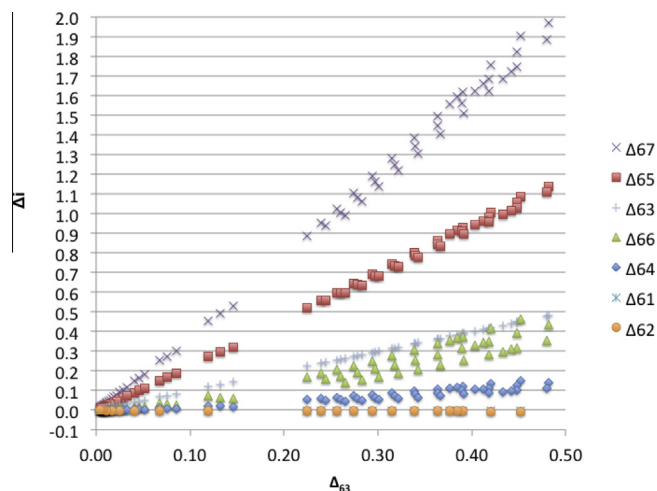


Fig. A6. Relationship between Δ_{63} and the other Δ_i for the 3 DIC supermolecular cluster models from B3LYP/6-311++G(2d,2p) from the temperature range 0 to 1000°C . Gaps in the graph are due to larger increments between temperature when $T > 100^\circ\text{C}$ (see Table B.3 in Appendix B, the Electronic supplement).

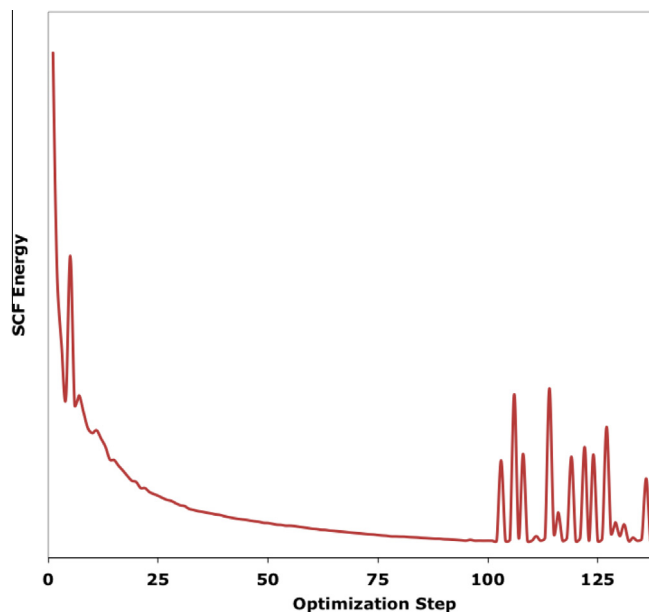


Fig. A7. Sample SCF energy plot versus a series of optimization steps in the process of searching for an optimized geometry for a supermolecular cluster containing a carbonate ion surrounded by 21 waters. After about 100 optimization iterations, the computational chemistry program is oscillating around a minimum energy point, having trouble finding the local minimum energy geometry due to the flatness of the potential energy field. User intervention is required to help the optimization converge (see Sections 2.5 and A.4).

Table A2

Results of convergence study. Comparison of Δ_{47} , Δ_{63} , $\beta^{13}\text{C}$, and $\beta^{18}\text{O}$, at 25 °C for selected species calculated using different combinations of ab initio/hybrid methods and basis sets (see Fig. A1A–E and Sections 2.5, 3.1.1 and A.2.1). Values are unscaled.

Method/Basis set	Δ_{47}	$\beta^{13}\text{C}$	ave $\beta^{18}\text{O}$
CO ₂ (g)			
B3LYP/SDD	0.826	1.178	1.108
B3LYP/6-31G*	0.918	1.194	1.120
B3LYP/6-311G*	0.927	1.197	1.121
B3LYP/cc-pVTZ	0.919	1.197	1.121
B3LYP/6-311++G(2d,2p)	0.912	1.196	1.120
B3LYP/aug-cc-pVTZ	0.911	1.196	1.120
M06/6-31G*	0.971	1.205	1.125
M06/6-311G*	0.981	1.208	1.126
M06/cc-pVTZ	0.972	1.207	1.126
M06/6-311++G(2d,2p)	0.966	1.206	1.125
M06/aug-cc-pVTZ	0.966	1.206	1.126
6-2X/6-31G*	0.959	1.202	1.126
M06-2X/6-311G*	0.964	1.205	1.126
M06-2X/cc-pVTZ	0.953	1.203	1.125
M06-2X/6-311++G(2d,2p)	0.948	1.203	1.125
M06-2X/aug-cc-pVTZ	0.948	1.203	1.125
MP2/6-31G*	0.921	1.195	1.117
MP2/6-311G*	0.933	1.198	1.119
MP2/cc-pVTZ	0.917	1.195	1.117
MP2/6-311++G(2d,2p)	0.904	1.194	1.116
MP2/aug-cc-pVTZ	0.905	1.194	1.116
CCSD/6-31G*	0.928	1.197	1.122
CCSD/6-311G*	0.944	1.201	1.123
CCSD/cc-pVTZ	0.934	1.200	1.123
CCSD/6-311++G(2d,2p)	0.921	1.198	1.121
CCSD/aug-cc-pVTZ	0.925	1.199	1.122

Table A2 (continued)

CO ₂ (g)			
Method/Basis set	Δ_{47}	$\beta^{13}\text{C}$	ave $\beta^{18}\text{O}$
QCISD/6-31G*	0.911	1.194	1.119
QCISD/6-311G*	0.928	1.198	1.121
QCISD/cc-pVTZ	0.920	1.197	1.121
QCISD/6-311++G(2d,2p)	0.906	1.196	1.119
QCISD/aug-cc-pVTZ	0.911	1.196	1.120
PBE/6-31G*	0.880	1.186	1.114
PBE/6-311G*	0.889	1.190	1.115
PBE/cc-pVTZ	0.880	1.189	1.115
PBE/6-311++G(2d,2p)	0.872	1.187	1.114
PBE/aug-cc-pVTZ	0.872	1.187	1.114
RHF/6-31G*	1.044	1.221	1.138
RHF/6-311G*	1.058	1.224	1.139
RHF/cc-pVTZ	1.046	1.223	1.138
RHF/6-311++G(2d,2p)	1.044	1.223	1.137
RHF/aug-cc-pVTZ	1.039	1.222	1.137
CO ₃ ²⁻ (g)			
Method/Basis set	Δ_{63}	R3666 ($\beta^{13}\text{C}$)	ave R2866 ($\beta^{18}\text{O}$)
B3LYP/SDD	0.347	1.180	1.076
B3LYP/6-31G*	0.413	1.204	1.086
B3LYP/6-311G*	0.396	1.199	1.085
B3LYP/cc-pVTZ	0.394	1.198	1.086
B3LYP/6-311++G(2d,2p)	0.337	1.177	1.081
B3LYP/aug-cc-pVTZ	0.331	1.174	1.080
M06/6-31G*	0.451	1.215	1.091
M06/6-311G*	0.433	1.210	1.090
M06/cc-pVTZ	0.430	1.208	1.091
M06/6-311++G(2d,2p)	0.370	1.187	1.085
M06/aug-cc-pVTZ	0.371	1.187	1.086
M06-2X/6-311G*	0.450	1.215	1.091
M06-2X/6-31G*	0.433	1.211	1.090
M06-2X/cc-pVTZ	0.428	1.209	1.090
M06-2X/6-311++G(2d,2p)	0.382	1.193	1.087
M06-2X/aug-cc-pVTZ	0.382	1.192	1.087
MP2/6-31G*	0.433	1.209	1.088
MP2/6-311G*	0.422	1.207	1.088
MP2/cc-pVTZ	0.414	1.203	1.087
MP2/6-311++G(2d,2p)	0.331	1.175	1.080
MP2/aug-cc-pVTZ	0.335	1.175	1.081
CCSD/6-31G*	0.444	1.214	1.090
CCSD/6-311G*	0.435	1.212	1.090
CCSD/cc-pVTZ	0.433	1.211	1.090
CCSD/6-311++G(2d,2p)	0.361	1.186	1.084
CCSD/aug-cc-pVTZ	0.356	1.182	1.083
QCISD/6-31G*	0.437	1.212	1.088
QCISD/6-311G*	0.428	1.210	1.089
QCISD/cc-pVTZ	0.428	1.209	1.089
QCISD/6-311++G(2d,2p)	0.349	1.182	1.082
QCISD/aug-cc-pVTZ			
RHF/6-31G*	0.523	1.243	1.102
RHF/6-311G*	0.505	1.238	1.101
RHF/cc-pVTZ	0.498	1.235	1.101
RHF/6-311++G(2d,2p)	0.455	1.220	1.098
RHF/aug-cc-pVTZ	0.454	1.220	1.098

Table A2 (continued)

M06L/6-31G*	0.427	1.207	1.087
M06L/6-311G*	0.407	1.201	1.086
M06L/cc-pVTZ	0.410	1.202	1.087
M06L/6-311++G(2d,2p)	0.345	1.179	1.082
M06L/aug-cc-pVTZ	0.348	1.179	1.083
PBE/6-31G*	0.382	1.192	1.081
PBE/6-311G*	0.366	1.188	1.080
PBE/cc-pVTZ	0.365	1.187	1.081
PBE/6-311++G(2d,2p)	0.305	1.163	1.075
PBE/aug-cc-pVTZ	0.294	1.158	1.075
$\text{H}_2\text{CO}_3(\text{g})$			
Method/Basis set	Δ_{63}	R3666 ($\beta^{13}\text{C}$)	ave R2866 ($\beta^{18}\text{O}$)
B3LYP/SDD	0.414	1.190	1.105
B3LYP/6-31G*	0.486	1.214	1.116
B3LYP/6-311G*	0.477	1.212	1.116
B3LYP/cc-pVTZ	0.470	1.210	1.115
B3LYP/6-311++G(2d,2p)	0.461	1.208	1.115
B3LYP/aug-cc-pVTZ	0.462	1.208	1.115
M06/6-31G*	0.518	1.223	1.121
M06/6-311G*	0.509	1.221	1.121
M06/cc-pVTZ	0.500	1.218	1.120
M06/6-311++G(2d,2p)	0.492	1.217	1.120
M06/aug-cc-pVTZ	0.493	1.216	1.119
M06-2X/6-31G*	0.523	1.225	1.122
M06-2X/6-311G*	0.513	1.223	1.122
M06-2X/cc-pVTZ	0.506	1.221	1.121
M06-2X/6-311++G(2d,2p)	0.496	1.218	1.120
M06-2X/aug-cc-pVTZ	0.499	1.219	1.120
MP2/6-31G*	0.496	1.217	1.117
MP2/6-311G*	0.495	1.218	1.119
MP2/cc-pVTZ	0.486	1.215	1.117
MP2/6-311++G(2d,2p)	0.464	1.209	1.115
MP2/aug-cc-pVTZ	0.473	1.211	1.115
CCSD/6-31G*	0.512	1.223	1.119
CCSD/6-311G*	0.512	1.224	1.121
CCSD/cc-pVTZ	0.508	1.223	1.120
CCSD/6-311++G(2d,2p)	0.486	1.217	1.118
QCISD/6-31G*	0.505	1.221	1.118
QCISD/6-311G*	0.504	1.221	1.120
QCISD/6-311++G(2d,2p)	0.479	1.215	1.117
QCISD/cc-pVTZ	0.501	1.221	1.119
RHF/6-31G*	0.593	1.252	1.136
RHF/6-311G*	0.585	1.250	1.137
RHF/cc-pVTZ	0.576	1.248	1.135
RHF/6-311++G(2d,2p)	0.570	1.247	1.135
RHF/aug-cc-pVTZ	0.570	1.246	1.135
$\text{HCO}_3^- \cdot 3(\text{H}_2\text{O})$			
Method/Basis set	Δ_{63}	R3666 ($\beta^{13}\text{C}$)	ave R2866 ($\beta^{18}\text{O}$)
B3LYP/6-31G*	0.434	1.205	1.108
B3LYP/6-311G*	0.421	1.201	1.107
B3LYP/cc-pVTZ	0.418	1.201	1.106
B3LYP/6-311++G(2d,2p)	0.410	1.198	1.105
B3LYP/aug-cc-pVTZ	0.412	1.199	1.106
M06/6-31G*	0.471	1.215	1.113
M06/6-311G*	0.455	1.210	1.112
M06/cc-pVTZ	0.449	1.209	1.111

Table A2 (continued)

Method/Basis set	Δ_{63}	R3666 ($\beta^{13}\text{C}$)	ave R2866 ($\beta^{18}\text{O}$)
M06/6-311++G(2d,2p)	0.440	1.207	1.110
M06/aug-cc-pVTZ	0.441	1.206	1.111
M06-2X/6-31G*	0.468	1.216	1.113
M06-2X/6-311G*	0.454	1.212	1.113
M06-2X/cc-pVTZ	0.451	1.212	1.112
M06-2X/6-311++G(2d,2p)	0.444	1.210	1.111
M06-2X/aug-cc-pVTZ	0.447	1.210	1.112
MP2/6-31G*	0.452	1.208	1.108
MP2/6-311G*	0.446	1.207	1.109
MP2/6-311++G(2d,2p)	0.406	1.199	1.107
RHF/6-31G*	0.540	1.242	1.125
RHF/6-311G*	0.527	1.239	1.124
RHF/cc-pVTZ	0.523	1.238	1.123
RHF/6-311++G(2d,2p)	0.514	1.236	1.122
RHF/aug-cc-pVTZ	0.516	1.236	1.122
$\text{H}_2\text{CO}_3^* \cdot 3(\text{H}_2\text{O})$			
Method/Basis set	Δ_{63}	R3666 ($\beta^{13}\text{C}$)	ave R2866 ($\beta^{18}\text{O}$)
B3LYP/6-31G*	0.449	1.212	1.120
B3LYP/6-311G*	0.449	1.212	1.120
B3LYP/cc-pVTZ	0.448	1.211	1.119
B3LYP/6-311++G(2d,2p)	0.442	1.210	1.119
B3LYP/aug-cc-pVTZ	0.443	1.210	1.119
M06/6-31G*	0.492	1.224	1.126
M06/6-311G*	0.478	1.221	1.126
M06/cc-pVTZ	0.477	1.220	1.125
M06/6-311++G(2d,2p)	0.472	1.218	1.124
M06/aug-cc-pVTZ	0.473	1.218	1.124
M06-2X/6-31G*	0.496	1.224	1.125
M06-2X/6-311G*	0.487	1.222	1.126
M06-2X/cc-pVTZ	0.480	1.221	1.124
M06-2X/6-311++G(2d,2p)	0.474	1.219	1.123
M06-2X/aug-cc-pVTZ	0.477	1.219	1.123
MP2/6-31G*	0.477	1.219	1.121
MP2/6-311G*	0.475	1.219	1.123
MP2/6-311++G(2d,2p)	0.449	1.212	1.119
RHF/6-31G*	0.574	1.253	1.140
RHF/6-311G*	0.564	1.250	1.140
RHF/cc-pVTZ	0.560	1.250	1.138
RHF/6-311++G(2d,2p)	0.554	1.248	1.137
RHF/aug-cc-pVTZ	0.555	1.248	1.137

A.1.3. Calculation of stochastic abundances for a carbonate phase

The stochastic isotopomer abundances (i.e., the denominator in Eq. (2)) do not depend upon temperature since they are determined from the isotopic makeup of the carbonate and the probability of the occurrence of each isotopologue within that configuration. For example, let $x_{13\text{C}}$ and $x_{12\text{C}}$ represent the relative abundances of ^{13}C and ^{12}C respectively in the carbonate, and similarly $x_{18\text{O}}$, $x_{17\text{O}}$, and $x_{16\text{O}}$, the relative amounts of ^{18}O , ^{17}O , and ^{16}O in the carbonate, such that $x_{12\text{C}} \cdot x_{13\text{C}} = 1$ and $x_{16\text{O}} \cdot x_{17\text{O}} \cdot x_{18\text{O}} = 1$. Then

$$x_{2666-r} = x_{12\text{C}} \cdot x_{16\text{O}} \cdot x_{16\text{O}} \cdot x_{16\text{O}} \quad (\text{A19})$$

$$x_{3866-r} = 3 \cdot (x_{13\text{C}} \cdot x_{18\text{O}} \cdot x_{16\text{O}} \cdot x_{16\text{O}}) \quad (\text{A20})$$

etc.

where x_{2666-r} = the stochastic (i.e., random) abundance of $^{12}\text{C}^{16}\text{O}_3$ and x_{3866-r} = the stochastic abundance of $^{13}\text{C}^{18}\text{O}^{16}\text{O}_2$, etc. The factor of 3 in Eq. (A20) reflects the assumption that all three isotopomers of x_{3866} have an equal chance of being chosen in a random distribution.

A.2. Convergence/sensitivity testing results: Choice of the best ab initio modeling techniques for clumped isotope signatures of aqueous DIC species

A.2.1. Ab initio/hybrid methods – basis set combinations

We compared values of Δ_{63} , $\beta^{13}\text{C}$, and $\beta^{18}\text{O}$ calculated by different levels of theory for $\text{CO}_2(\text{g})$, $\text{CO}_3^{2-}(\text{g})$, $\text{H}_2\text{CO}_3(\text{g})$, $\text{HCO}_3^- \cdot 3(\text{H}_2\text{O})$, and $\text{H}_2\text{CO}_3^* \cdot 3(\text{H}_2\text{O})$ (Table A1, Section 2.5). Each ab initio/hybrid method

Table A3

Comparison of Δ_{63} , $\beta^{13}\text{C}$, and composite $\beta^{18}\text{O}$, and as calculated using the four solvation techniques with B3LYP and 3 different Pople basis sets at 25 °C (see Fig. A2A–C). Also included are the oxygen fractionation between DIC species and water ($\alpha^{18\text{O}}(\text{DIC}^- \text{H}_2\text{O}(l))$); carbon isotope fractionation between DIC species and $\text{CO}_2(\text{g})$ ($\alpha^{18\text{O}}(\text{DIC}^- \text{CO}_2(\text{g}))$); and the difference between the two sides of the Redlich Teller product rule (Eq. (15)) (RT diff). $\alpha^{18\text{O}}(\text{CO}_3^{2-} \text{H}_2\text{O}(l))$ and $\alpha^{13\text{C}}(\text{CO}_3^{2-} \text{CO}_2(\text{g}))$ are compared with experimental values from Beck et al. (2005) (Table 4, Fig. A3) and Zhang et al. (1995) (Table 5, Fig. A4) respectively. E-nn notation is equivalent to 10^{-nn} . Values are unscaled.

CO_3^{2-}							
Solvation technique	Method/Basis Set	$\beta^{13}\text{C}$	Comp $\beta^{18}\text{O}$	Δ_{63}	RT diff	$\alpha^{18\text{O}}(\text{CO}_3^{2-} \text{H}_2\text{O}(l))$	$\alpha^{13\text{C}}(\text{CO}_3^{2-} \text{CO}_2(\text{g}))$
Gas	B3LYP/6-31G*	1.204	1.086	0.413	3.7E-07	1.0096	1.0080
	B3LYP/6-311G*	1.199	1.085	0.396	6.2E-07	1.0082	1.0015
	B3LYP/6-311++G(2d,2p)	1.177	1.081	0.337	3.8E-07	1.0040	0.9843
Implicit	B3LYP/6-31G*	1.204	1.089	0.418	8.6E-07	1.0128	1.0084
	B3LYP/6-311G*	1.199	1.088	0.398	7.8E-07	1.0112	1.0012
	B3LYP/6-311++G(2d,2p)	1.179	1.084	0.343	6.4E-07	1.0073	0.9864
Explicit	B3LYP/6-31G*	1.200	1.097	0.391	-1.1E-06	1.0198	1.0052
	B3LYP/6-311G*	1.195	1.095	0.370	1.5E-06	1.0177	0.9980
	B3LYP/6-311++G(2d,2p)	1.189	1.092	0.351	1.2E-06	1.0148	0.9943
Average of supermolecular clusters	B3LYP/6-31G*	1.2072	1.1029	0.3992	-1.8E-04	1.0256	1.0109
	standard error	0.0004	0.0003	0.0013	3.9E-05	0.0003	0.0003
	B3LYP/6-311G*	1.2033	1.1015	0.3818	2.0E-04	1.0237	1.0049
	standard error	0.0003	0.0003	0.0014	4.2E-05	0.0003	0.0003
	B3LYP/6-311++G(2d,2p)	1.1993	1.0988	0.3702	-1.5E-04	1.0209	1.0030
standard error	0.0004	0.0004	0.0011	4.3E-05	0.0004	0.0003	
HCO_3^-							
Solvation technique	Method/Basis Set	$\beta^{13}\text{C}$	Comp $\beta^{18}\text{O}$	Δ_{63}	RT diff	$\alpha^{18\text{O}}(\text{CO}_3^{2-} \text{H}_2\text{O}(l))$	$\alpha^{13\text{C}}(\text{CO}_3^{2-} \text{CO}_2(\text{g}))$
Gas	B3LYP/6-31G*	1.201	1.099	0.458	-4.0E-04	1.0216	1.0026
	B3LYP/6-311G*	1.197	1.099	0.446	-3.7E-04	1.0213	0.9995
	B3LYP/6-311++G(2d,2p)	1.188	1.097	0.417	-3.7E-04	1.0194	0.9923
Implicit	B3LYP/6-31G*	1.199	1.101	0.443	-2.9E-04	1.0234	1.0038
	B3LYP/6-311G*	1.194	1.100	0.427	-3.0E-04	1.0224	0.9974
	B3LYP/6-311++G(2d,2p)	1.185	1.098	0.394	-2.6E-04	1.0202	0.9912
Explicit	B3LYP/6-31G*	1.205	1.108	0.434	-1.6E-05	1.0299	1.0092
	B3LYP/6-311G*	1.201	1.107	0.421	-2.0E-05	1.0287	1.0028
	B3LYP/6-311++G(2d,2p)	1.198	1.105	0.410	-4.9E-07	1.0268	1.0022
Average of supermolecular clusters	B3LYP/6-31G*	1.2098	1.1114	0.4268	-4.2E-04	1.0334	1.0132
	standard error	0.0006	0.0004	0.0017	1.5E-04	0.0004	0.0005
	B3LYP/6-311G*	1.2062	1.1106	0.4124	-2.9E-04	1.0321	1.0102
	standard error	0.0006	0.0004	0.0017	9.2E-05	0.0004	0.0005
	B3LYP/6-311++G(2d,2p)	1.2025	1.1080	0.4033	-5.8E-04	1.0293	1.0057
standard error	0.0005	0.0004	0.0013	2.1E-04	0.0003	0.0004	
H_2CO_3							
Solvation technique	Method/Basis set	$\beta^{13}\text{C}$	Comp $\beta^{18}\text{O}$	Δ_{63}	RT diff		
Gas	B3LYP/6-31G*	1.214	1.116	0.486	-2.4E-04		
	B3LYP/6-311G*	1.212	1.116	0.477	-2.6E-04		
	B3LYP/6-311++G(2d,2p)	1.208	1.115	0.461	-2.4E-04		
Implicit	B3LYP/6-31G*	1.210	1.116	0.467	-2.0E-04		
	B3LYP/6-311G*	1.207	1.116	0.455	-2.1E-04		
	B3LYP/6-311++G(2d,2p)	1.202	1.114	0.435	-2.0E-04		

Table A3 (continued)

Explicit	B3LYP/6-31G*	1.212	1.120	0.449	−4.6E−05
	B3LYP/6-311G*	1.212	1.120	0.449	−4.9E−05
	B3LYP/6-311++G(2d,2p)	1.210	1.119	0.442	−8.6E−05
Average of supermolecular clusters	B3LYP/6-31G*	1.2160	1.1210	0.4522	−2.5E−04
	standard error	0.0004	0.0004	0.0012	6.6E−05
	B3LYP/6-311G*	1.2130	1.1211	0.4413	−2.9E−04
	standard error	0.0005	0.0004	0.0017	8.5E−05
	B3LYP/6-311++G(2d,2p)	1.2105	1.1191	0.4344	−3.3E−04
standard error	0.0006	0.0004	0.0016	9.9E−05	
Calcite cluster					
	Method/Basis set	$\beta^{13}\text{C}$	Comp $\beta^{18}\text{O}$	Δ_{63}	
	B3LYP/6-31G*	1.2174	1.113	0.435	
	B3LYP/6-311G*	1.2107	1.109	0.406	
	B3LYP/6-311++G(2d,2p)	1.2077	1.106	0.394	
Aragonite cluster					
	Method/Basis set	$\beta^{13}\text{C}$	Comp $\beta^{18}\text{O}$	Δ_{63}	
	B3LYP/6-31G*	1.2194	1.1120	0.4385	
	B3LYP/6-311G*	1.2130	1.1086	0.4161	
	B3LYP/6-311++G(2d,2p)	1.2110	1.1075	0.4060	

was paired with 3 to 5 basis sets of different complexities. These comparisons show that for models using the same ab initio method, the use of increasingly complex basis sets (i.e., adding polarity and then diffuse functions) lowers Δ_{63} . In general, Δ_{63} (6-31G*) > Δ_{63} (6-311G*) > Δ_{63} (cc-pVTZ) > Δ_{63} (aug-cc-pVTZ) and Δ_{63} (cc-pVTZ) > Δ_{63} (6-311++G(2d,2p)). CO₂ was the main exception where Δ_{63} (6-31G*) < Δ_{63} (6-311G*) but Δ_{63} (6-31G*) > Δ_{63} (6-311++G(2d,2p)) and Δ_{63} (6-31G*) > Δ_{63} (aug-cc-pVTZ). Calculations of Δ_{63} using the 6-311++G(2d,2p) and aug-cc-pVTZ valence triple zeta basis sets were very close, and deviated from each other by an average of <0.001‰ (range 0.000 to 0.006‰), most likely indicating a convergence close to the complete basis set limit.

Overall, we found that results from different levels of theory showed similar trends for the five species investigated (Fig. A1A–E). Δ_{63} , $\beta^{13}\text{C}$, and $\beta^{18}\text{O}$ of a given species showed similar trends across the methods. RHF, the simplest level of theory, had consistently higher results than high-accuracy methods. In general, M06 and M06-2X were next highest; B3LYP values were similar to MP2, and very close or slightly lower than QCISD. CCSD values were slightly higher than QCISD values. PBE models gave the lowest values. Rustad et al. (2008) found that of the combinations they tested, the B3LYP method combined with the aug-cc-pVDZ basis set (correlation-consistent polarized valence double zeta with polarization augmented with diffuse functions) gave the best match to experiment for $\beta^{13}\text{C}$. Use

of the 6-311++G(2d,2p) basis set gives similar results to the even larger aug-cc-pVTZ (valence triple zeta), but is less computer intensive. We conclude that the B3LYP/6-311++G(2d,2p) model is a reasonable compromise between accuracy and computer efficiency for the calculation of Δ_{63} , $\beta^{13}\text{C}$, and $\beta^{18}\text{O}$ (see Fig. A7).

A.2.2. Comparison of measured and model CO₂(g) vibrational frequencies and bond lengths

We compared the CO₂(g) vibrational frequencies and C=O bond lengths using each method/basis set combination with measured frequencies, corrected for anharmonicity (Table A4) (Tashkun et al., 1998; Ding et al., 2004). The QCISD/6-311++G(2d,2p) model has the smallest root-mean squared misfit (RMS¹¹) (13.8 cm^{−1}); the B3LYP/6-311++G(2d,2p) model has the next best RMS (14.0). In general, the QCISD and the B3LYP methods yield the smallest RMS values. The RHF models have the largest RMS misfits (245.0 to 279.2 cm^{−1}). Next highest are the M06 and M06-2X models ranging from 83.8 to 141.5 cm^{−1}.

The QCISD/6-311G* and the QCISD/6-311++G(2d,2p) predicted C–O bond lengths that were the closest to the experimental length of 1.1621 Å (Oliphant and Bartlett, 1994): (1.1621 Å and 1.1617 Å respectively).

¹¹ RMS = $\sqrt{(\sum(\text{residuals between predicted and measured vibrational frequencies})^2)/(\text{number of frequencies})}$.

Table A4

CO₂(g) bond lengths and vibrational frequencies from several ab initio method and basis set combinations compared to experimental harmonic values. The deviation of the model bond length from the experimental length is shown as well as the root mean square of all 3 vibrational frequencies compared to the experimental frequencies. Note that the O–C–O bending mode is degenerate due to the symmetry of the CO₂ molecule (Section A.2.2).

Method/Basis set	C–O bond lth (Å)	Dev from Exp't	O–C–O bend vib freq (cm ⁻¹)	C–O sym stretch vib freq (cm ⁻¹)	C–O asym stretch vib freq (cm ⁻¹)	RMS err (vib freq)
Experimental ^a	1.1621	0	672.83	1353.65	2390.3	0
<i>B3LYP</i>						
6-31G*	1.1692	-0.0071	640.0318	1372.0103	2436.2473	34.27
6-311G*	1.1604	0.0017	666.5054	1375.5077	2435.8784	29.41
cc-pVTZ	1.1604	0.0017	671.7897	1371.6471	2416.7626	18.49
6-311++G(2d,2p)	1.1604	0.0017	675.9948	1363.8623	2399.3326	8.08
aug-cc-pVTZ	1.1604	0.0017	673.5411	1369.5778	2401.1794	11.14
<i>CCSD</i>						
6-31G*	1.1704	-0.0083	659.478	1385.1931	2441.7571	35.69
6-311G*	1.1598	0.0023	682.4316	1394.1757	2454.7911	44.32
cc-pVTZ	1.1592	0.0029	684.5488	1389.5602	2434.3932	33.52
6-311++G(2d,2p)	1.1595	0.0026	692.1163	1373.594	2405.0558	18.14
aug-cc-pVTZ	1.1595	0.0026	688.2243	1385.8763	2414.612	24.94
<i>M06-2X</i>						
6-31G*	1.1628	-0.0007	668.1874	1421.7868	2492.5552	70.99
6-311G*	1.1546	0.0075	689.6297	1421.8265	2485.8468	68.46
cc-pVTZ	1.1554	0.0067	693.4366	1413.7713	2463.0743	55.78
6-311++G(2d,2p)	1.1551	0.0070	699.1919	1407.8216	2448.5858	48.40
aug-cc-pVTZ	1.1553	0.0068	696.0565	1412.2007	2449.5534	49.93
<i>M06</i>						
6-31G*	1.1641	-0.0020	672.1039	1405.2606	2512.5545	76.62
6-311G*	1.1547	0.0074	691.3407	1413.4777	2517.1761	81.69
cc-pVTZ	1.1545	0.0076	702.0111	1409.1921	2493.2013	69.58
6-311++G(2d,2p)	1.1545	0.0076	702.4276	1402.1132	2479.259	60.93
aug-cc-pVTZ	1.1545	0.0076	704.3044	1407.3354	2479.0954	62.60
<i>MP2</i>						
6-31G*	1.1797	-0.0176	636.1065	1333.0759	2447.569	41.04
6-311G*	1.169	-0.0069	657.6529	1341.3982	2456.0945	39.62
cc-pVTZ	1.1694	-0.0073	655.8008	1331.9973	2426.0527	26.06
6-311++G(2d,2p)	1.1695	-0.0074	662.8297	1316.983	2397.0388	22.29
aug-cc-pVTZ	1.1702	-0.0081	658.9605	1325.8074	2401.4476	19.08
<i>PBE</i>						
6-31G*	1.1803	-0.0182	611.2251	1322.7506	2386.5368	39.85
6-311G*	1.1718	-0.0097	635.4068	1326.2016	2387.5912	26.84
cc-pVTZ	1.1719	-0.0098	640.37	1322.1455	2367.6069	29.22
6-311++G(2d,2p)	1.172	-0.0099	643.3531	1314.9803	2349.8274	36.53
aug-cc-pVTZ	1.172	-0.0099	641.87	1319.3474	2350.7166	35.13
<i>QCISD</i>						
6-31G*	1.1729	-0.0108	652.1706	1364.0492	2416.8106	20.31
6-311G*	1.1621	0.0000	675.1745	1374.3493	2431.1062	26.45
cc-pVTZ	1.1613	0.0008	677.9894	1372.3034	2413.9679	17.65
6-311++G(2d,2p)	1.1617	0.0004	684.7	1355.5649	2383.5952	7.95
aug-cc-pVTZ	1.1617	0.0004	682.0499	1368.3275	2393.4722	10.17
<i>RHF</i>						
6-31G*	1.1433	0.0188	745.8143	1518.4826	2585.0052	153.20
6-311G*	1.1352	0.0269	767.1984	1522.1681	2592.1527	161.30
cc-pVTZ	1.1362	0.0259	772.9755	1511.2303	2564.3449	147.37
6-311++G(2d,2p)	1.1355	0.0266	780.0991	1505.9484	2553.0072	142.80
aug-cc-pVTZ	1.1362	0.0259	774.795	1509.4917	2549.5419	141.47

^a Tashkun et al. (1998) and Ding et al. (2004).

Table A5

Bond lengths and select vibrational frequencies from B3LYP/6-311++G(2d,2p) models of different solvation techniques compared to experimental values

CO ₃ ²⁻	Bond lengths (Å)				Select vibrational frequencies (cm ⁻¹)		
	C–O	C–O	C–O		Out-of-plane	Sym stretch	Asym stretch
Gas	1.3068	1.3068	1.3068		858.7128	1008.545	1309.0252
Implicit	1.2984	1.2984	1.2984		864.6562	1036.6728	1320.4542
3(H ₂ O)	1.3011	1.3011	1.3011		854.2013	1025.4838	1361.4046
Ave supermolecular clusters	1.2849	1.2899	1.2998		Smeared		1395.0706
Exp't (aq) (Rudolph et al., 2006)					884	1066	1385
HCO ₃ ⁻	C–O	C–O	C–O	O–H	Out-of-plane	Sym stretch	Asym stretch
Gas	1.2502	1.2338	1.4501	0.9625	820.1593	1289.2348	1750.6803
Implicit	1.2503	1.2436	1.4122	0.9641	819.8281	1292.2129	1665.3384
Explicit	1.2634	1.2408	1.3943	0.9696	829.8463		
Ave supermolecular clusters	1.2429	1.2595	1.379	0.9889	Smeared	1349.9065	1669.5742
Exp't (aq)					843	1312/1360	1630

Table A6

Scaling factors for the predictions of harmonic frequencies and zero-point vibrational energies (adapted from Table 24 in Zhao and Truhlar, 2008). These factors are used for comparison with unscaled vibration frequencies in the calculations of carbon and oxygen isotope fractionations and clumped isotope signatures. Zhao & Trudhal did not consider scaling factors for MP2.

Method	Harmonic scaling factor	ZPVE scaling factor
B3LYP	0.998	0.985
M06	0.994	0.983
M06-2X	0.982	0.972
M06-L	0.996	0.980
HF	0.932	0.921
PBE	1.025	1.012

All B3LYP methods (except 6-31G*) predict a bond length of 1.1604 Å. Eight of the ten M06 and M06-2X model bond length predictions deviate by more than .0067 Å from the experimental value. Again, the B3LYP method, combined with the valence triple zeta, polarized 6-311++G(2d,2p) basis set with diffuse functions appears to be the best balance between accuracy and computational efficiency.

A.2.3. Comparison of DIC Species with experimental bond lengths and vibrational frequencies

Table A5 shows bond lengths and select vibrational frequencies for each DIC species with the 4 solvation techniques for B3LYP/6-311++G(2d,2p) models. In general, the more accurately solvated models have smaller intramolecular bond lengths. Vibrational frequencies com-

Table A7

Effect of scaling vibrational frequencies on Δ_{63} , $\beta^{13}\text{C}$, composite $\beta^{18}\text{O}$, composite $\beta^{17}\text{O}$, and composite K3866 for the calcite and aragonite lattices, and one conformer from each DIC species. Results are shown with no scaling (scale factor = 1.0), harmonic scale factor (.998) and zero point vibrational energy scale factor (.985) for B3LYP ab initio method (see Table A6) at 25 °C. All results are from the B3LYP/6-311++G(2d,2p) models.

Species	Conformer	Scale factor	Δ_{63}	$\beta^{13}\text{C}$	Comp $\beta^{18}\text{O}$	Comp $\beta^{17}\text{O}$	Comp K3866
CO ₃ ²⁻	9a	0.985	0.3599	1.1954	1.0970	1.0502	1.000387822
	9a	0.998	0.3703	1.1996	1.0992	1.0513	1.000398972
	9a	1.000	0.3719	1.2002	1.0995	1.0514	1.000400694
HCO ₃ ⁻	5b	0.985	0.3902	1.1957	1.1039	1.0537	1.000421168
	5b	0.998	0.4011	1.1998	1.1061	1.0548	1.000432894
	5b	1.000	0.4028	1.2005	1.1065	1.0550	1.000434704
H ₂ CO ₃	1a	0.985	0.4221	1.2028	1.1148	1.0591	1.000456187
	1a	0.998	0.4334	1.2070	1.1172	1.0603	1.000468404
	1a	1.000	0.4352	1.2077	1.1175	1.0605	1.000470289
Calcite		0.985	0.3818	1.2028	1.1034	1.0534	1.000411586
		0.998	0.3924	1.2071	1.1057	1.0545	1.000422993
		1.000	0.3940	1.2078	1.1060	1.0547	1.000424753
Aragonite		0.985	0.3935	1.2060	1.1048	1.0541	1.000424426
		0.998	0.4043	1.2103	1.1071	1.0553	1.000436012
		1.000	0.4060	1.2110	1.1075	1.0554	1.000437799

Table A8

Comparison of theoretical clumped isotope signatures of CO₂ (g) for T = 300K (26.85 °C) from this work with values from two different models presented in Wang et al. (2004) (Fig. A5). Values from this work are unscaled.

Method/Basis set	Δ_{45}	Δ_{46}	Δ_{47}	Δ_{48}	Δ_{49}
Vib. Freq. Set I, Wang et al. (2004)	−0.0044	−0.0104	0.9138	0.3381	2.2192
Vib Freq. Set II, Wang et al. (2004)	−0.0044	−0.0106	0.9243	0.3956	2.3296
B3LYP/6-31G*	−0.0043	−0.0103	0.9081	0.3590	2.2257
B3LYP/6-311G*	−0.0043	−0.0104	0.9175	0.3648	2.2514
B3LYP/cc-pVTZ	−0.0043	−0.0103	0.9096	0.3644	2.2349
B3LYP/6-311++G(2d,2p)	−0.0043	−0.0102	0.9019	0.3600	2.2148
B3LYP/aug-cc-pVTZ	−0.0043	−0.0102	0.9019	0.3640	2.2187
MO6-2X/6-31G*	−0.0045	−0.0108	0.9491	0.4054	2.3553
MO6-2X/6-311G*	−0.0045	−0.0109	0.9538	0.4055	2.3660
MO6-2X/cc-pVTZ	−0.0044	−0.0108	0.9432	0.4010	2.3398
MO6-2X/6-311++G(2d,2p)	−0.0044	−0.0107	0.9382	0.3979	2.3258
MO6-2X/aug-cc-pVTZ	−0.0044	−0.0107	0.9376	0.4017	2.3282
M06/6-31G*	−0.0045	−0.0109	0.9606	0.3837	2.3586
M06/6-311G*	−0.0046	−0.0110	0.9706	0.3933	2.3890
M06/cc-pVTZ	−0.0045	−0.0109	0.9623	0.3939	2.3728
M06/6-311++G(2d,2p)	−0.0045	−0.0109	0.9555	0.3887	2.3529
M06/aug-cc-pVTZ	−0.0045	−0.0109	0.9563	0.3953	2.3610
MP2/6-31G*	−0.0043	−0.0103	0.9112	0.3206	2.1964
MP2/6-311G*	−0.0044	−0.0104	0.9236	0.3289	2.2308
MP2/cc-pVTZ	−0.0043	−0.0102	0.9071	0.3242	2.1916
MP2/6-311++G(2d,2p)	−0.0042	−0.0101	0.8944	0.3145	2.1561
MP2/aug-cc-pVTZ	−0.0042	−0.0101	0.8952	0.3216	2.1649
PBE/6-31G*	−0.0041	−0.0098	0.8708	0.3168	2.1091
PBE/6-311G*	−0.0041	−0.0099	0.8794	0.3217	2.1320
PBE/cc-pVTZ	−0.0041	−0.0098	0.8708	0.3205	2.1131
PBE/6-311++G(2d,2p)	−0.0041	−0.0097	0.8627	0.3170	2.0926
PBE/aug-cc-pVTZ	−0.0041	−0.0097	0.8627	0.3213	2.0965
QCISD/6-31G*	−0.0043	−0.0102	0.9019	0.3550	2.2096
QCISD/6-311G*	−0.0043	−0.0104	0.9186	0.3652	2.2538
QCISD/cc-pVTZ	−0.0043	−0.0103	0.9105	0.3659	2.2383
QCISD/6-311++G(2d,2p)	−0.0042	−0.0102	0.8968	0.3548	2.1994
QCISD/aug-cc-pVTZ	−0.0043	−0.0102	0.9013	0.3654	2.2189
CCSD/6-31G*	−0.0043	−0.0104	0.9180	0.3724	2.2601
CCSD/6-311G*	−0.0044	−0.0106	0.9340	0.3818	2.3021
CCSD/cc-pVTZ	−0.0044	−0.0105	0.9245	0.3809	2.2812
CCSD/6-311++G(2d,2p)	−0.0043	−0.0104	0.9114	0.3697	2.2441
CCSD/aug-cc-pVTZ	−0.0043	−0.0104	0.9153	0.3798	2.2613

pare reasonably well with experiment. Rustad et al. (2008) has a detailed discussion of the effects of gas vs. implicit solvation vs. cluster models on the vibrational frequencies and the bond lengths, with which our results generally agree.

A.2.4. Effects of scaling the vibrational frequencies

Model predictions for a few species were calculated using both unscaled and scaled vibrational frequencies. Two kinds of method- and basis-set-specific scaling factors were used (Table A6): based on fitting to (1) harmonic frequencies and (2) zero-point vibrational energies (ZPVE) as described in Zhao and Truhlar (2008). The scaling factors are different for each ab initio and DFT method (Table A7).

In most cases, unscaled models predict $\beta^{18}\text{O}$, $\beta^{13}\text{C}$, and Δ_{63} slightly larger than equivalent models using harmonic scaling, which are in turn slightly larger than equivalent

models with ZPVE scaling. In general, the unscaled models did a better job of predicting oxygen and carbon isotope fractionations than did the scaled models. In the absence of a compelling case for scaling, our results presented in this work use unscaled vibrational frequencies.

A.3. Renormalizing the fractional abundances of DIC species when omitting the CO₂(aq)

The fractional abundances of the 3 DIC species [CO₂(aq) + H₂CO₃], HCO₃[−], and CO₃^{2−}, are calculated using the equations of Millero et al. (2006) with Eqs. (2) and (3). The very small amount of H₂CO₃ is included with the CO₂(aq) species. These abundances are shown in Table 10 and Fig. 6. However, as discussed in Section 4.1.2, the CO₂(aq) portion of the DIC pool is omitted from the calculation of the composite DIC Δ_{63} since CO₂ does not

have 3 oxygens and is not in rapid exchange equilibrium with carbonate species.

$[\text{H}_2\text{CO}_3]$ is assumed to be $= .001 * [\text{CO}_2(\text{aq})]$. Then to determine the contribution of H_2CO_3 , HCO_3^- , and CO_3^{2-} the relative abundances must be renormalized such that they add to unity (Eq. (21)) (i.e., $f'(\text{H}_2\text{CO}_3) + f'(\text{HCO}_3^-) + f'(\text{CO}_3^{2-}) = 1$). This is done as follows:

Let $s = 0.001 * f(\text{H}_2\text{CO}_3 + \text{CO}_2(\text{aq})) + f(\text{HCO}_3^-) + f(\text{CO}_3^{2-})$ where $f(x)$ is the fractional abundance of species x when $[\text{CO}_2(\text{aq}) + \text{H}_2\text{CO}_3]$, HCO_3^- , and CO_3^{2-} are included and $f'(x)$ is the fractional abundance of species x when $\text{CO}_2(\text{aq})$ is omitted. Then

$$f'(\text{H}_2\text{CO}_3) = 0.001 * f(\text{H}_2\text{CO}_3 + \text{CO}_2(\text{aq}))/s \quad (\text{A21})$$

$$f'(\text{HCO}_3^-) = f(\text{HCO}_3^-)/s$$

$$f'(\text{CO}_3^{2-}) = f(\text{CO}_3^{2-})/s$$

For example, at $\text{pH} = 5$, $T = 25$, and $S = 0$, $f(\text{H}_2\text{CO}_3 + \text{CO}_2(\text{aq})) = .974$, $f(\text{HCO}_3^-) = .026$, and $f(\text{CO}_3^{2-}) = 0$ (Table 9). Then $s = 0.001 * .974 + .026 + 0 = .026974$, $f'(\text{H}_2\text{CO}_3) = .001 * .974 / .026974 = .036109$, $f'(\text{HCO}_3^-) = .026 / .026974 = .963891$, and $f'(\text{CO}_3^{2-}) = 0$. These are the values used to calculate Δ_{63} as shown in Table 10.

A.4. Strategies for finding optimized geometries for large supermolecular clusters in Gaussian09

We found it very difficult to obtain optimized geometries of supermolecular clusters containing DIC species surrounded by multiple water molecules, presumably because the potential energy field of the cluster is very flat due to numerous weak H bonds. Often the geometry iteration process (a gradient based optimization) proceeds smoothly for several steps but then oscillates around a stationary point without being able to converge (see Fig. A6). In such cases, one can intervene and choose the molecular geometry of one of the iteration steps preceding the start of the oscillations and then restart automatic optimization. Regenerating an initial Hessian is also helpful.

If self-consistent field (SCF) iterations do not converge, then it is helpful to try a different method, such as Fermi temperature broadening or a quadratically convergent SCF procedure. If an error occurs in which there are atoms too close together, it is necessary to back up a few iterations and start over with an earlier geometry. If an internal coordinate error occurs, indicating a problem with the automatic generation of redundant internal coordinates, then it is necessary to optimize using Cartesian coordinates.

It is useful to save the checkfile file in order to save the Hessian, which can be used to obtain the vibrational frequencies of the different isotopologues. It also useful if a long-running job needs to be restarted.

In order to facilitate optimizations of systems using larger and larger basis sets, we used the “bootstrap” method. We first obtained the optimized geometry with a small basis set, such as 6-31G* and determined the force constant Hessian analytically. This Hessian was reused as an initial guess for the next larger basis set, and so forth.

Sometimes a system optimizes to an apparently satisfactory stationary point but has trouble converging during the frequency calculations. In such cases it is useful to tighten the quadrature grid used by the DFT method. During long frequency calculations, it is also helpful to use the read-write file (xx.rwf) to save intermediate calculation results that are not saved in the checkpoint file.

APPENDIX B. SUPPLEMENTARY DATA

Supplementary data associated with this article can be found, in the online version, at <http://dx.doi.org/10.1016/j.gca.2013.06.018>

REFERENCES

- Adamczyk K., Premont-Schwarz M., Pines D., Pines E. and Nibbering E. T. J. (2009) Real-Time observation of carbonic acid formation in aqueous solution. *Science* **326**, 1690–1694.
- Affek H. P., Bar-Matthews M., Ayalon A., Matthews A. and Eiler J. M. (2008) Glacial/interglacial temperature variations in Soreq cave speleothems as recorded by ‘clumped isotope’ thermometry. *Geochim. Cosmochim. Acta* **72**, 5351–5360.
- Al-Horani F. A., Al-Moghrabi S. M. and de Beer D. (2003) The mechanism of calcification and its relation to photosynthesis and respiration in the scleractinian coral *Galaxea Fascicularis*. *Marine Biology* **142**, 419–426.
- Bartlett R. J. (1995) Coupled-cluster theory: an overview of recent developments. In *Modern Electronic Structure Theory, Part II* (ed. D. R. Yarkony). World Scientific Publishing Co., Singapore, pp. 1047–1131.
- Bartlett R. J. and Musial M. (2007) Coupled-cluster theory in quantum chemistry. *Rev. Mod. Phys.* **79**, 291.
- Beck W. C., Grossman E. L. and Morse J. W. (2005) Experimental studies of oxygen isotope fractionation in the carbonic acid system at 15°, 25°, and 40 °C. *Geochim. Cosmochim. Acta* **69**, 3493–3503.
- Becke D. (1993) A new mixing of Hartree-Fock and local density-functional theories. *J. Chem. Phys.* **98**, 1372–1377.
- Bigeleisen J. and Mayer M. G. (1947) Calculation of equilibrium constants for isotopic exchange reactions. *J. Chem. Phys.* **15**, 261–267.
- Blaudeau J.-P., McGrath M. P., Curtiss L. A. and Radom L. (1997) Extension of Gaussian-2 (G2) theory to molecules containing third-row atoms K and Ca. *J. Chem. Phys.* **107**, 5016.
- Bryantsev V. S., Diallo M. S., van Duin A. C. T. and Goddard, III, W. A. (2009) Evaluation of B3LYP, X3LYP, and M06-class density functionals for predicting the binding energies of neutral, protonated, and deprotonated water clusters. *J. Chem. Theory Comput.* **5**, 1016–1026.
- Cao X. and Liu Y. (2012) Theoretical estimation of the equilibrium distribution of clumped isotopes in nature. *Geochim. Cosmochim. Acta* **77**, 292–303.
- Chacko T. and Deines P. (2008) Theoretical calculation of oxygen isotope fractionation factors in carbonate systems. *Geochim. Cosmochim. Acta* **72**, 3642–3660.
- Chacko T. K., Mayeda P., Clayton R. N. and Goldsmith J. R. (1991) Oxygen and carbon isotope fractionations between CO_2 and calcite. *Geochim. Cosmochim. Acta* **55**, 2867–2882.
- Chamberlin A. C., Cramer C. J. and Truhlar D. G. (2008) Performance of SM8 on a test to predict small-molecule solvation free energies. *J. Phys. Chem. B* **112**, 8651–8655.
- Cizek J. (1969). In *Advances in Chemical Physics*, vol. 14 (ed. P. C. Hariharan). Wiley Interscience, New York, p. 35.

- Cramer C. J. and Truhlar D. G. (2008) The SM8 solvation model. *Acc. Chem. Res.* **41**, 760–768.
- Crawford T. D. and Schaefer H. F. (2000) An introduction to coupled cluster theory for computational chemists. In *Reviews in Computational Chemistry*, vol. 14 (eds. K. B. Lipkowitz and D. B. Boyd). VCH Publishers, New York, pp. 33–136.
- Daeron M., Guo W., Eiler J., Genty D., Blamart D., Boch R., Drysdale R., Maire R., Wainer K. and Zanchetta G. (2011) ^{13}C – ^{18}O clumping in speleothems: observations from natural caves and precipitation experiments. *Geochim. Cosmochim. Acta* **75**, 3303–3317.
- Dennis P. (2004) Carbon isotope effects in carbonate systems. *Geochim. Cosmochim. Acta* **68**, 2659–2679.
- Dennis K. J. and Schrag D. P. (2010) Clumped isotope thermometry of carbonates as an indicator of diagenetic alteration. *Geochim. Cosmochim. Acta* **74**, 4110–4122.
- Dennis K. J., Affek H. P., Passey B. H., Schrag D. P. and Eiler J. M. (2011) Defining an absolute reference frame for ‘clumped’ isotope studies of CO_2 . *Geochim. Cosmochim. Acta* **75**, 7117–7131.
- Ding Y., Macko P., Romanini D., Perevalov V. G., Tashkun S. A., Teffo J.-L., Hu S.-M. and Campargue A. J. (2004) High sensitivity CW-cavity ringdown and Fourier transform absorption spectroscopies of $(\text{CO}_2)\text{-C-13}$. *Mol. Spectrosc.* **226**, 146–160.
- Dunning, Jr., T. H. and Hay P. J. (1976). In *Modern Theoretical Chemistry*, vol. 3 (ed. , IIIH. F. Schaefer). Plenum, New York, pp. 1–28.
- Eagle R. A., Schauble E., Tripathi A., Tutken T., Hulbert R. and Eiler J. (2010) Body temperatures of modern and extinct vertebrates from $(^{13}\text{C})\text{-(}^{18}\text{O)}$ bond abundances in biapatite. *PNAS* **107**, 10377–10382.
- Eagle R. A., Eiler J. M., Tripathi A. K., Ries J. B., Freitas P. S., Hiebenthal C., Wanamaker, Jr., A. D., Taviani M., Elliot M., Marensi S., Nakamura K., Ramirez P. and Roy K. (2013) The influence of temperature and seawater carbonate saturation state on ^{13}C – ^{18}O bond ordering in bivalve mollusks. *Biogeosciences* **10**, 4591–4606.
- Eiler J. M. (2007) Clumped-isotope geochemistry—the study of naturally-occurring, multiply substituted isotopologues. *Earth Planet. Sci. Lett.* **262**, 309–327.
- England A. H., Duffin A. M., Schwartz C. P., Uejio J. S., Prendergast D. and Saykally R. J. (2011) On the hydration and hydrolysis of carbon dioxide. *Chem. Phys. Lett.* **514**, 187–195.
- Falcke H. and Eberle S. H. (1990) Raman spectroscopic identification of carbonic acid. *Water Res.* **24**, 685–688.
- Faure G. and Mensing T. M. (2004) *Isotopes: Principles and Applications*, Third ed. John Wiley & Sons Inc., Hoboken, NJ, 896pp.
- Fuentealba P., von Szentpaly L., Preuss H. and Stoll H. (1985) Pseudopotential calculations for alkaline-earth atoms. *J. Phys. B* **18**, 1287–1296.
- Gaussian 09, Revision B.1, (2010) Frisch, M. J.; Trucks, G. W.; Schlegel, H. B.; Scuseria, G. E.; Robb, M. A.; Cheeseman, J. R.; Scalmani, G.; Barone, V.; Mennucci, B.; Petersson, G. A.; Nakatsuji, H.; Caricato, M.; Li, X.; Hratchian, H. P.; Izmaylov, A. F.; Bloino, J.; Zheng, G.; Sonnenberg, J. L.; Hada, M.; Ehara, M.; Toyota, K.; Fukuda, R.; Hasegawa, J.; Ishida, M.; Nakajima, T.; Honda, Y.; Kitao, O.; Nakai, H.; Vreven, T.; Montgomery, Jr., J. A.; Peralta, J. E.; Ogliaro, F.; Bearpark, M.; Heyd, J. J.; Brothers, E.; Kudin, K. N.; Staroverov, V. N.; Kobayashi, R.; Normand, J.; Raghavachari, K.; Rendell, A.; Burant, J. C.; Iyengar, S. S.; Tomasi, J.; Cossi, M.; Rega, N.; Millam, J. M.; Klene, M.; Knox, J. E.; Cross, J. B.; Bakken, V.; Adamo, C.; Jaramillo, J.; Gomperts, R.; Stratmann, R. E.; Yazyev, O.; Austin, A. J.; Cammi, R.; Pomelli, C.; Ochterski, J. W.; Martin, R. L.; Morokuma, K.; Zakrzewski, V. G.; Voth, G. A.; Salvador, P.; Dannenberg, J. J.; Dapprich, S.; Daniels, A. D.; Farkas, Ö.; Foresman, J. B.; Ortiz, J. V.; Cioslowski, J.; Fox, D. J. Gaussian, Inc., Wallingford CT, 2009.
- Ghosh P., Adkins J., Affek H., Balta B., Guo W., Schauble E., Schrag D. and Eiler J. (2006) ^{13}C – ^{18}O bonds in carbonate minerals: a new kind of paleothermometer. *Geochim. Cosmochim. Acta* **70**, 1439–1456.
- Guo W., Mosenfelder J. L., Goddard, III, W. A. and Eiler J. M. (2009) Isotopic fractionations associated with phosphoric acid digestion of carbonate minerals: insights from first-principal modeling and clumped isotope measurements. *Geochim. Cosmochim. Acta* **73**, 7203–7225.
- Guo W. (2008) Carbonate clumped isotope thermometry: application to carbonaceous chondrites and effects of kinetic isotope fractionation. Ph.D. dissertation, California Institute of Technology.
- Halls M. D. and Schlegel H. B. (1998) Comparison of the performance of local, gradient-corrected, and hybrid density functional models in predicting infrared intensities. *J. Chem. Phys.* **109**, 10587–10593.
- Hamman D. R. (1997) H_2O hydrogen bonding in density-functional theory. *Phys. Rev. B* **55**, R10157–R10160.
- Hariharan P. C. and Pople J. A. (1973) Influence of polarization functions on molecular-orbital hydrogenation energies. *Theor. Chim. Acta* **28**, 213–222.
- Head-Gordon M., Pople J. A. and Frisch M. J. (1988) MP2 energy evaluation by direct methods. *Chem. Phys. Lett.* **153**, 503–506.
- Kendall R. A., Dunning, Jr., T. H. and Harrison R. J. (1992) Electron affinities of the first-row atoms revisited. Systematic basis sets and wave functions. *J. Chem. Phys.* **96**, 6796–6806.
- Herzberg G. (1966). *Molecular Spectra and Molecular Structure. III. Electronic Spectra and Electronic Structure of Polyatomic Molecules*. Van Nostrand Reinhold, New York, pp. 598.
- Horita J. and Wesolowski D. J. (1994) Liquid-vapor fractionation of oxygen and hydrogen isotopes of water from the freezing to the critical-temperature. *Geochim. Cosmochim. Acta* **58**, 3425–3437.
- Huntington K. W., Eiler J. M., Affek H. P., Guo W., Bonifacie W. M., Yeung L. Y., Thiagarajan N., Passey B., Tripathi A., Daeron M. and Came R. (2009) Methods and limitations of ‘clumped’ CO_2 isotope ($\Delta 47$) analysis by gas-source isotope ratio mass spectrometry. *J. Mass Spectrom.* **44**, 1318–1329.
- Jmol: an open-source Java viewer for chemical structures in 3D. <http://www.jmol.org/>.
- Johnson B. G., Gill P. M. W. and Pople J. A. (1993) The performance of a family of density functional methods. *J. Chem. Phys.* **98**, 5612.
- Kim S. and O’Neil J. (1997) Equilibrium and nonequilibrium oxygen isotope effects in synthetic carbonates. *Geochim. Cosmochim. Acta* **61**, 3461–3475.
- Krishnan R., Binkley J. S., Seeger R. and Pople J. A. (1980) Self-consistent molecular-orbital methods. 20. Basis set for correlated wave-functions. *J. Chem. Phys.* **72**, 650–654.
- Lee C., Yang W. and Parr R. G. (1988) Development of the Colle–Salvetti correlation-energy formula into a functional for the electron density. *Phys. Rev. B* **37**, 785–789.
- Lee T. J. and Scuseria G. E. (1995) Achieving chemical accuracy with coupled-cluster theory. In *Quantum Mechanical Electronic Structure Calculations with Chemical Accuracy* (ed. S. R. Langhoff). Kluwer Academic Publishers., Dordrecht, pp. 47–108.
- Lécuyer C., Hutzler A. and Amiot R., et al. (2012) Carbon and oxygen isotope fractionations between aragonite and calcite

- of shells from modern molluscs. *Chemical geology* **332**, 92–101.
- Liu Y. and Tossell J. A. (2005) Ab initio molecular orbital calculations for boron isotope fractionations on boric acids and borates. *Geochim. Cosmochim. Acta* **69**, 3995–4006.
- Majoube M. (1971) Fractionnement en oxygène n 18 et en deutérium entre l'eau et sa vapeur. *J. Chim. Phys.* **68**, 1423–1436.
- Marenich A. V., Cramer C. J. and Truhlar D. G. (2009) Universal solvation model based on the generalized Born approximation with asymmetric descreening. *J. Chem. Theory Comput.* **5**, 2447–2464.
- McCrea J. M. (1950) On the isotopic geochemistry of carbonates and a paleotemperature scale. *J. Chem. Phys.* **18**, 849–857.
- Miertus S., Scrocco E. and Tomasi J. (1981) Electrostatic interaction of a solute with a continuum. A direct utilization of ab initio molecular potentials for the prevision of solvent effects. *Chem. Phys.* **55**, 117–129.
- Millero D. J., Graham T. B., Huang F., Bustos-Serrano H. and Pierrot D. (2006) Dissociation constants of carbonic acid in seawater as a function of salinity and temperature. *Marine Chem.* **100**, 80–94.
- Molnar L. F., He X., Wang B. and Merz, Jr., H. M. (2009) Further analysis and comparative study of intermolecular interactions using dimers from the S22 database. *J. Chem. Phys.* **131**, 065102.
- Nakamoto K. (1997) *Infrared and Raman Spectra of Inorganic and Coordination Compounds Part A: Theory and Applications in Inorganic Chemistry*. John Wiley & Sons Inc., New York.
- Oliphant N. and Bartlett R. J. (1994) A systematic comparison of molecular properties obtained using Hartree–Fock, a hybrid Hartree–Fock density-functional-theory, and coupled-cluster methods. *J. Chem. Phys.* **100**, 6550.
- Perdew J. P., Burk K. and Ernzerhof M. (1996) Generalized gradient approximation made simple. *Phys. Rev. Lett.* **77**, 3865–3868.
- Perdew J. P., Burke K. and Ernzerhof M. (1997) Generalized gradient approximation made simple. *Phys. Rev. Lett.* **78**, 1396.
- Pople J. A., Head-Gordon M. and Raghavachari K. (1987) Quadratic configuration interaction – a general technique for determining electron correlation energies. *J. Chem. Phys.* **87**, 5968–5975.
- Powell M. J. D. (1970) A fortran subroutine for solving systems of nonlinear algebraic equations. In *Numerical Methods for Nonlinear Algebraic Equations* (ed. P. Rabinowitz). Gordon and Breach Science Publishers, London.
- Rassolov V. A., Pople J. A., Ratner M. A. and Windus T. L. (1998) 6-31G(d) basis set for atoms K through Zn. *J. Chem. Phys.* **109**, 1223–1229.
- Redlich O. Z. (1935) A general relationship between the oscillation frequency of isotropic molecules – (with remarks on the calculation of harmonious force constants). *Phys. Chem. B* **28**, 371–382.
- Refson K. (2000) Moldy: a portable molecular dynamics simulation program for serial and parallel computers. *Comp. Phys. Commun.* **126**, 310–329.
- Richet P., Bottinga Y. and Javoy M. (1977) A Review of Hydrogen, carbon, Nitrogen, Oxygen, Sulphur, and Chlorine Stable Isotope Fractionation among Gaseous Molecules. *Ann. Rev. Earth Planet. Sci.* **5**, 65–110.
- Romanek C., Grossman E. and Morse J. (1992) Carbon isotopic fractionation in synthetic aragonite and calcite: Effects of temperature and precipitation rate. *Geochimica et Cosmochimica Acta* **56**, 419–430.
- Rudolph W. W., Fischer D. and Irmer G. (2006) Vibrational spectroscopic studies and density functional theory calculations of speciation in the CO₂–water system. *Appl. Spectrosc.* **60**, 130–144.
- Rustad J. R. and Bylaska E. J. (2007) Ab initio calculation of isotopic fractionation in B(OH)₃(aq) and BOH₄(aq). *J. Am. Chem. Soc.* **129**, 2222–2223.
- Rustad J. R., Nelmes S. L., Jackson V. E. and Dixon D. A. (2008) Quantum-chemical calculations of carbon-isotope fractionation in CO₂(g), aqueous carbonate species and carbonate minerals. *J. Phys. Chem. A* **112**, 542–555.
- Rustad J. R., Bylaska E. J., Jackson V. E. and Dixon D. A. (2010a) Calculation of boron-isotope fractionation between B(OH)₃(aq) and B(OH)₄(aq). *Geochim. Cosmochim. Acta* **74**, 2843–2850.
- Rustad J. R., Casey W. H., Yin Q.-Z., Bylaska E. J., Felmy A. R., Bogatko S. A., Jackson V. E. and Dixon D. A. (2010b) Isotopic fractionation of Mg²⁺(aq), Ca²⁺(aq), and Fe²⁺(aq) with carbonate minerals. *Geochim. Cosmochim. Acta* **74**, 6301–6323.
- Saenger C., Affek H. P., Felis T., Thiagarajan N., Lough J. M. and Holcomb M. (2012) Carbonate clumped isotope variability in shallow water corals: Temperature dependence and growth-related vital effects. *Geochimica et Cosmochimica Acta* **99**, 224–242.
- Schauble E. A. (2004) Applying stable isotope fractionation theory to new systems. In *Geochemistry of Non-Traditional Stable Isotopes: Reviews in Mineralogy & Geochemistry*. vol. 55, pp. 65–111.
- Schauble E., Ghosh P. and Eiler J. (2006) Preferential formation of ¹³C–¹⁸O bonds in carbonate minerals, estimated using first-principles lattice dynamics. *Geochim. Cosmochim. Acta* **70**, 1439–1456.
- Scilab Consortium – Digiteo (2011) Scilab: free and open source software for numerical computation (OS, Version 5.3.3) [running on Apple OSX 10.6.8]. Available from: <http://www.scilab.org>.
- Scott A. P. and Radom L. (1996) Harmonic vibrational frequencies: an evaluation of Hartree–Fock, Møller–Plesset, quadratic configuration interaction, density functional theory and semi empirical scale factors. *J. Phys. Chem.* **100**, 16502–16513.
- Scuseria G. E., Janssen C. L. and Schaefer, III, H. F. (1988) An efficient reformulation of the closed-shell coupled cluster single and double excitation (CCSD) equations. *J. Chem. Phys.* **89**, 7382–7387.
- Shackleton N. J. and Opdyke N. D. (1973) Oxygen isotope and palaeomagnetic stratigraphy of Equatorial Pacific Core V28-238: oxygen isotope temperatures and ice volumes on a 105 year and 106 year scale. *Quatern. Res.* **3**, 39–55.
- Shackleton N. J. (1974) Attainment of isotopic equilibrium between ocean water and the benthonic foraminifera genus *Uvigerina*: isotopic changes in the ocean during the last glacial. In *Colloques Internationaux du C.N.R.S.* vol. 219, pp. 203–209.
- Sim F., St. Amant A., Papai I. and Salahub D. R. J. (1992) Gaussian density functional calculations on hydrogen-bonded systems. *Am. Chem. Soc.* **114**, 4391–4400.
- Soli A. L. and Byrne R. H. (2002) CO₂ system hydration and dehydration kinetics and the equilibrium. *Marine Chem.* **78**, 65–73.
- Suárez D., Rayón V. M., Díaz N. and Valdés H. (2011) Ab initio benchmark calculations on Ca(II) complexes and assessment of density functional theory methodologies. *J. Phys. Chem. A* **115**, 11331–11343.
- Swart P. K., Burns S. J. and Leder J. J. (1991) Fractionation of the stable isotopes of oxygen and carbon in carbon dioxide during the reaction of calcite with phosphoric acid as a function of temperature and technique. *Chem. Geol. Isotope Geosci. Sect.* **86**, 89–96.

- Tashkun S. A., Perevalov V. I., Teffo J.-L., Rothman L. S. and Tyuterev V. G. J. (1998) Global fitting of (CO₂)-C-12-O-16 vibrational-rotational line positions using the effective Hamiltonian approach. *Quantum Spectrosc. Radiat. Transfer* **60**, 785.
- Thiagarajan N., Adkins J. and Eiler J. (2011) Carbonate clumped isotope thermometry of deep-sea corals and implications for vital effects. *Geochim. Cosmochim. Acta* **75**, 4416–4425.
- Thomas J. R., DeLeeuw B. J., Vacek G. and Schaefer H. F. (1993a) A systematic theoretical study of the harmonic vibrational frequencies for polyatomic molecules: the single, double, and perturbative triple excitation coupled-cluster [CCSD(T)] method. *J. Chem. Phys.* **98**, 1336, 1993.
- Thomas J. R., DeLeeuw B. J., Vacek G., Crawford T. D., Yamaguchi Y. and Schaefer H. F. (1993b) The balance between theoretical method and basis set quality: a systematic study of equilibrium geometries, dipole moments, harmonic vibrational frequencies, and infrared intensities. *J. Chem. Phys.* **99**, 403.
- Tossell J. A. (2006) H₂CO₃ and its oligomers: structures, stabilities, vibrational and NMR spectra, and acidities. *Inorg. Chem.* **45**, 5961–5970.
- Tripathi A., Eagle R., Thiagarajan N., Gagnon A., Bauch H., Halloran P. and Eiler J. (2010) ¹³C–¹⁸O bond ordering and clumped isotope thermometry in foraminifera and coccoliths. *Geochim. Cosmochim. Acta* **74**, 5697–5717.
- Urey H. C. (1947) The thermodynamic properties of isotopic substances. *J. Chem. Soc.*, 562–581.
- Wang Z., Schauble E. and Eiler J. (2004) Equilibrium thermodynamics of multiply substituted isotopologues of molecular gases. *Geochim. Cosmochim. Acta* **68**, 4779–4797.
- Wong M. W. (1996) Vibrational frequency prediction using density functional theory. *Chem. Phys. Lett.* **256**, 391–399.
- Woon D. E. and Dunning, Jr., T. H. (1993) Gaussian-basis sets for use in correlated molecular calculations. 3. The atoms aluminum through argon. *J. Chem. Phys.* **98**, 1358–13571.
- Xantheas S. S. (1995) Ab initio studies of cyclic water clusters (H₂O)_n, n = 1–6. III. Comparison of density functional with MP2 results. *J. Chem. Phys.* **102**, 4505.
- Yang K., Zheng J. J., Zhao Y. and Truhlar D. G. (2010) Tests of the RPBE, revPBE, tau-HCTHhyb, omega B97X-D, and MOHLYP density functional approximations and 29 others against representative databases for diverse bond energies and barrier heights in catalysis. *J. Chem. Phys.* **132**, 164117.
- Zeebe R. E. (2007) An expression for the overall oxygen isotope fractionation between the sum of dissolved inorganic carbon and water. *Geochim. Geophys. Geosyst.* **8**. <http://dx.doi.org/10.1029/2003GC001663>.
- Zeebe R. E. (2011) On the molecular diffusion coefficients of dissolved CO(2), HCO(3)(-), and CO(3)(2-) and their dependence on isotopic mass. *Geochim. Cosmochim. Acta* **75**, 2483–2498.
- Zeebe R. E. (2009) Hydration in solution is critical for stable oxygen isotope fractionation between carbonate ion and water. *Geochim. Cosmochim. Acta* **73**, 5283–5291.
- Zeebe R. E. and Wolf-Gladrow D. A. (2001) *CO₂ in Seawater: Equilibrium, Kinetics, Isotopes*. Elsevier Science, Amsterdam, 346 pp.
- Zhang J., Quay P. D. and Wilbur D. O. (1995) Carbon isotope fractionation during gas-water exchange and dissolution of CO₂. *Geochim. Cosmochim. Acta* **59**, 107.
- Zhao Y. and Truhlar D. G. (2008a) Density functionals with broad applicability in chemistry. *Acc. Chem. Res.* **41**, 157–167.
- Zhao Y. and Truhlar D. G. (2008b) The M06 suite of density functionals for main group thermochemistry, thermochemical kinetics, noncovalent interactions, excited states, and transition elements: two new functionals and systematic testing of four M06-class functionals and 12 other functionals. *Theor. Chem. Acc.* **120**, 215–241.

Associate editor: Claire Rollion-Bard